

LIFE CYCLE COST OPTIMIZATION OF A SOLAR COMBISYSTEM IN NEPAL

by

Bishan Thapa

A thesis submitted to the faculty of  
The University of North Carolina at Charlotte  
in partial fulfillment of the requirements  
for the degree of Master of Science in  
Applied Energy and Electromechanical Systems

Charlotte

2019

Approved by:

---

Dr. Weimin Wang

---

Dr. Umit Cali

---

Dr. Wesley Williams

©2019  
Bishan Thapa  
ALL RIGHTS RESERVED

## ABSTRACT

BISHAN THAPA. Life Cycle Cost Optimization of a Solar Combisystem in Nepal. (Under the direction of DR. WEIMIN WANG)

Nepal has a huge potential for solar energy utilization to meet the growing energy demand. Solar thermal systems have been used in Nepal since the 1960s. In the past two decades, much work was done with a focus on improving design, fabrication, and installation practices of using solar thermal collectors for heating domestic hot water. Little work has been found in literature on the design and analysis of solar combisystems in Nepal. The work presented in this thesis includes the design, modeling, and optimization of a solar combisystem for typical single-family houses in Nepal. The proposed solar combisystem consists of solar thermal collectors, one preheating water tank, one domestic hot water tank with auxiliary electric resistance heating, an electric instantaneous water heater and circulation pumps. TRNSYS software is used to model the solar combisystem. For optimization, life cycle cost is the objective function. The number of hours not satisfying the thermostat set points is treated as the constraint of the optimization problem. Major optimization variables include the thermal collector area, the volumes of both tanks, the flow rate of water circulating between the thermal collectors and the preheating tank, and several building envelope variables such as the wall insulation and roof insulation. The particle swarm optimization and the Hooke-Jeeves algorithms are combined to solve the optimization problem.

The solar combisystem is modeled and optimized in two different climatic regions in Nepal: the Terai region and the Hilli region. The optimization for both locations starts from an initial design based on guidelines, conventional construction practices, and

engineering judgement. Relative to the initial design, the life cycle cost is reduced by 63% and 72% respectively for the Terai and the Hilli region respectively. The optimization results in a lower collector area and a lower storage tank size for the Terai region but a higher collector area for the Hilli region. One of the important aspects of this research was to include building insulation variables during optimization. The drastic reduction in objective function is also due to the effect of insulation in building envelope which allowed the usage of low value of instantaneous water heater. Lastly this study emphasizes the importance of using optimization tool to achieve the best performance even for the initial design.

## ACKNOWLEDGEMENTS

First and foremost, I would like to express my sincerest gratitude to Dr. Weimin Wang for his dedicated time from inception to the completion of this thesis. I am looking forward to imbibing his professional integrity in my career. His insistence on quality rather than quantity of work is always etched in my mind. Living in the other side of the world from family is never easy but his occasional personal attendance was very helpful to get me going. I am equally thankful to Dr. Umit Cali and Dr. Wesley Williams for their valuable suggestions to construct the thesis.

I am incredulous to all the help that came along my way. When I began to remember names of all those who helped me during this research, I feel that I have only been an arranger for this thesis. I am thankful to Srijana Koirala for sending the drawing of reference house in Nepal, Sanjay Kumar Tulsayan for sending me the cost of solar thermal components in Nepal and Amirahmad Zare for his invaluable help during modeling of combisystem in TRNSYS. I am grateful to Nita Khanal for helping me in formatting the thesis.

Finally, it goes without saying that I am thankful to my parents and relatives who have given me impetus to complete this thesis.

## DEDICATION

This thesis is dedicated to my parents.

## TABLE OF CONTENTS

LIST OF TABLES .....	x
LIST OF FIGURES .....	xi
LIST OF ABBREVIATIONS.....	xiii
CHAPTER 1: INTRODUCTION.....	1
1.1 Solar Thermal Energy Around the Globe .....	1
1.2 Energy Scenario in Nepal .....	2
Residential Energy Consumption .....	3
1.3 Solar Energy in Nepal.....	4
Solar Water Heating Systems in Nepal.....	6
1.4 Research Objectives.....	8
CHAPTER 2: LITERATURE REVIEW .....	9
2.1 Background on Solar Combisystem.....	9
2.2 Feasibility Study of Solar Combisystems .....	13
2.3 Life Cycle Analysis.....	15
2.4 Optimization of Solar Thermal Systems.....	19
2.5 Optimization of Solar Combisystem.....	21
2.6 Solar Space Heating in Nepal .....	23
CHAPTER 3: CLIMATE OF NEPAL AND HOUSE PROTOTYPE DEVELOPMENT	25
3.1 Climate of Nepal.....	25
3.1.1 Terai Region.....	25
3.1.2 Hilli Region.....	27
3.1.3 Himalayan Region .....	27

3.2 House Construction in Nepal .....	27
CHAPTER 4: SYSTEM DESCRIPTION AND MODELING IN TRNSYS .....	35
4.1 Combisystem Design and Description .....	35
4.2 Modeling in TRNSYS .....	37
4.2.1 Solar Collector Loop.....	37
4.2.1.1 Weather Data Reader- Type 15.....	38
4.2.1.2 Solar Collector -Type 1b.....	39
4.2.1.3 Storage Tank-Type 534.....	42
4.2.1.4 Pump-Type 114.....	44
4.2.1.5 Controller-Type 165 d.....	45
4.2.2 DHW Loop of the Combisystem .....	46
4.2.2.1 Load Profile – Type 14 h .....	46
4.2.2.2 Equation Tab.....	47
4.2.2.3 Diverter- 11f.....	48
4.2.2.4 Valve control – Type 115 .....	48
4.2.2.5 Storage Tank – Type 534.....	48
4.2.2.6 DHW tank –Type 158.....	48
4.2.2.7 Tank Stat- Type 106.....	49
4.2.2.8 Mixing Valve-Type 11h.....	50
4.2.3 Space Heating Loop.....	51
4.2.3.1 Storage Tank – Type 534.....	51
4.2.3.2 Pump –Type 114.....	52
4.2.3.3 Thermostat – Type 166.....	52

4.2.3.4 Instantaneous Water Heater- Fluid Heater Type 138 .....	53
4.2.3.5 Multi-zone Building-Type 56 .....	53
4.2.4 Thermal Comfort Measurement -Type 584 .....	59
CHAPTER 5: LIFE CYCLE COST OPTIMIZATION .....	62
5.1 Variables .....	62
5.2 Objective Function.....	67
5.2.1 Investment Cost .....	68
5.2.2 Operating Cost .....	70
5.2.3 Penalty Function .....	70
5.3 Selection of Optimization Tool.....	72
5.4 Optimization Algorithm.....	73
5.4.1 Particle Swarm Optimization.....	74
5.4.2 Hooke Jeeves Algorithm.....	79
CHAPTER 6: OPTIMIZATION RESULTS .....	85
6.1 Results for the Terai Region .....	85
6.2 Results for the Hilli Region .....	91
CHAPTER 7: CONCLUSIONS .....	100
7.1 Summary of Results .....	100
7.2 Future Work .....	101
REFERENCES .....	103
APPENDIX A.....	107
APPENDIX B .....	110

## LIST OF TABLES

TABLE 1: Envelope of Typical Modern Construction in Nepal .....	34
TABLE 2: Type 1b parameter settings .....	41
TABLE 3: Parameters of DHW tank .....	49
TABLE 4: Optimization variables used with their boundary conditions .....	63
TABLE 5: The cost of major solar combisystem components .....	68
TABLE 6: Optimization parameter for PSO algorithm (Hin 2013) .....	76
TABLE 7: Optimization parameters for the Hooke-Jeeves algorithm .....	84
TABLE 8: Initial values and final values of the optimization variables for Terai region .	89
TABLE 9: Initial values and final values of the optimization variables for Hilli region ..	95

## LIST OF FIGURES

FIGURE 1: Global solar thermal capacity in operation and annual energy yields from 2000-2017 (Weiss and Spork-dur 2018) .....	1
FIGURE 2: Sectoral Energy Consumption for year 2015 (Rajbhandari and Nakarmi 2015) .....	3
FIGURE 3: Residential energy consumption by end use for year 2015 (Bhandari and Pandit 2018) .....	4
FIGURE 4: Global horizontal irradiation of Nepal (ESMAP 2017) .....	5
FIGURE 5: Map of Nepal showing three different geographical features (Wikipedia)....	25
FIGURE 6: Climate comparison of southern city of Nepal with New-Delhi .....	26
FIGURE 7: Typical Newari house.....	29
FIGURE 8: Typical house during Rana regime.....	29
FIGURE 9: Typical rural house in Nepal .....	30
FIGURE 10: Modern housing in Kathmandu.....	30
FIGURE 11: Schematic of the solar combisystem .....	37
FIGURE 12: Modeling of solar collector loop in TRNSYS.....	38
FIGURE 13: Schematic of storage tank.....	44
FIGURE 14: Operation of controller type 165d .....	45
FIGURE 15: DHW loop of the combisystem.....	46
FIGURE 16: Hourly representation of DHW consumption profile.....	47
FIGURE 17: Modeling of space heating in TRNSYS .....	51
FIGURE 18: External wall construction for reference building and its TRNSYS representation (right).....	55
FIGURE 19: Roof construction for reference building and its TRNSYS representation (Right).....	56
FIGURE 20: Construction of radiant floor heating system in TRNSYS.....	58

FIGURE 21: Calculation of thermal comfort by Type 584 .....	60
FIGURE 22: TRNSYS model of the solar combisystem.....	61
FIGURE 23: Cost vs. Power of instantaneous heater .....	69
FIGURE 24: Interface between GenOpt and simulation program (Wetter 2016) .....	73
FIGURE 25: Gbest and lbest neighborhood topology .....	77
FIGURE 26: Von Neumann neighborhood topology .....	77
FIGURE 27: Exploratory move of Hooke-Jeeves algorithm.....	80
FIGURE 28: Pattern move of the Hooke-Jeeves algorithm.....	82
FIGURE 29: Evolution of the objective function values with the generation for the particle swarm optimization in Terai region .....	87
FIGURE 30: Evolution of the objective function values with the generation for the particle swarm optimization in Terai, after excluding the outliers due to the triggering of the penalty function .....	87
FIGURE 31: Evolution of the objective function with the iteration for the Hooke-Jeeves optimization .....	88
FIGURE 32: Evolution of the objective function values with the generation for the particle swarm optimization in Hilli region. ....	93
FIGURE 33: Evolution of the objective function values with the generation for the particle swarm optimization in Hilli region without outliers.....	93
FIGURE 34: Evolution of the objective function values in Hooke-Jeeves for Hilli region .....	94
FIGURE 35: Impact of collector slope on Life Cycle Cost.....	97
FIGURE 36: Impact of collector slope on annual energy generation for Sterling, VA.....	97

## LIST OF ABBREVIATIONS

AEPC - Alternative Energy Promotion Center

ANSYS – Analysis of Systems

ASHRAE – American Society of Heating Refrigeration and Air Conditioning Engineers

CHREM – Canadian Hybrid Residential End-Use Energy Model

CHS – Canadian Housing Stock

CSTB – Centre Scientifique et Technique du Batiment

DHW – Domestic Hot Water

EPS – Expanded Polystyrene

ESMAP – Energy Sector Management Assistance Program

FSC – Fractional Solar Consumption

GJ – Giga Joule

HJ – Hooke Jeeves

HUSP – Hours Under Set Point

IEA – International Energy Agency

IEE – Intelligent Energy Europe

LCC – Life Cycle Cost

LPG – Liquefied Petroleum Gas

MOPSO – Multi Objective Particle Swarm Optimization

NRB – Nepal Rastra Bank

NREL – National Renewable Energy Laboratory

NZEH – Net Zero Energy House

PEX – Cross Linked Polyethylene

PSO – Particle Swarm Optimization

PVT – Photovoltaic Thermal

SEL – Solar Energy Laboratory

SHC – Solar Heating and Cooling

SWH – Solar Water Heating

TESS – Thermal Energy Systems Specialists

TRNSYS – Transient System Simulation

VRF – Variable Flow Refrigerant

# CHAPTER 1: INTRODUCTION

## 1.1 Solar Thermal Energy Around the Globe

According to the International Energy Agency (Weiss and Spork-dur 2018), the total solar thermal capacity in operation by the end of 2017 was 472 GW<sub>th</sub>. This amount of solar thermal power comes from 675 million square meters of collector area, which grew by a factor of eight relative to the year 2000 as shown in FIGURE 1. The installed solar thermal systems yielded 388 TWh solar thermal energy in 2017, which led to the savings of 41.7 million tons of oil and the reduction of 134.7 million tons of CO<sub>2</sub>.

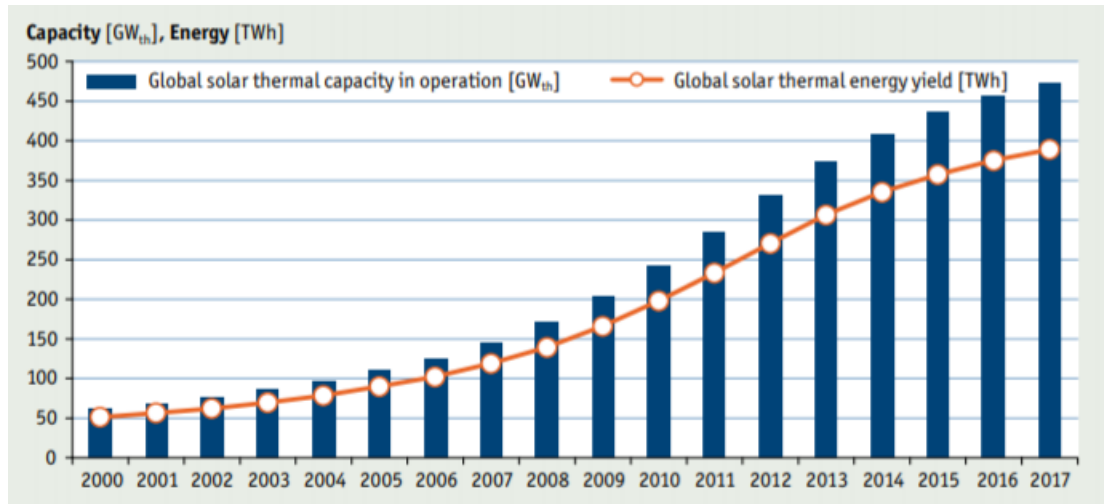


FIGURE 1: Global solar thermal capacity in operation and annual energy yields from 2000-2017 (Weiss and Spork-dur 2018)

Despite of the historical rapid growth, the global solar thermal market has faced challenging times in recent years. This is especially evident in China and Europe, where the traditional mass markets for small-scale solar water heating systems for single-family houses and apartment buildings are under market pressure from heat pumps and photovoltaic systems. In total, the global market declined by 4.2% in 2017 compared to 2016. However, positive market developments were recorded in India (26%), Mexico

(7%), and in Turkey (4%), where the number in parenthesis indicates the percentage of increase from 2016 to 2017. In 2016, most of the solar thermal capacity was installed in China (324.5 GWth) and Europe (51.8 GWth), the combination of which accounted for 82.3% of the global installed capacity. The remaining installed capacity was shared between the United States and Canada (18.6 GWth), Asia excluding China (12.1 GWth), Latin America (12.3 GWth), the Middle East and North Africa region (6.8 GWth), Australia and New Zealand (6.5 GWth), Sub-Saharan African countries (1.5 GWth), and all other countries not mentioned above (22.8 GWth) (Weiss and Spork-dur 2018).

## **1.2 Energy Scenario in Nepal**

In Nepal, energy consumption sectors include residential, commercial, transportation, industrial, agriculture, and others. The sector of “others” accounts for the energy consumption for street lights, temples, mosques, and churches. In the year of 2015, the national total energy consumption was 475 million GJ. As FIGURE 2 shows, the residential sector accounted for the predominant share of energy consumption (80%), followed sequentially by industrial (8%), transportation (7%), commercial (4%), the agricultural and others (Rajbhandari and Nakarmi 2015).

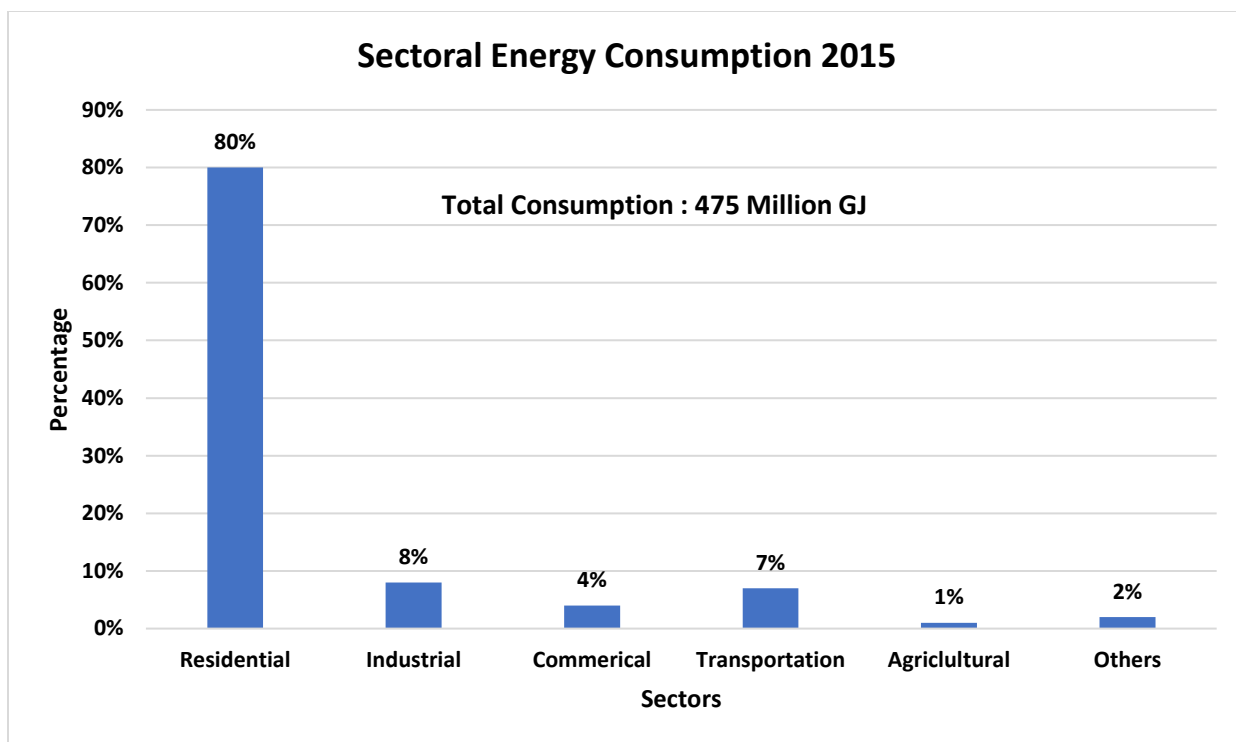


FIGURE 2: Sectoral Energy Consumption for year 2015 (Rajbhandari and Nakarmi 2015)

### Residential Energy Consumption

Residential sector energy consumption is related to the number of households and population. The population growth rate and the economic situation of the households are the two main factors that affect the residential energy consumption and fuel types in Nepal. The residential sector consumed 350 million GJ in the year of 2015. Major share of residential energy consumption goes towards cooking (60%), lighting (12%), domestic hot water (DHW) (12%), and space heating (10%), as shown in FIGURE 3.

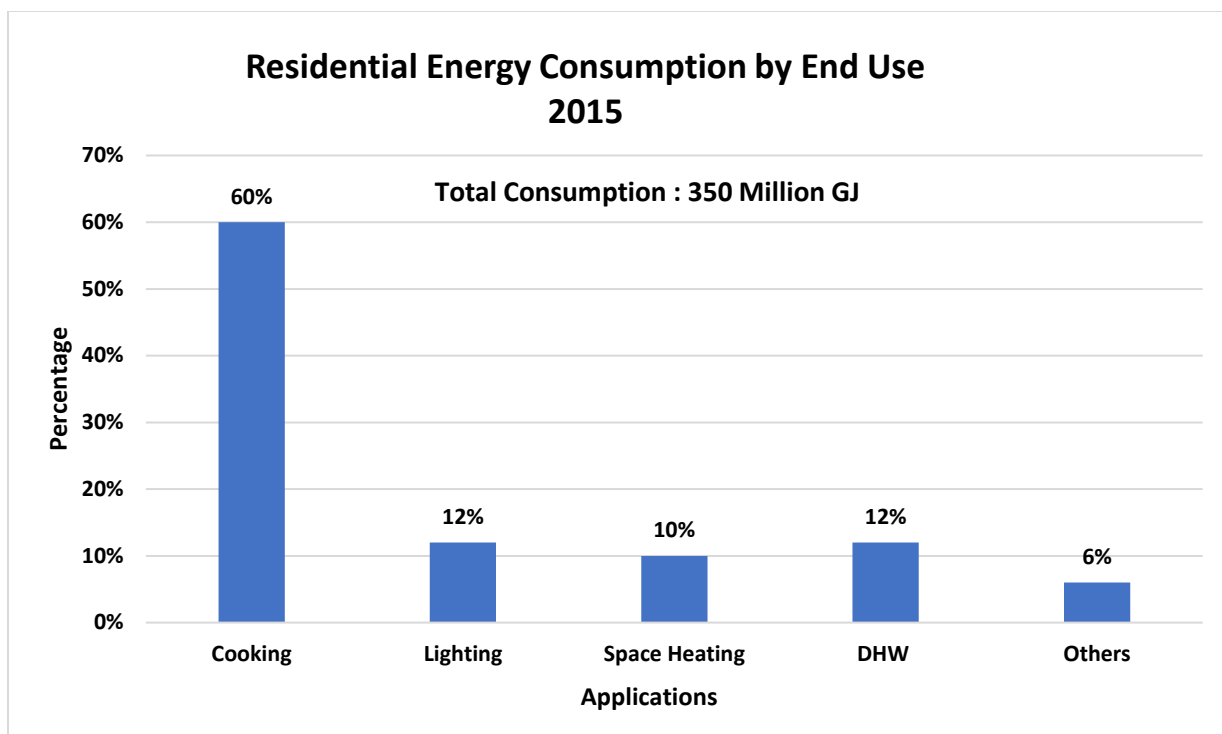


FIGURE 3: Residential energy consumption by end use for year 2015 (Bhandari and Pandit 2018)

### 1.3 Solar Energy in Nepal

Nepal is endowed with a huge amount of natural resources. In addition to the huge hydro power potential, the country is bestowed with favorable solar insolation. On average there are 300 sunny days in a year with 6.8 sunshine hours per day. This means that Nepal has a high potential for solar energy utilization to meet the growing energy demand. The northwest part of Nepal has the highest solar irradiation reaching up to 5.5 kWh/m<sup>2</sup>/day as shown in FIGURE 4. Other regions in the country have average daily global horizontal irradiation (GHI) value in the range between 4.4 kWh/m<sup>2</sup>/day and 4.9 kWh/m<sup>2</sup>/day (ESMAP 2017).

# GLOBAL HORIZONTAL IRRADIATION

## NEPAL

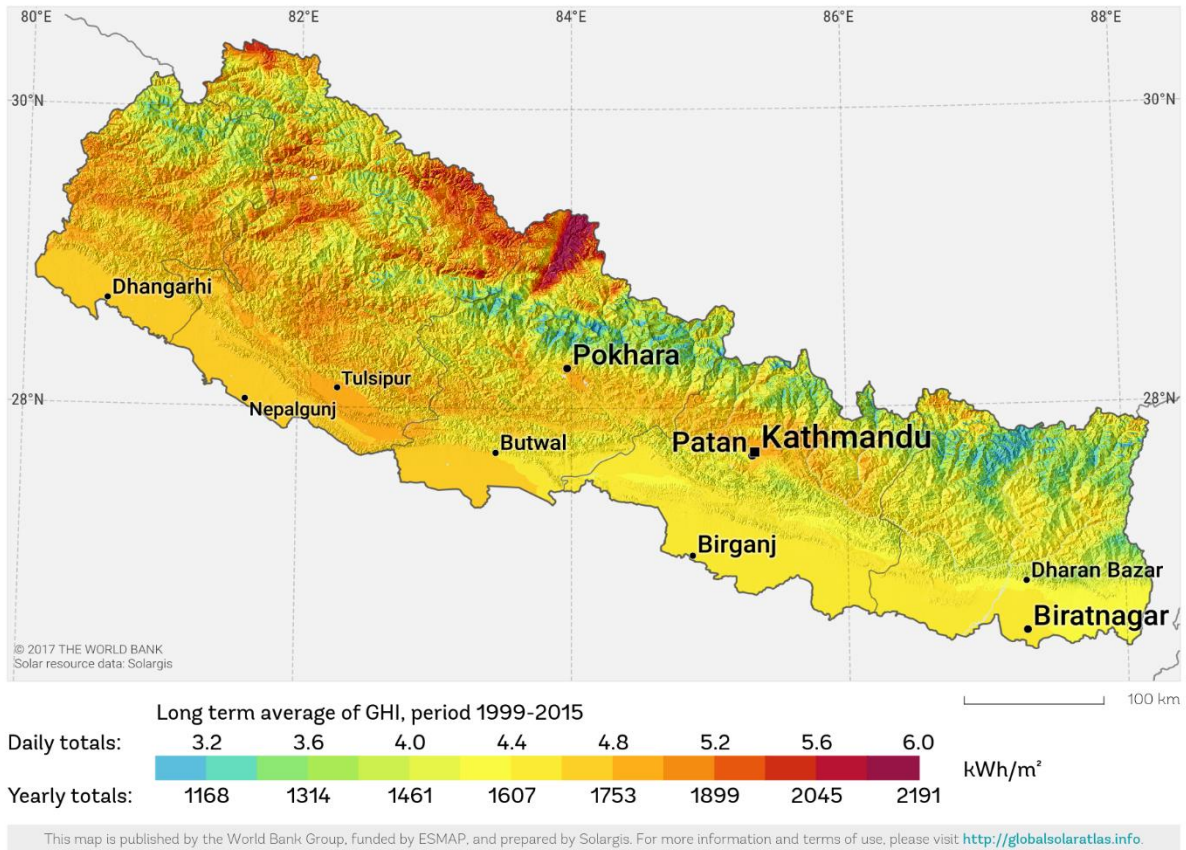


FIGURE 4: Global horizontal irradiation of Nepal (ESMAP 2017)

Since the residential sector is the largest energy consumer in Nepal, cost-effective renewable energy technology is expected to play a significant role towards the country's sustainable development. In particular, solar energy has a great potential in reducing fossil fuel energy consumption for residential space heating and domestic hot water generation (Papillon *et al.* 2010).

## **Solar Water Heating Systems in Nepal**

After the introduction of solar water heating (SWH) back in 1960s, the technology has evolved dramatically. Many private companies and research institutions have been working aggressively to improve the design, fabrication and installation practices (Shakya and Bajracharya 2003).

Solar systems are becoming common for service water heating in hotels, guesthouses, and even in solitary mountain lodges and tourist trekking trails. Locally fabricated solar thermal systems, most of which are passive solar systems, have been used widely in various parts of the country. In the field, black painted aluminum plate is usually used as the solar absorber and it is welded to galvanized steel tubes and covered with glazing. The collectors are fabricated manually in local shops, which made them not as efficient as various types of collectors manufactured in developed countries. The operating efficiency of solar thermal systems is constrained not only by the simple type of collector constructions but mainly due to the lack of sufficient piping insulation. Though the local fabrication technology cannot produce solar collectors with efficiency as high as those manufactured in developed countries, some users claimed they had used the solar collectors are robust to last up to 30 years without any issues. It was estimated that solar thermal collectors with approximately a total of 100,000 m<sup>2</sup> of surface area was installed in the country, which was equivalent to a collector surface area of 5-7 m<sup>2</sup> per 1,000 inhabitants. The installation of solar collectors is predicted to grow by 50,000 m<sup>2</sup> every year (Peuser *et al.* 2011).

Private companies importing solar thermal systems and components from India and China are instrumental for the rapid growth of solar thermal systems in Nepal. These

imported technologies are aesthetic and efficient compared to locally fabricated solar thermal systems. Alternative Energy Promotion Center (AEPC), an organization responsible for governing the promotion of renewable technologies in Nepal, certified 21 companies to disseminate the solar thermal technologies (AEPC 2018). However, because the AEPC certification is not mandatory to provide services related to solar thermal technology, there are hundreds of companies nationwide active in this field. Though solar thermal systems for service water heating have deep penetration in the residential sector, using solar energy for space heating is rare. On the other hand, it is common to have snow in the northern part of Himalayan nation. Although Kathmandu is known to have most amicable weather throughout the country, it witnessed snow in February 2019 after 63 years (reported by Himalayan Times on February 10, 2019). Apart from snow, Kathmandu had prolonged period of coldness throughout the winter. In cold weather conditions, the occupants' thermal comfort cannot be satisfied without the use of appropriate space heating systems.

Solar combisystem is a kind of system that relies on solar to provide both domestic hot water and space heating. The design and implementation of solar combisystems is new to Nepal. No reference has been found in literature to investigate the system configuration and performance analysis of solar combisystems. This thesis intends to address the gap in the current literature on solar combisystems and provide meaningful contributions in the usage of solar energy for buildings.

## **1.4 Research Objectives**

Recognizing the importance of thermal comfort in modern residential buildings and the abundant source of solar energy in Nepal, this research aims to achieve the following objectives:

- Propose a solar combisystem for Nepal;
- Model the proposed system performance with TRNSYS, a detailed transient simulation program;
- Optimize the system design with respect to the life cycle cost; and
- Analyze the optimized system design over different climate zones in the country.

## **CHAPTER 2: LITERATURE REVIEW**

Since the invention of solar thermal collectors in 1896 in the U.S., there have been many studies on both the component level and the system level. Studies on the component level have focused on the efficiency improvement of the major components of solar thermal systems, of which the solar collector is the foremost important one. Studies on the system level have worked on the enhancement of system performance, including both the energy performance and the economic performance. Since this thesis focuses on solar combisystem for domestic hot water and space heating, some organizational as well as general individual contributions are summarized at first. After reviewing few literatures on feasibility of solar combisystem across the world, solar thermal systems optimizations are reviewed with focus on solar combisystem optimization. Finally, a brief summary of studies on solar thermal heating in Nepal is also discussed.

### **2.1 Background on Solar Combisystem**

The concept of solar combisystems came into being in the late twentieth century. Since then, many research programs were implemented across the world to delve into the complex nature of combisystem design. For example, the International Energy Agency Solar Heating and Cooling Programme (IEA-SHC) dedicated one of their working tasks - Task 26- to solar combisystems (Weiss 2003). From 1998 to 2002, IEA-SHC Task 26 made a thorough analysis of different combisystem design options and synthesized them into 21 alternative system configurations. For nine of those configurations, detailed investigations were performed via TRNSYS simulations to obtain the recommended values for certain design parameters (Hin 2013).

Of all solar thermal systems in operation worldwide, solar combisystems account for only a small portion and most of them are deployed in Europe. As of 2009, approximately 18% of the installed solar thermal capacity in Europe is from solar combisystems (Weiss *et al.* 2013) The immense European interest in solar combisystems can be demonstrated through several renowned international research programs. From 2001 to 2003, the Altener programme under the European Commission, in collaboration with IEA-SHC Task 26, studied over 200 combisystems and monitored 39 different systems, based on which the guidelines for installation and design were developed and the approaches for characterization and comparison of different systems were documented (Ellehaug 2003). From 2007 to 2010, Intelligent Energy Europe (IEE) commissioned a project known as Combisol (Papillon *et al.* 2010). The objectives of Combisol were to develop best practices, standards, and recommendations for manufacturers, installers, authorities and technical experts. The project also grouped the combisystems in Europe to six different categories. A number of combisystems installed in Europe were evaluated and monitored in-situ. The project showed that significant energy savings could be achieved if the system was properly designed and installed (Hin 2013).

Apart from the above mentioned two comprehensive organizational effort to delve into solar combisystem, all the researches related to combisystems are individual and they have contributed great deal in demystifying many aspects of combisystems. Their studies on various components (e.g., solar collector and heat storage), the heat distribution mechanisms, the controls and various auxiliary heating mechanisms, and the whole systems performance have led to fruitful findings which have become guidelines for the designers, planners and installers.

To increase the performance of a solar combisystem, one may consider many possible design features, such as large thermal storage, highly efficient auxiliary heaters, and low-temperature space heating systems), stratifiers, tank-in-tank configurations, high efficiency pumps, and increased storage tank insulation (Streicher *et al.* 2004).

Similarly, several researchers have focused on the sizing of individual components of solar combisystems. Lund (2005) studied the effects of collector area and heat storage volume on system performance. Lund concluded that solar combisystems with oversized collector areas performed well but oversizing collectors was not favorable for the economic performance of the system. Lund also found that increasing the storage volume marginally improved the amount of solar heat delivered to the system. In another study, Lundh *et al.* (2010) investigated the impact of storage dimensions and auxiliary volume configurations on system performance. Auxiliary volume can be internal and external storage. Internal auxiliary volume was created with a thin membrane which separates the main store volume. They concluded that a storage size up to 4 m<sup>3</sup> could be used for the collector area of 30 m<sup>2</sup>. The simulations also showed that the performance of an internal auxiliary volume configuration exceeded that of a system with an external auxiliary unit in most cases.

Some studies investigated the impact of load and weather profiles on combisystem performance. For example, Ulrike and Klaus (2000) demonstrated how different domestic hot water load profiles could affect the thermal performance of a combisystem. They found that if simplified load profiles with either a fixed number of draw-offs every day or with relatively long draw-off durations are used, the thermal performance of the system tends to be overestimated. Though they did not recommend the specific DHW profile for use, they highly recommended to use profiles with small time steps (Bales and Persson 2003)

compared seven different external DHW units, comprising flat plate heat exchanger and flow control, with a reference method for preparing hot water in a combisystem. These DHW units used different control methods. The objective of that study was to determine which methods are most effective in solar combisystems and to identify factors that strongly influence the energy savings of the system. The study concluded that the best performance was obtained in the units which had maximum primary flow suitable to the load profile and that system which returned low temperature to the storage. The hot water load profile was also shown to have large impact on energy savings.

Andersen and Furbo (2009) showed that the annual thermal performance of solar collectors could not be predicted from the global radiation, but both the annual thermal performance and the annual utilized solar energy could be fitted to a linear function of the yearly solar radiation on the collector for both flat plate and evacuated tubular solar collectors.

Though combisystems present many opportunities for detailed studies on different designs, configurations, performances and external influences due to its complexity, for the same reason it is difficult to characterize and compare different combisystems. For example, a combisystem that works well for a single-family detached house in Athens, Greece does not necessarily work well for a similar residential building in Stockholm, Sweden. In this respect, a few numbers of studies tried to develop various methods to characterize the combisystem performance but there is still no widely accepted approach to compare and characterize solar combisystems. Letz *et al.* (2009) proposed a method to compare solar combisystems independently of climate conditions and building loads. They developed a metric called fractional solar consumption (FSC), which is a dimensionless

quantity that takes into account climate, DHW and space heating load, collector size, and tilt but does not take into account the system being studied. The study showed that the fractional energy savings with or without parasitic energy can be expressed as a quadratic function of FSC. This method was proved to be effective for wide range of conditions but limited to certain orientation and hot water loads. Later it was used to create a nomogram and a computer program called CombiSun. Leconte *et al.* (2012) attempted to combine artificial neural networks with a test bench in order to characterize a solar combisystem's performance in different climates. They proposed a method based on the short cycle system performance test procedure which tests each combisystem as a whole system on a semi-virtual test bench. Experimental results were used to identify a "Gray Box" model of the tested solar combisystem. The grey box model could then simulate the behavior of the system for any climate and any building, which was not possible solely with FSC. Results of all those simulations were finally used according to the FSC procedure in order to characterize the tested combisystem performances with a simple curve. When this methodology was tested against the results from two installed solar combisystems, the proposed methodology was found promising.

## **2.2 Feasibility Study of Solar Combisystems**

The cost effectiveness of solar combisystems has been properly documented by the IEA task 26 and several other European programs. Apart from these studies, a number of techno-economic studies on solar combisystems were conducted for different climates across the world.

Sustar (2011) investigated whether the solar combisystem was more cost effective than the domestic solar water heating (SWH) system. TRNSYS models were created to

study the annual performance of a conventional SWH and a solar combisystem of the same size for residential applications in six locations (i.e., Denver, Boston, San Francisco, Chicago, Phoenix and Atlanta) in the U.S. The highest annual energy savings was achieved in Denver, followed by San Francisco and Boston. The high annual energy savings in Denver and Boston was largely due to their relatively significant space heating loads and relatively high incident solar radiation. In the case of San Francisco, the space heating loads and the high incident solar radiation in the late spring played a large role in yielding high energy savings of the solar combisystem than the conventional SWH. In terms of the cost savings relative to the reference system (which can be gas or electric), the annual cost savings for an electric system was the largest in San Francisco and Boston due to their high electricity costs. Annual cost savings was the highest for the gas system in Georgia due to the extremely high gas cost.

Asaee *et al.* (2014) conducted a feasibility study of using an enhanced solar combisystem plus (DHW, space heating, space cooling) to achieve a net zero energy house design in four climatic conditions in Canada. The results showed that solar combisystems provided a substantial fraction of energy used for space heating, space cooling and domestic hot water heating for a simple house in all major climatic regions of Canada. Inspired by the results of this study, Asaee *et al.* (2016) performed a techno-economic analysis of retrofitting solar combisystem in Canadian housing stock (CHS). A hybrid energy modeling approach - Canadian Hybrid Residential End-Use Energy Model (CHREM) and Green House Gas Emissions- was employed in their work. The results showed that around 40% of houses in the CHS were eligible for solar combisystem retrofit, and if all eligible houses were retrofitted, the annual energy consumption and greenhouse

gas emissions of the CHS would be reduced by about 19%. The tolerable capital cost varied significantly amongst provinces. Governmental subsidies or incentive programs were suggested to promote the deployment of solar combisystems in some provinces.

### **2.3 Life Cycle Analysis**

Life cycle analysis was used in several studies because of its advantage of comprehensively measuring the effectiveness of solar thermal systems. Depending on the focused aspects, life cycle analysis was performed in the perspective of life cycle cost, life cycle energy and life cycle exergy. Most life cycle analyses tried to answer the following two questions: 1) is the solar thermal system financially feasible? 2) does the solar thermal system save more energy during its operation than the energy required in the manufacture phase?

Kalogirou (2009) answered both questions for a residential thermo-siphon solar hot water system in Nicosia, Cyprus. It was determined that an electric backup thermosiphon solar hot water system had a payback time of 2.7 years and life cycle savings of 2240 € while the same system with a diesel backup had a payback time of 4.5 years and life cycle savings of 1056 €. As of life cycle energy, the energy payback time was only 13 months, which means that the solar energy utilized in 13 months matches the energy used in the production phase of all system components.

Crawford and Treloar (2004) attempted to answer the second question by analyzing the net energy consumption of both solar and conventional domestic hot water systems in Melbourne, Australia. They determined that in comparison with the conventional system, the solar hot water systems compensated the extra embodied energy in 0.5 years for the electric hot water system and 2 years for the gas-boosted hot water systems.

Ardente *et al.* (2005) performed a thorough analysis of a thermo-siphon solar water heating system for the city of Palermo, Italy. They calculated the energy payback time, defined as the primary energy used during all the life cycle phases of the system divided by the annual energy saving. For simple thermo-siphon solar collectors, the energy payback time was determined to be less than two years. In their calculation, the embodied energy considered all phases of the solar collector life cycle, including production, transportation, installation, maintenance, and disposal.

Battisti and Corrado (2005) performed a similar analysis on solar thermal collectors with integrated water storage in Rome, Italy. The collector tubes of this collector design were of a larger diameter which allowed for extra storage within the collector array itself and thereby no external storage tank was required. The study found that for an integrated water storage volume of 100 L, the system had a primary energy payback time of 5 to 16 months depending on the type of backup system (electric or natural gas boiler) and whether a transparent insulation material was used.

Leckner (2008) performed a life cycle analysis of a solar combisystem installed in a typical house built in Montreal, Canada, which was renovated to become a net-zero energy house. He compared flat plate and evacuated tube collectors for a number of collectors (one to six) installed. The results showed that the flat plate collectors had a shorter pay back economically than the evacuated tube collectors. However, in both cases, the payback time was too long to be financially viable. When the inflation rate, the rising cost of electricity, the discount rate and the cost of equipment replacement and maintenance were accounted for, the solar combisystem could be never paid back financially. For life cycle energy, Leckner found that a combisystem with two solar collectors had an energy

payback time of 7.5 years and a system with six solar collectors had an energy payback time of 9.6 years.

Hugo (2008) modelled a typical house in Montreal, Quebec with a solar combisystem and seasonal thermal storage. For the purpose of seasonal thermal storage, Hugo assumed that the tank volume and collector area could be large enough to store sufficient energy collected in summer for space heating and domestic hot water heating over the winter. Hugo determined that the financial payback of such a system ranged from 26 to 55 years depending on the system configuration and economic parameters, such as government incentives, the rising cost of electricity and the inflation rate. Hugo also determined that such a system had an energy payback time of 4.9 to 6 years, which was much longer than the energy payback time for typical solar thermal systems. Hugo attributed the high energy payback time to the efficient hydro power generation in Quebec.

Hernandez and Kenny (2012) compared the predicted and actual energy payback times for six different solar domestic hot water heating systems installed in Ireland. The systems differed in the collector areas, storage volumes, auxiliary energy sources, collector tilts and collector types (flat plate or evacuated tube). The domestic hot water demand profiles for the houses served by the studied systems were also different. The predicted energy payback times for these systems ranged from 1.2 years to 3.5 years. Based on the real measured energy savings, they calculated the actual payback times to be in the range from 2.5 to 15.9 years. Several systems performed much worse than the prediction due to the poor quality of installation and equipment malfunctions. In addition to the energy payback time, they determined the net energy ratios of the six systems, where the net energy ratio means 'how many times' the embodied energy is paid back over the service

life of the system. The net energy ratio ranged between 1.3 and 7.9 based on the measured performance. These results showed that even for systems with malfunctions and installation problems, the saved energy during the operation phase was always higher than the solar system's embodied energy.

Chow *et al.* (2009) analyzed the performance of solar assisted heat pump for pool water heating and pool space heating. They relied on TRNSYS simulation for the economic analysis of the system. Because the solar collectors dominated the capital cost of the system, the initial cost could be lower with a smaller scale of solar heating employed. However, from the energy saving perspective, it was obvious that a large collector area led to more energy savings compared to the conventional system without solar collectors. The implementation cost can be reduced with the use of smaller collector area, even if more heat pump units have to be employed. Consequently, more auxiliary energy will be needed to satisfy the energy demands. However, the increase in energy saving is higher than the cost growth rate of collectors. The payback period is therefore shorter when more collector area was considered. The payback period for the proposed combination systems is less than 5 years. Better system utilization and hence cost saving may be achieved by extending the services to space cooling and dehumidification in the summer period.

Patil (2010) studied the impact of climate change on R-2000 houses built in Montreal, Canada. Four cases were considered with difference combinations of the energy efficiency of houses and the climate conditions. The two energy efficiency levels included R-2000 houses and the net zero energy houses (NZEH) using the solar PVT (photovoltaic thermal) system and many other energy efficient features. The two climate conditions included the present climate and the climate of 2050. For the R-2000 house, the heating

load would reduce by 11 to 22%, while the cooling load would increase by 25 to 93% by the mid-century. The life cycle analysis indicated that the NZEH was cost competitive with the base R-2000 house over the life span of 50 years although the former had a higher initial cost. The NZEH had 40% higher embodied energy than the base R-2000 house, however, it had a lower life cycle energy and life cycle emission t than the R-2000 house.

In summary, all reviewed studies indicated that solar thermal systems can pay back the system's embodied energy before the end of its operating life. The number of years required to pay back the embodied energy depends mostly on the system design and the climate conditions. For financial payback times, however, residential solar thermal systems can vary significantly as they depend not only on the design and climate but also the utility tariff and equipment cost. A solar thermal system is likely to pay back financially within its lifetime at locations where energy is expensive and the climate is characterized with warm and sunny weather (e.g., Mediterranean countries). In places like Montreal, Quebec, where the electricity cost is low, solar thermal systems are unlikely viable economically.

## **2.4 Optimization of Solar Thermal Systems**

Optimization is a powerful approach to improve solar system design and operation. Hin (2013) lists out earlier attempts to optimize solar thermal systems include Bar-Cohen (1978), Barnes (1981), and Michelson (1982). Bar-Cohen (1978) developed a model for compact solar water heaters to optimize the ratio between the storage volume and the collector area for maximizing the storage temperature of the collector in the early morning. It was concluded that a storage temperature of more than 40°C was possible in early morning. Barnes (1981) determined the optimal collector area to be 4.8 m<sup>2</sup> to minimize the annualized cost of a solar collector. Barnes further stated that even with a larger collector

area ( $>4.8 \text{ m}^2$ ), there were no severe economic penalties because the marginal cost increase with collector area was small. Michelson (1982) optimized a solar air heater using a simplex optimization method to minimize the simple payback by modifying the collector specifications such as tilt angle, azimuth, collector area, and storage volume.

In the recent two decades, the research on solar system optimization has gained growing momentum due to the development of sophisticated modeling, simulation programs and optimization techniques. Using fractional energy savings as the design criteria, Loomans (2002) applied a genetic algorithm to find the optimal configuration of a large scale solar hot water heater. Kraus et al (2002) combined the use of a classical gradient-based simplex method with a genetic algorithm to minimize the cost of a large solar domestic hot water system. They relied on TRNSYS for performance simulation and succeeded in reducing the solar heating cost by 18% compared to a conventionally planned and installed solar thermal systems. Kalogirou (2004) combined the use of artificial neural networks and a genetic algorithm to maximize the life cycle savings of an industrial solar water heater. They managed to increase the life cycle savings by 3.1%-4.9% compared to a traditionally designed system, depending whether subsidized fuel prices were considered. Lima *et al.* (2006) used a modified simplex algorithm to optimize a thermo-syphon solar domestic water heater in Sao Paolo, Brazil. Depending on the electricity price, the optimized systems were found to have financial pay back periods between 5.25 and 9.75 years. In order to determine the best optimization criteria, Fraisse *et al.* (2009) compared the results from the single objective and multi-objective optimization criteria. They cautioned that using a single optimization criterion instead of multiple optimization criteria (e.g. both the cost savings and energy savings) took the risk of obtaining a solution with

much worse performance in other unconsidered performance criteria. The author also pointed out that with relatively low energy prices, the energy savings from optimization would always be greater than the cost savings.

Kalogirou et al. (2008) attempted to optimize various aspects of the heat exchanger design located at the back of the PV. Using TRNSYS as the simulation program and Type 50d as the component for the PVT collector, they recommended that relative to aluminum or steel, copper was a better choice collector fins and tubes. They also found the optimum values of collector parameters, for example, 10 mm for the tube diameter, 8 cm for the tube spacing, and 0.2 mm for the fin thickness.

## **2.5 Optimization of Solar Combisystem**

Regarding to the solar combisystem optimization, Bales (2002) optimized the generic combisystem design alternative 11 from the IEA Task 26 for minimum cost and maximum fractional energy savings. They used TRNSYS models for system performance simulation and a Hooke-Jeeves algorithm for optimization. This optimization managed to increase fractional energy savings by 17% to 30% compared to the base case depending on the design parameter settings.

Calise *et al.* (2011) used a modified Hooke-Jeeves algorithm to minimize the payback period and annual cost of three different solar heating and cooling systems that were modelled in TRNSYS. This optimization was able to decrease the payback period from 28.3 to 25.2 years or from 21.5 to 14.8 years, depending on the system and subsidy assumed.

Bornatico *et al.* (2012) conducted an optimization study on solar combisystems for a mid-sized single-family house in Zurich, Switzerland. The optimal solution resulted in a

collector size of 14.5 m<sup>2</sup>, a tank volume of 498.98 L, and an auxiliary nominal power of 8.5 kW. The solar fraction of 21.8% was achieved for the optimal system design. A subsequent parameter sensitivity analysis showed that the collector size had the greatest impact on the solar fraction, energy use and the installation cost, while the tank volume had significant impact on solar fraction and installation but not energy use. The auxiliary heater size had relatively small impact on both energy use and installation cost. They used particle swarm optimization (PSO) and genetic algorithms for the optimization. When the implementation effort and the computational resources were considered, PSO was found to be a better choice for solving the problem.

Bornatico et al. (2012) optimized the sizes of the main components of a solar combisystem. They used Polysun software for the system simulation. The objective function was a weighted combination of solar fraction, energy use and cost. They used two different starting points and tested two different optimization algorithms, a particle swarm optimization algorithm and a genetic algorithm. Both algorithms resulted in similar optimal solutions.

Hin (2013) conducted an optimization of the system designed by Leckner. The base system designed by Leckner was optimized with respect to life cycle cost, life cycle energy and life cycle exergy. The optimized design was compared with the base system. The optimized system reduced the life cycle cost by 19%, the life cycle energy by 34 % and the life cycle exergy by 34%. Though the system had unreasonably high financial payback period due to the low cost of electricity and high cost of solar components, the solar combisystem was paid back energy wise within 7 years. In another study, Rey (2017) conducted a multi-objective optimization of the same system using life cycle cost and life

cycle energy. They developed a micro-time variant Multi-Objective Particle Swarm Optimization (MOPSO) algorithm to handle the large number of computations in multi-objective optimization. When this multi-objective framework was applied to the system in Montreal and Massachusetts, it was found that the algorithm was able to reduce the objective functions up to 45.1% and 64.3% respectively.

## **2.6 Solar Space Heating in Nepal**

As of 2009, of all installed solar combisystems, Asia had less than 1% (Weiss *et al.* 2013). No studies on solar combisystem in Nepal was found. However, recently, there was a few studies on space heating system either through solar air collectors or through solar thermal collectors. They are summarized below.

Timilsina *et al.* (2018) compared a variable refrigerant flow (VRF) system and a radiant floor heating system for a resort in Nepal. Heat gained from solar collectors were provided at 20° to the radiant floor system. Though the solar underfloor heating system costs three times more than the VRF system, the annual operating cost is twelve times less. If annual savings was considered as revenue, the solar underfloor heating system was financially feasible with a rate of return at 9.94 % and a payback period of 12.91 years. The levelized cost of energy from the solar system was found to be NRs.13.18 with subsidies and NRs. 27.47 without subsidies. The levelized cost of solar powered system for the case with subsidies was slightly more than the rate of electricity (NRs. 11.31). If the tariff rate was increased by more than 15 %, the solar system would be cheaper than the system powered with electricity. Major components of the underfloor system such as collectors, pumps, piping materials were quoted from the international market, which caused the high upfront cost. The large footprint of underfloor system compared to VRF,

the lack of attractive subsidies for solar heating system, and the low electricity tariff contributed to the economic infeasibility of solar floor heating systems.

Giri *et al.* (2013) conducted a research on heating a single room in the morning and night time during winter in Kathmandu, Nepal using solar air collectors with heat storage. The performance of the overall system was evaluated through ANSYS and Energy-Plus simulation software. ANSYS was used to investigate the collector performance by comparing the ambient temperature and the theoretical output with the simulation output. A pebble heat storage system and a conventional liquefied petroleum gas (LPG) system were compared with respect to the operating cost. The results revealed that the solar system with pebble heat storage saved NRs 40,500 energy cost per year for a single bed room in a residence in Kathmandu valley. The result showed that packed bed heat storage system with solar air collector was financially feasible with an internal rate of return 13% and a net present value of NRs 54,946. If the solar system was adopted for the whole house with dedicated place allocated for storage, the system would reduce the energy cost significantly for heating on the long-term basis.

## CHAPTER 3: CLIMATE OF NEPAL AND HOUSE PROTOTYPE DEVELOPMENT

### 3.1 Climate of Nepal

Nepal is located in South Asia, bordering China in the north and India in the other three directions. The country lies from 26° to 28° north latitude and from 80° to 88° east longitude. Though Nepal measures approximately 200 km from north to south, the rapid change of altitude leads to significant variations of the climate across the country. Considering that the average outdoor air temperature drops by 6° for every 1000 m rise in altitude, the country can be divided into three main regions according to the climate.

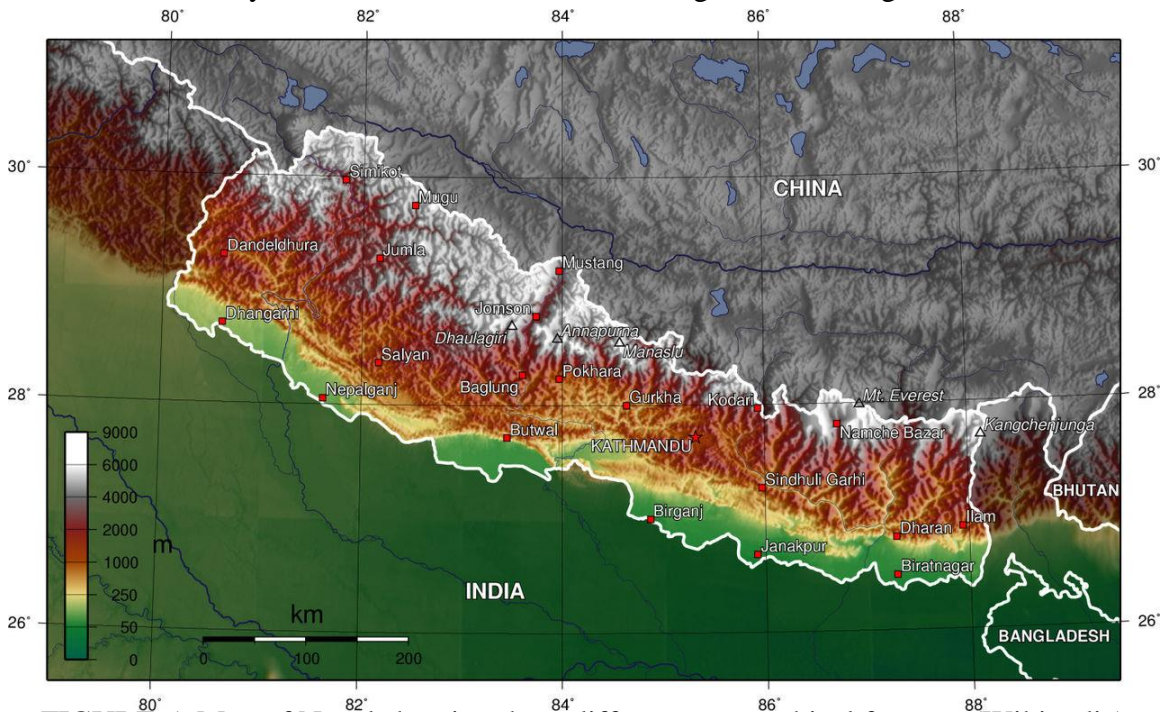


FIGURE 5: Map of Nepal showing three different geographical features (Wikipedia)

#### 3.1.1 Terai Region

The Terai region, with a width of about 26 km to 32 km on the south and an altitude of about 60 m to 305 m from mean sea level, occupies about 17% of the total land area of Nepal. The Terai region is marked as green on the Nepal map in FIGURE 5. In this region,

the summer temperature exceeds 37°C and even higher, while the winter temperature ranges from 8°C to 23°C. Although there are no severe cold weather conditions in winter, this region experiences the death of at least a dozen people every year due to cold waves as reported by (Pradhan *et al.* 2019). Biratnagar, Janakpur, Birganj, Butwal, Nepalganj and Dhangadi are the representative cities of this region. The optimal design of the solar combisystem and the house is performed in this region. However, the TRNSYS software, the simulation program used to evaluate the energy performance of the solar combisystem, does not have a weather file for any cities located in this region. Hence, the weather file for the city of New Delhi in India, which has similar climate as the Terai region, is selected for TRNSYS simulation. FIGURE 6 compares the temperature statistics of Birganj and New Delhi, which indicate their similar year-round temperature patterns.

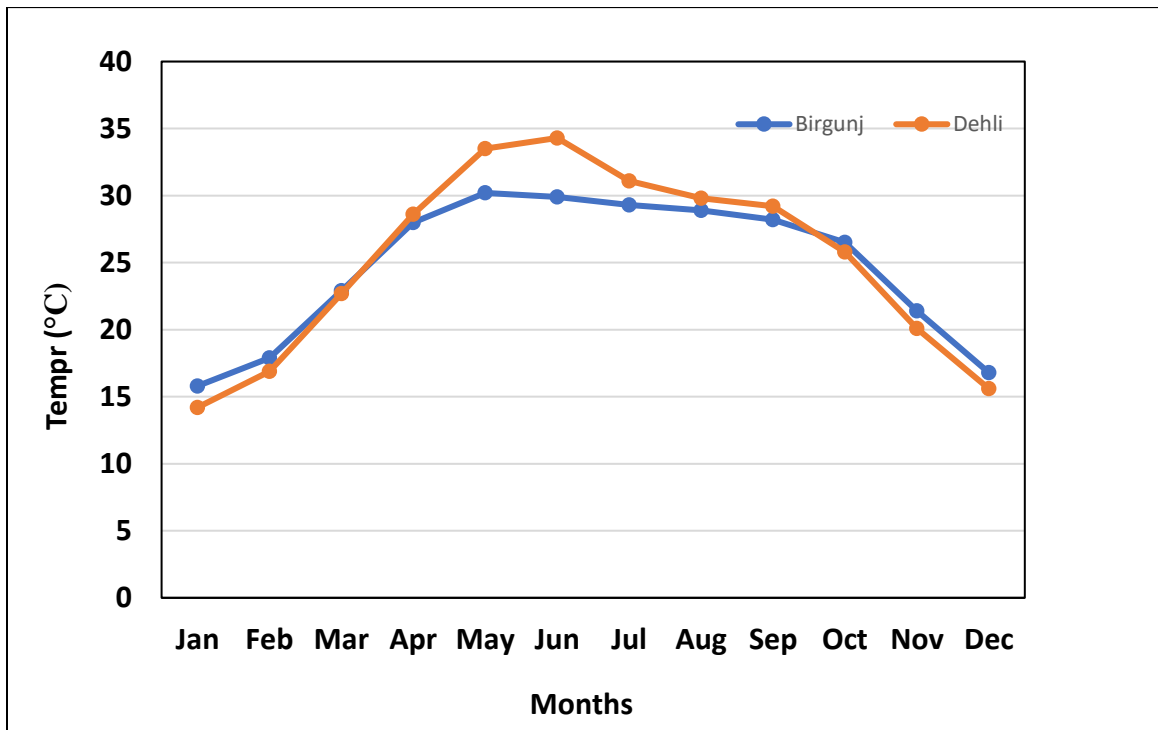


FIGURE 6: Climate comparison of southern city of Nepal with New-Delhi

### **3.1.2 Hilli Region**

The Hilli region lies in north of the Terai region. The Hilli region ranges from 305 m to 3000 m above the sea level (as presented in Nepal Tourism Board website) north - south and it is marked with brown color in FIGURE 5. Kathmandu, the capital of Nepal, lies in this region and it will be used as the representative location to analyze the climate zone. Kathmandu has an average temperature from 19°C to 30 °C in summer and from 2°C to 12°C in winter. The heating season for Kathmandu is from November to March (Giri 2013).

### **3.1.3 Himalayan Region**

The Himalayan region has an altitude of more than 3000 m above the sea level. Marked with white color in FIGURE 5, this region comprises mountains, alpine pastures and temperate forests. The climate of this region is characterized with a cool summer and a severe cold winter. Due to the severe cold winter weather conditions, the typical house construction defined for the other two regions cannot be used in the Himalayan region. Because there is a lack of data regarding typical house construction in the Himalayan region, this region is not used in this work for the optimal design of solar combisystems.

## **3.2 House Construction in Nepal**

This section explains the pattern of building construction in Nepal for past a few centuries and narrows down to why a particular house type has been chosen for this research study.

Typical Newari houses, which flourished during the Medieval era (1200-1769 AD), are mainly constructed from bricks. They usually have wit-pitched or pen roof with roof tiles, as shown in FIGURE 7. Balconies, windows and doors carved with woodwork

representing cultural values are the notable aspects of these buildings. During the Medieval era, this type of buildings was built by wonderfully skilled community of Newars. These buildings are still in existence after renovation with modern technologies (Sengupta and Upadhyaya 2016).

During the British colonization in India, the ruling Rana regime introduced the neo-classical, baroque or industrial style of buildings in Nepal. These buildings typically had hundreds of rooms and were built for the Royal members as shown in FIGURE 8. They are currently being utilized as various governmental organizations and ministries (Sengupta and Upadhyaya 2016).



FIGURE 7: Typical Newari house



FIGURE 8: Typical house during Rana regime



FIGURE 9: Typical rural house in Nepal



FIGURE 10: Modern housing in Kathmandu

Rural houses in Nepal are usually built from bricks, stone, timber and metal works as shown in FIGURE 9. They are less complicated because they use traditional materials

with local craftsmanship. The materials from a collapsed building can be easily salvaged and reused. Rural people still adopt this technology (Subedi 2010).

Modern Nepali houses are the direct influence of globalization and westernization in the country. Modern buildings were constructed sporadically when they were introduced in the mid-twentieth century. However, they gained momentum after the emergence of privately planned residential enclaves in the city due to the enactment of Apartment Act and the deregulation of housing finance in the year of 2000. More recently, apartment towers have been built across the city, adding a new dimension to residential modernity (Sengupta and Upadhyaya 2016). FIGURE 10 shows the eclectic mixture of modern-day homes in Kathmandu. After analyzing the various architecture and construction practices, (Sengupta and Upadhyaya 2016) termed Kathmandu as a city in transition. They explained the existing housing scenario of Kathmandu within the blurred lines of tradition and modernity. The modern buildings are constructed with a diversity of materials such as reinforced concrete, glasses, marble stones, and steel (Subedi 2010). In addition, architectural elements originated from Europe, such as triangular pediments and French windows, are frequently adopted in modern buildings. Though Nepal is one of the developing countries in South Asia, Kathmandu exhibits real estate values similar to a second-tier city in United Kingdom or Australia. A typical new house costs from NRs. 10 million to NRs. 25 million (roughly \$0.1 to \$0.25 million) (Sengupta and Upadhyaya 2016). Modern buildings are becoming popular because people realized that they are more robust than traditional buildings after the recent devastating earthquake in 2015, which flattened over 600,000 buildings and killed over 8,000 people.

The National Building Code established in 1994 classifies buildings into four categories: Class A for state of art buildings, Class B for professionally engineered buildings, Class C for buildings with floor area less than 1,000sq ft and structural span less than 4.5m, and Class D for low-strength masonry buildings. The code requirements vary with building classes. Engineers, architects and mid-level technicians are responsible for the design and construction of buildings belonging to Classes A, B and C. For Class-D buildings, it is the responsibility of house owners to comply with the building code. In addition to the national building code, there are a set of building by-laws enacted by local municipalities. These by-laws do not cover building structural safety but include appropriate urban planning measures such as the right-of-way of adjacent roads, ground coverage and other requirements (e.g., height restrictions and open spaces). In rural areas, there are no building by-laws. However, traditional communities have certain community rules and practices for the location and construction of (Subedi 2010).

Currently, the National Building Code regulates the design and construction for structural integrity and safety but not energy performance. There is no national code in Nepal that specifies the minimum energy performance requirement and thermal comfort of occupants.

The house prototype developed in this study is a typical Nepali modern Class B house, which means that the house design and construction is performed by professionals. The house has a two and half stories with a total floor area of 232 m<sup>2</sup>, which is representative of single-family houses for most of the region in Terai and Hilli belt of Nepal.

For most residential buildings, regardless of whether they are professionally engineered or built with local craftsmanship, the construction material and technology are very similar. Generally, the building is built with full brick wall (230 mm) for external walls and half brick wall (110 mm) for internal walls, with 10 to 12 mm plaster on both interior and exterior sides or only on the interior side. The roof is 100 mm reinforced concrete slab with 12 to 15 mm cement plaster on the interior side. False ceiling is not used. No thermal insulation is used in building envelope. It is assumed that windows have single-pane glazing with wooden frame because double-pane glazing is not a common practice (Subedi 2010). TABLE 1 summarizes the envelope construction for the house prototype in Kathmandu. The detailed construction of the house is placed in Appendix A.

TABLE 1: Envelope of Typical Modern Construction in Nepal

<b>EXTERNAL WALL CONSTRUCTION</b>				
<b>Type</b>	<b>Thickness(mm)</b>	<b>Density(kg/m<sup>3</sup>)</b>	<b>Conductivity (W/(m-K))</b>	<b>Capacity (kJ/(kg-K))</b>
Cement Plaster	12	1860	0.72	0.84
Brick Wall	230	2400	1.34	0.1
Cement Plaster	12	1860	0.72	0.84
<b>GROUND FLOOR CONSTRUCTION</b>				
<b>Type</b>	<b>Thickness(mm)</b>	<b>Density(kg/m<sup>3</sup>)</b>	<b>Conductivity (W/(m-K))</b>	<b>Capacity (kJ/(kg-K))</b>
Cement Plaster	12	1860	0.72	0.84
Concrete	100	1950	1.64	0.1
<b>ROOF CONSTRUCTION</b>				
<b>Type</b>	<b>Thickness(mm)</b>	<b>Density(kg/m<sup>3</sup>)</b>	<b>Conductivity(W/(m-K))</b>	<b>Capacity (kJ/(kg-K))</b>
Cement Plaster	12	1860	0.72	0.84
Concrete Slab	100	1950	1.64	0.1

Sources of data: the material layer thickness is from (Subedi 2010) and all others are from (ASHRAE 2007).

## CHAPTER 4: SYSTEM DESCRIPTION AND MODELING IN TRNSYS

### 4.1 Combisystem Design and Description

Recall that a solar combisystem refers to a system that uses solar as the main source of energy for both space heating and domestic hot water generation. Since the availability of solar energy is intermittent and the magnitude of solar energy depends on weather conditions, it is not realistic to expect solar energy as the solely source in many locations. Therefore, an auxiliary heating mechanism is needed to satisfy the heating load during unfavorable weather conditions. Theoretically, the auxiliary heating source can be electricity, natural gas, or other fuel types. Electricity is selected as the auxiliary source of heating in this work because the suffice of electricity infrastructure with hydropower as the main source of electricity in Nepal.

There is no standardized configuration for solar combisystems. A combisystem that works for one situation may not necessarily work for other situations. Designers, engineers and installers vary the solar combisystem configuration, component sizing, and controls according to their specific needs (Hin 2013). FIGURE 11 shows the schematic of the solar combisystem used for this thesis. Irrespective of the energy sources for auxiliary heating and the component sizes, a solar combisystem consists of three loops: the solar collector loop, the domestic hot water loop, and the space heating loop, which are described next.

The main function of solar collector loop is to collect heat energy from sun during day. The major components in the solar collector loop include solar collectors, a storage tank, and a circulating pump as shown in FIGURE 11. Because of the use of a pump, this system is referred as an active system. Instead of using pure water as the heat transfer fluid, propylene glycol and water mixture in the ratio of 3:2 is used to prevent liquid freezing in

winter. An internal heat exchanger at the bottom of the storage tank transfers heat from the liquid circulated from the solar collectors to the tank water outside of the heat exchanger. In the solar loop, the pump is on and circulates the fluid when the outlet temperature of the solar collectors is greater than the tank water temperature by more than 10°C. Once the pump is on, it keeps running until the sensed temperature difference falls below 2°C. The pump will shut off irrespective of any pre-conditions., if the temperature inside the tank reaches 90°C to protect the system.

The DHW loop provides domestic hot water at the desired temperature. The DHW tank has an electric heater to maintain the tank water temperature at its thermostat setpoint. A mixing valve is used to mix the hot water from the DHW tank and the cold water from the city mains or a water reservoir in the house for appropriate delivery water temperature. Whenever hot water is consumed, the same amount of cold water must be supplied to the DHW tank. This makeup cold water goes through the storage tank first to be preheated as shown in FIGURE 11.

The space heating loop consists of the storage tank, a circulation pump, an electric instantaneous water heater, and radiant floors as shown in FIGURE 11. When the space temperature falls below the thermostat set point, the pump is on and it supplies water to the building. The instantaneous heater is on during the heating season only which has been defined as different time for the different locations used. At other times of year, the heating system is turned off to avoid the risk of house overheating.

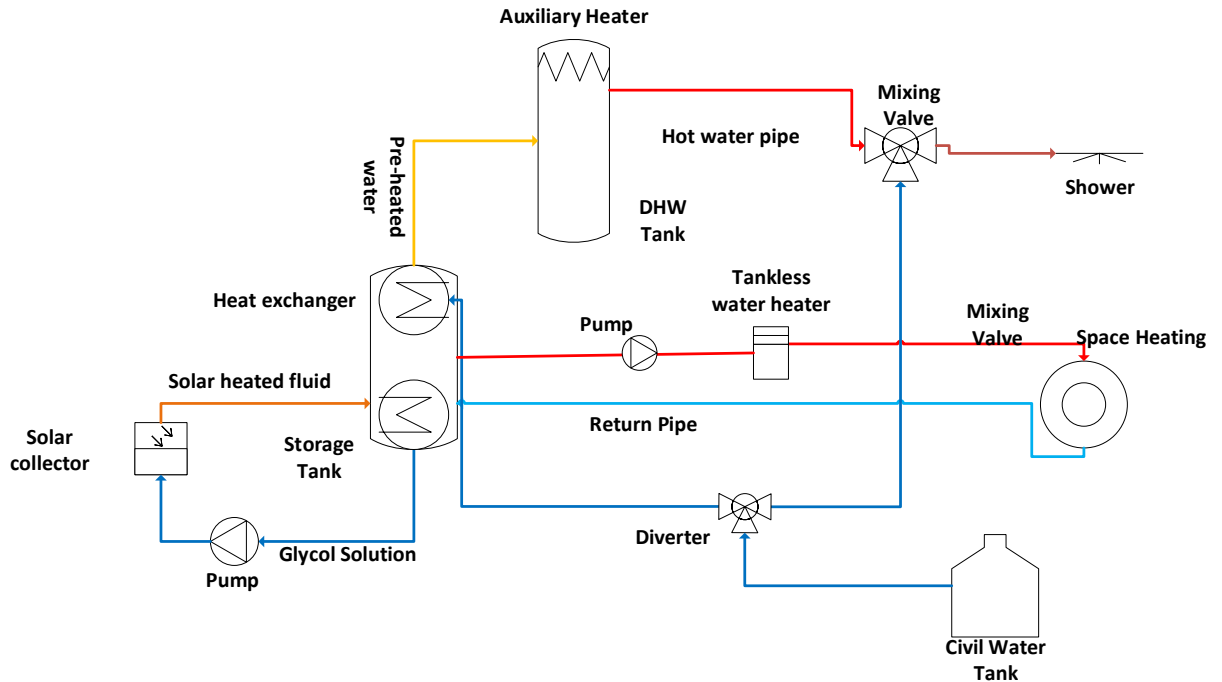


FIGURE 11: Schematic of the solar combisystem

## 4.2 Modeling in TRNSYS

TRNSYS software (Klein *et al.* 2018) is used to model the solar combisystem. TRNSYS stands for TRaNsient SYstem Simulation program. It is a versatile, component-based, and extensible energy simulation tool that can be used for simulation of simple systems as well as complete energy simulation of multi-zone buildings. The software was originally developed by the University of Wisconsin's Solar Energy Laboratory (SEL) and has been commercially available since 1975. Since then this tool has been under continuous development; currently the joint team includes the Centre Scientifique et Technique du Batiment (CSTB) in France, Transsolar Energietechnik GmbH in Germany, and Thermal Energy Systems Specialists (TESS) in Madison, Wisconsin, along with the Solar Energy lab at the University of Wisconsin (Patil 2010).

### 4.2.1 Solar Collector Loop

Solar collector loop is modeled as shown in FIGURE 12.

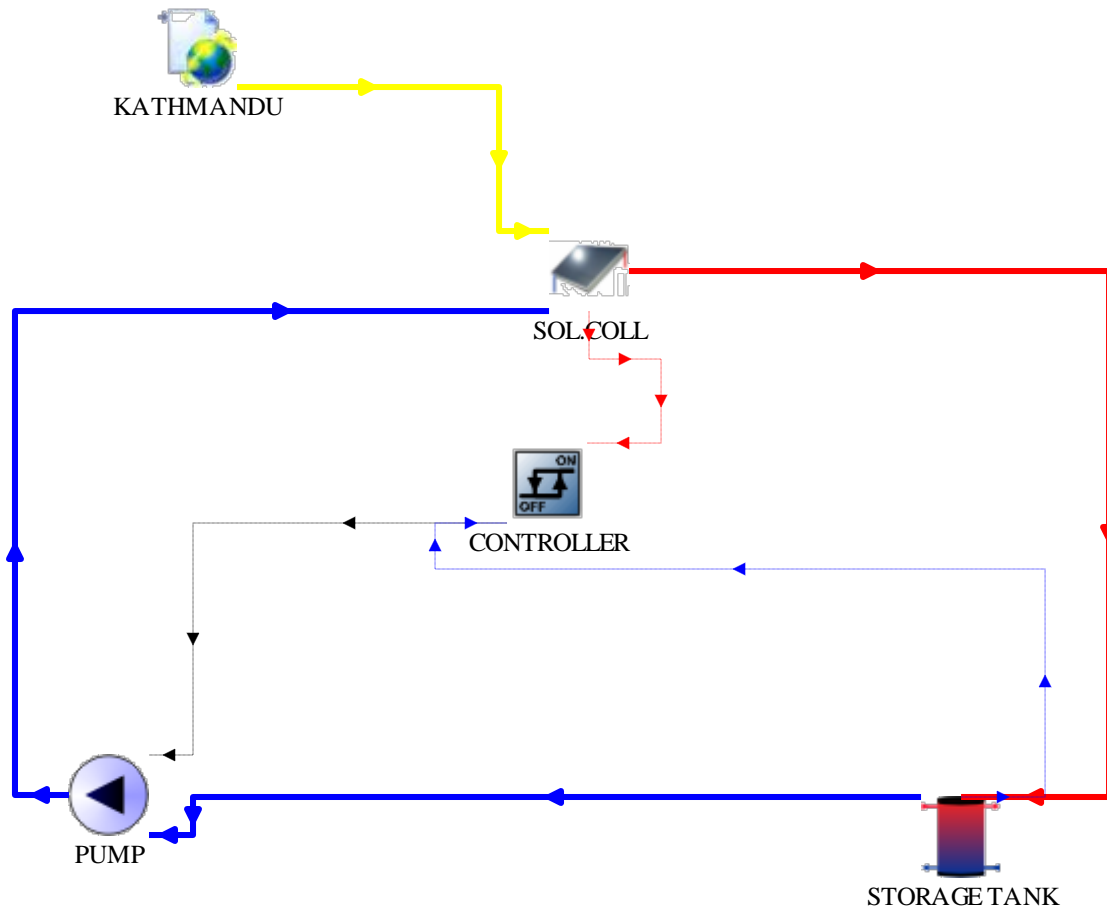


FIGURE 12: Modeling of solar collector loop in TRNSYS

#### 4.2.1.1 Weather Data Reader- Type 15

This component reads data at a regular time interval from an external weather data file, interpolates the data (including solar radiation for tilted surfaces) at sub-hourly time steps, and make the data available to other TRNSYS components, such as Type 56 for buildings and Type 1 for solar collectors. Type 15 model also calculates several useful weather-related variables, including the mains water temperature, effective sky temperature etc.

#### 4.2.1.2 Solar Collector -Type 1b

Solar collector is a key component of the solar combisystem. The Solar Flame FMAX collector with a gross area of 2 m<sup>2</sup> per module is used in this work. A total collector area of 20 m<sup>2</sup> is assumed for the initial design.

In TRNSYS, Type 1b models the thermal performance of flat-plate solar collectors using a standard quadratic efficiency equation. The quadratic equation correlates the collector's thermal efficiency with the ratio of temperature difference to solar radiation ( $\Delta T/I_T$ ), where the temperature difference refers to the difference between the fluid inlet temperature and the ambient temperature. Type 1b provides the flexibility of connecting collectors in series, in parallel or both. The overall thermal performance of the collector array is determined by the number of modules in series and the characteristics of each module.

A general equation for solar thermal collector efficiency can be obtained from the Hottel-Whillier equation:

$$\eta = \frac{Q_u}{A I_T} = \frac{m C_{pf} (T_o - T_i)}{A I_T} = F_r (\tau \alpha)_n - F_R U_L \frac{(T_i - T_a)}{I_T} \dots \dots \dots 1$$

Where,

$\eta$  = Thermal efficiency of the collector

$Q_u$  = Heat collected from the collector

$A$  = Total collector area or gross area

$I_T$  = Global radiation incident on the solar collector (Tilted surface)

$m$  = mass flow rate at use conditions

$C_{pf}$  = Specific heat of collector fluid

$T_o$  = Outlet temperature from the collector

$T_i$  = Inlet temperature of fluid to collector

$T_a$  = Ambient (air) temperature

$F_R$  = Overall collector heat removal efficiency factor

$(\Gamma\alpha)_n$  = Transmittance absorptance product

$U_L$  = Loss coefficient

Because the thermal loss coefficient  $U_L$  varies with respect to temperature, a better expression is obtained by taking into account a linear dependency of  $U_L$  versus  $(T_i - T_a)$ .

$$\eta = \frac{Qu}{AI_T} = F_r(\tau\alpha)_n - F_R U_L \frac{(T_i - T_a)}{I_T} - F_R U_L \frac{(T_i - T_a)^2}{\bar{t} I_T} \dots \dots \dots 2$$

where,

$U_L/T$  = Loss coefficient with reference to difference in temperature

The equation above can be rewritten as.

$$\eta = a_0 - a_1 \frac{(\Delta T)}{I_T} - a_2 \frac{(\Delta T)^2}{I_T} \dots \dots \dots 3$$

where,

$a_0$  = Intercept (maximum) of the collector efficiency

$a_1$  = Negative of the first-order coefficient in collector efficiency equation/ Slope of the efficiency curve

$a_2$  = Negative of the second-order coefficient in collector efficiency equation/ Curvature of the efficiency curve

This is the general solar collector thermal efficiency equation used in Type 1. The thermal efficiency is defined by three coefficients:  $a_0$ ,  $a_1$  and  $a_2$ . The coefficients required for the quadratic efficiency equation can be obtained from standard collector performance tests. The coefficient values are from (Banister and Collins 2015) and they are listed in TABLE 2.

TRNSYS Type1 offers a total of 5 options to consider the impact of “off -normal solar incidence”. For Type1b, a second order quadratic function is used to compute the incidence angle modifier (IAM):

$$\frac{(\Gamma\alpha)_b}{(\Gamma\alpha)_n} = 1 - b_0 \left( \frac{1}{\cos\theta} - 1 \right) - b_1 \left( \frac{1}{\cos\theta} - 1 \right)^2 \dots \dots \dots .4$$

Where,

$b_0$  = Negative of the second-order coefficient in collector efficiency equation

$b_1$  = Negative of the 2nd-order coefficient in the IAM curve fit equation

TABLE 2 summarizes the parameter settings for Type 1b used in this work.

TABLE 2: Type 1b parameter settings

Particulars	Value	Units	Source
Number in series	1	-	-
Collector area	AREA	string	-
Fluid specific heat	3.370	kJ/kg-K	(Leckner 2008)
Tested flow rate	71.21	kg/hr-m <sup>2</sup>	(Banister and Collins 2015)
Intercept efficiency	0.769	-	”
Efficiency slope	13.0104	kg/hr-m <sup>2</sup>	”
Efficiency curvature	0.04889	kg/hr-m <sup>2</sup>	”
Optical mode 2	2	-	”
1st-order IAM	0.32	-	”
2nd-order IAM	0.0	-	”

Apart from the parameters of the collector, reflectance and collector slope are important properties to be provided as input to inside the component. The reflectance is the

property of the surface above which the solar collector is positioned and is defined by the ratio of reflected radiation to total incident radiation and therefore must be between 0 and 1. Typical values are 0.2 for ground not covered by snow and 0.7 for snow-covered ground. The collector slope which is an input from the weather file of the location used, is also considered as the optimization variable.

#### **4.2.1.3 Storage Tank-Type 534**

The storage tank uses water for sensible heat storage. In the proposed solar combisystem, the storage tank plays the following roles: 1) acting as the thermal storage for the energy collected from solar collectors; 2) preheating the makeup water supplied to the domestic hot water tank; and 3) supplying hot water to the building for space heating.

The storage tank has a height of 1.5m and has a volume of 1000 liters for the initial design. This tank volume deemed appropriate for the initial collector area (20 m<sup>2</sup>) based on the simulation trial runs. The storage tank volume will be treated as variable to be optimized. The tank has two immersed coils. One coil is assigned for exchanging heat between the tank water and the glycol circulated from the solar collectors and the other coil is assigned to preheat the makeup water supplied from the city mains to the DHW tank.

The storage tank is modeled with TRNSYS Type 534. The model captures the heat transfer through the immersed heat exchangers and the parasitic heat losses to the surroundings through the tank surface. The tank heat loss coefficient is assumed to be 1.181 kJ/ (hr-m<sup>2</sup>-K) from (Leckner 2008). Since no gas burner is used, the flue loss coefficient is set to 0. The resolution of temperature stratification modeling is governed by the number of nodes, representing the number of equally divided tank water volume. Each node interacts thermally with the nodes above and below through thermal conduction and fluid

movement (either forced movement from inlet flow streams or natural destratification mixing due to temperature inversions in the tank). Type 534 supports up to 20 nodes. Increasing the number of nodes leads to a high resolution of temperature stratification but also slows down the simulation time. In this work, the tank is divided into five isothermal temperature nodes to model the tank water stratification.

Both coils are divided into 5 nodes along the flow direction. The heat exchanger nodes and their locations relative to the tank nodes are illustrated in FIGURE 13. To be favorable for the heat exchange and the system performance, the collector coil is placed at the bottom with glycol liquids from the solar collector entering the coil at tank Node 4 and leaving the coil at Node 5. The pre-heat coil is placed at the top of the storage tank with the makeup water entering the coil at tank Node 2 and leaving the coil at tank Node 1. The tank has one pair of ports for space heating. Water leaves the tank for space heating at the topmost node (Node 1) and returns back to the tank at the bottommost node (Node 5). Temperature inversion is the phenomenon when a node has a higher water temperature than the node above. To avoid temperature inversion, a negative value-(e.g., -100 kg/hr can be used for the parameter of inversion mixing flow rate. When the inversed temperature occurs at the end of a time step, the water between the involved nodes are mixed instantaneously in an adiabatic manner. The detailed construction of this tank is presented in Appendix B.

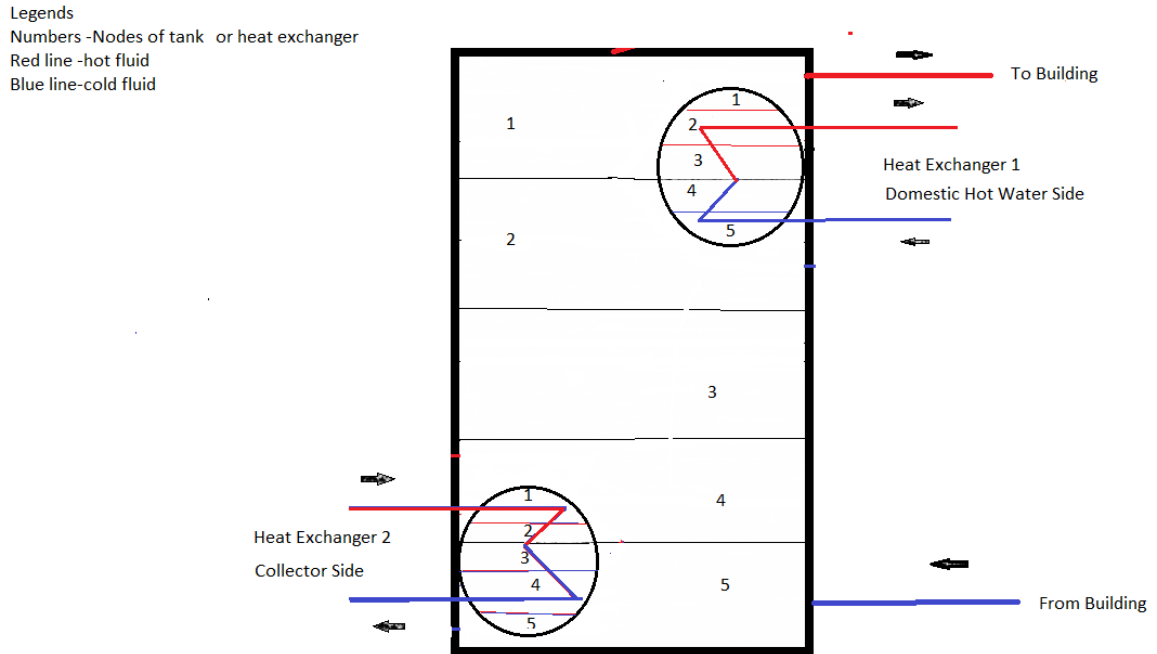


FIGURE 13: Schematic of storage tank

#### 4.2.1.4 Pump-Type 114

The solar collector pump drives the flow of glycol liquid through the solar collector loop. GRUNDFOS Alpha 2 pump is used and it has a rated power between 5 W and 45 W depending upon the pump speed (derived from TAS Pvt. Ltd. Nepal as of Nov. 18, 2018). The 45 W pump is used for the initial design.

Type 114 models a constant-speed pump that can maintain a constant mass flow rate. The flow rate of the pump is treated as a variable to be optimized. Transient characteristics (e.g., the impact on power and pressure) are not modeled during pump starting and stopping.

#### 4.2.1.5 Controller-Type 165 d

Type 165d controller is used to operate the pump conditionally by generating a control function  $\gamma_0$  that can have a binary value of 0 or 1. The value of  $\gamma_0$  is a function of 1) the temperature difference between two sensed points ( $T_H$  and  $T_L$ ); 2) the two dead band temperature differences ( $\Delta T_H$  and  $\Delta T_L$ ); and 3) the control signal at the previous time step

FIGURE 14 illustrates the operation of the controller. If the control signal in the previous time step is 0, it will turn to 1 in the current step only if the condition  $T_H - T_L > \Delta T_H$  satisfies. Once the control signal becomes 1 in the current step, it will continuously keep at the value of 1 until the condition  $T_H - T_L < \Delta T_L$  satisfies. For the solar collector loop control in this work,  $T_H$  and  $T_L$  refer to the collector outlet temperature and inlet temperature respectively. The dead bands are set to 10°C for  $\Delta T_H$  and 2°C for  $\Delta T_L$ . For safety protection, the pump will be turned off irrespective of the above conditions if the tank water temperature of the topmost node reaches the high limit of 90°C.

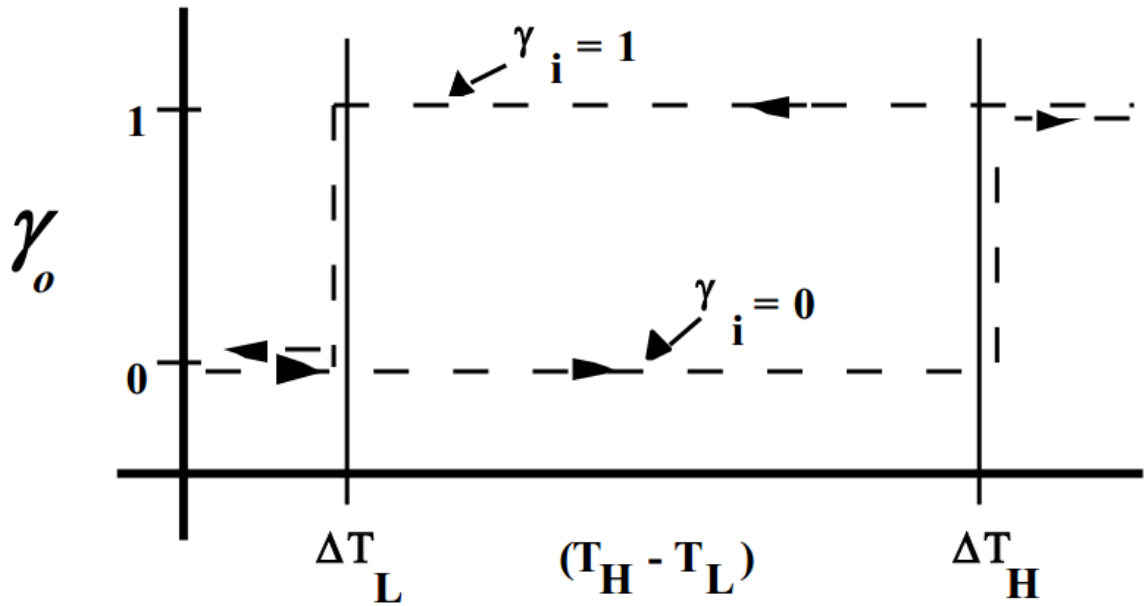


FIGURE 14: Operation of controller type 165d

## 4.2.2 DHW Loop of the Combisystem

All components of the DHW loop modeling as shown in FIGURE 15 are described in detail in following section.

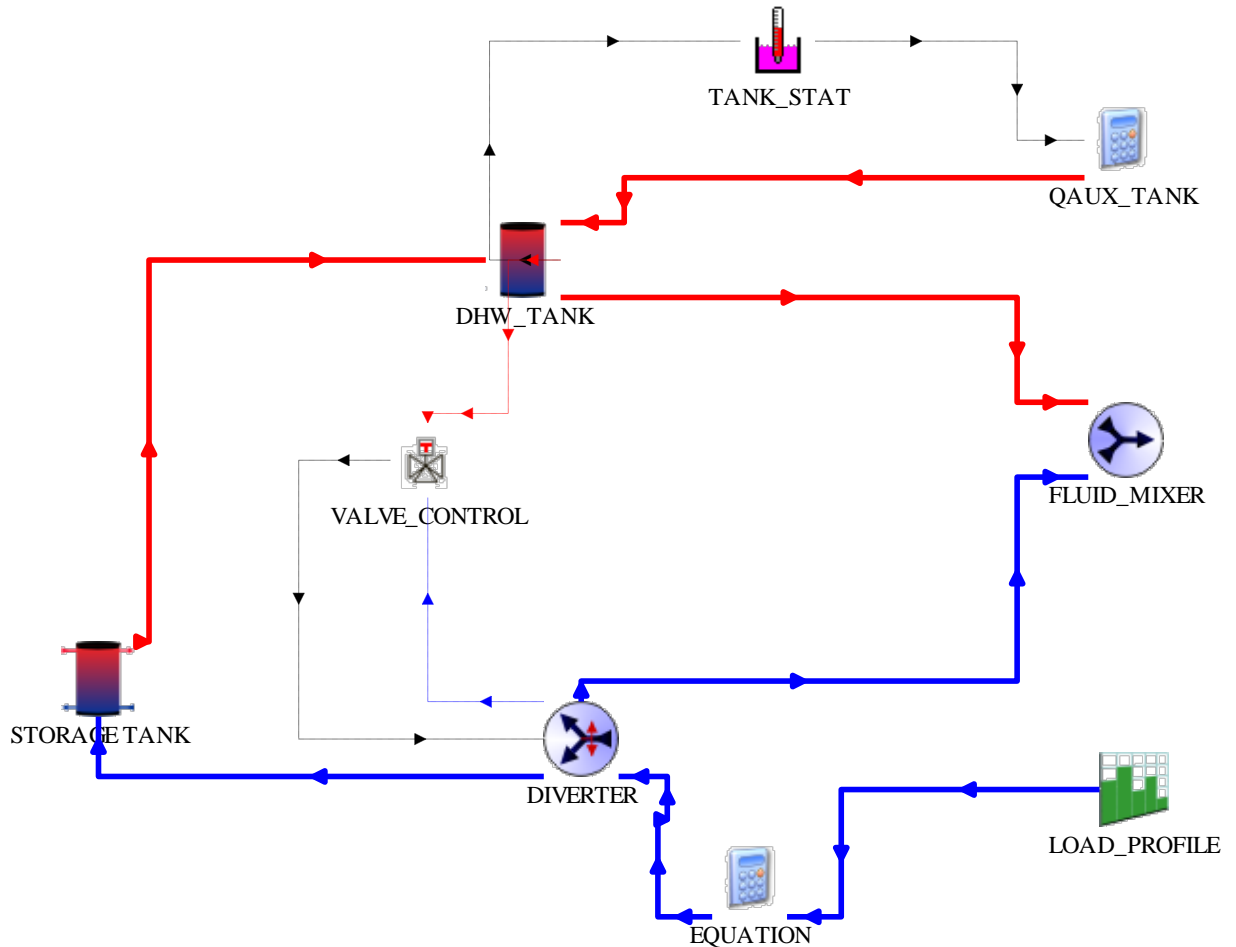


FIGURE 15: DHW loop of the combisystem

### 4.2.2.1 Load Profile – Type 14 h

The DHW load profile refers to the typical amount hot water consumption across a whole day. Many DHW profiles were reviewed by (Fairy and Parker 2004). The hourly profile from ASHRAE 90.2 was used by many studies and it approximates the actual hot water consumption more closely than other profiles. Therefore, the DHW profile from ASHRAE 90.2 is employed in this work and it is depicted in FIGURE 16. In TRNSYS, the

DHW profile is defined using the forcing function, Type 14, with its graphical plug-in. The graphical plug-in is an external executable program that allows the definition of DHW profile via a graphical user interface. Based on the defined DHW profile, Type 14 transfers the instantaneous/ average values to its downstream component, which is the diverter in this solar combisystem.

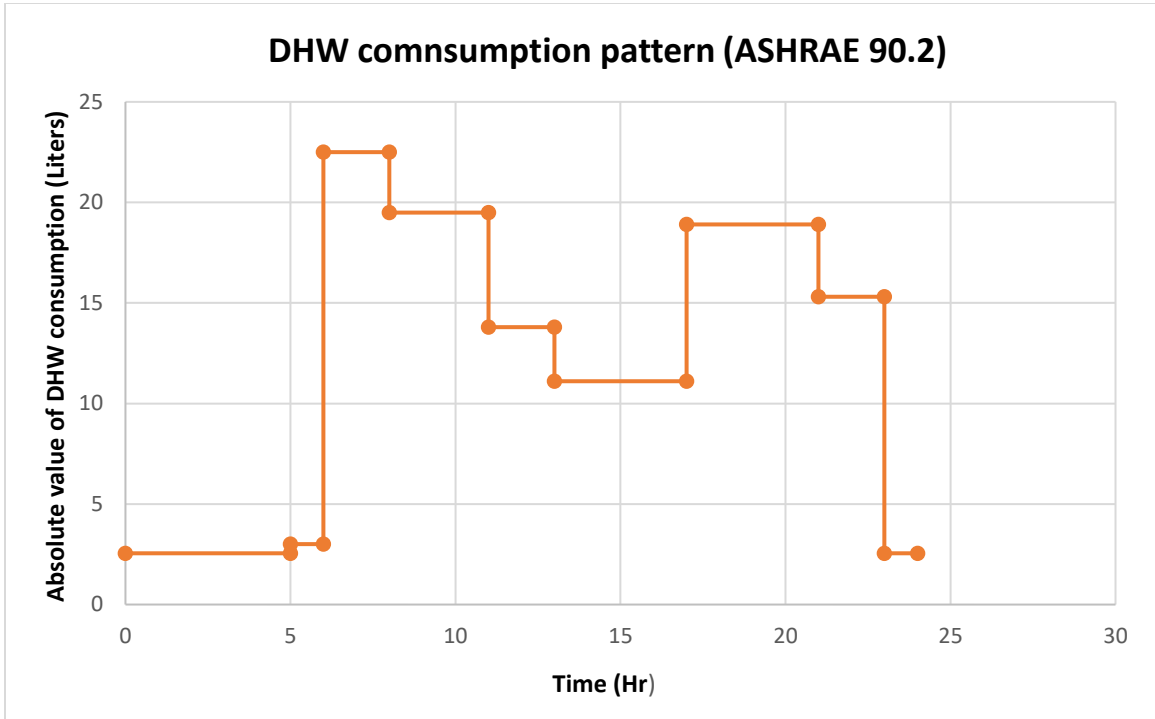


FIGURE 16: Hourly representation of DHW consumption profile

#### 4.2.2.2 Equation Tab

As shown in Equation 1, the equation tab calculates the DHW consumption in kg/hr by multiplying the average value of DHW load profile over a given timestep with daily hot water consumption.

$$mDHW = DHW_{Profile} * 300 \dots \dots \dots 4$$

where,

$mDHW$  = mass flow rate of water (kg/hr) drawn at a given time

$DHW\_Profile$  = DHW consumption defined inside Type 14 in fraction of total consumption

#### **4.2.2.3 Diverter- 11f**

The diverter is simulated by Type 11f in TRNSYS. The temperature of the city water varies throughout the year and it is supplied from the weather file to the diverter. The purpose of the diverter is to divide the total mass of fluid into two outlets: one for the storage tank and another for the mixing valve. In this regard, valve control comes to play as discussed next.

#### **4.2.2.4 Valve control – Type 115**

Valve control is modeled by Type 115 and it helps the diverter to take intelligent decision based on the temperature differential. The valve control receives two temperature inputs: one from the DHW tank outlet and another from the city water tank. After assessing the temperature of each input, the valve control gives command (in the form of control signal) to the diverter to release an appropriate quantity of fluid to each outlet.

#### **4.2.2.5 Storage Tank – Type 534**

This tank was explained earlier.

#### **4.2.2.6 DHW tank –Type 158**

Commercial installers of solar thermal systems recommend that the DHW tank be sized at 80 gallons (300 Liters) for a household with 5 people. Therefore, an 80-gallon tank with 1 kW electric heater is used as the initial design.

TRNSYS Type 158 is used to model the DHW tank. TABLE 3 lists the DHW tank parameter settings. The DHW tank volume is a variable to be optimized. The thermostat is located at the three-fourth of the tank height. If the sensed water temperature is below 60°C,

the auxiliary electric heater is activated. The purpose of maintaining tank water temperature more than 60°C is to avoid the growth of Legionella bacteria (Weiss 2003). Similar to the storage tank, a total of 5 nodes are defined with Node 1 being the highest one and Node 5 being the lowest one. The height, top, edge and bottom heat losses are taken from (Leckner 2008). The makeup water inlet is located at the tank bottom and the hot water outlet is at the top.

TABLE 3: Parameters of DHW tank

Parameters	Value	Unit	Source
Tank volume	DHW_VOL	variable name	
Tank height	1.5	m	(Leckner 2008)
Number of tank nodes	5	-	
Top loss coefficient	1.181	KJ/hr-m <sup>2</sup> -K	(Leckner 2008)
Edge loss coefficient	1.181	KJ/hr-m <sup>2</sup> -K	(Leckner 2008)
Bottom loss coefficient	1.181	KJ/hr-m <sup>2</sup> -K	(Leckner 2008)
Fluid specific heat	4.19	kJ/kg-K	
Fluid density	1000	kg/m <sup>3</sup>	
Fluid thermal conductivity	2.14	kJ/hr-m-K	
Height fraction of inlet 1	0	Fraction	
Height fraction of outlet 1	1.0	Fraction	
Height fraction of inlet 2	0.	Fraction	
Height fraction of outlet 2	1.	Fraction	
Number of thermostats	1	-	
Height fraction of thermostat	0.75	Fraction	
Number of auxiliary heat inputs	1	-	
Height fraction of auxiliary input	0.75	Fraction	

#### 4.2.2.7 Tank Stat- Type 106

TRNSYS Type 106 represents the tank thermostat. The thermostat controls the auxiliary heater status based on the set point and the temperature of water nearby the thermostat. The thermostat has a set point of 60°C with a dead band of 4°C. This means that the electrical heater is turned on when the sensed water reaches 58°C and is deactivated after the sensed water temperature reaches 62°C.

Type 106 sends the applicable control signal to the DHW tank heater. Based on the control signal, the heater is simulated as the following equation shows:

$$Q_{\text{aux}} = (D_P) * y_{\text{tank stat}} \dots \dots \dots 5$$

Where,

$D_P$  = Power of auxiliary heater inside the DHW tank in kJ/hr

$y_{\text{tank stat}}$  = Control signal in the form of either 0 or 1 from Type 106

#### **4.2.2.8 Mixing Valve-Type 11h**

TRNSYS Type 11h simulates the mixing valve. It reads the upstream water flow rates and temperatures and mixes the upstream of water appropriately to deliver the water at 45°C. This delivery water temperature complies with the practice and the recommendation by IEA Task 26.

### 4.2.3 Space Heating Loop

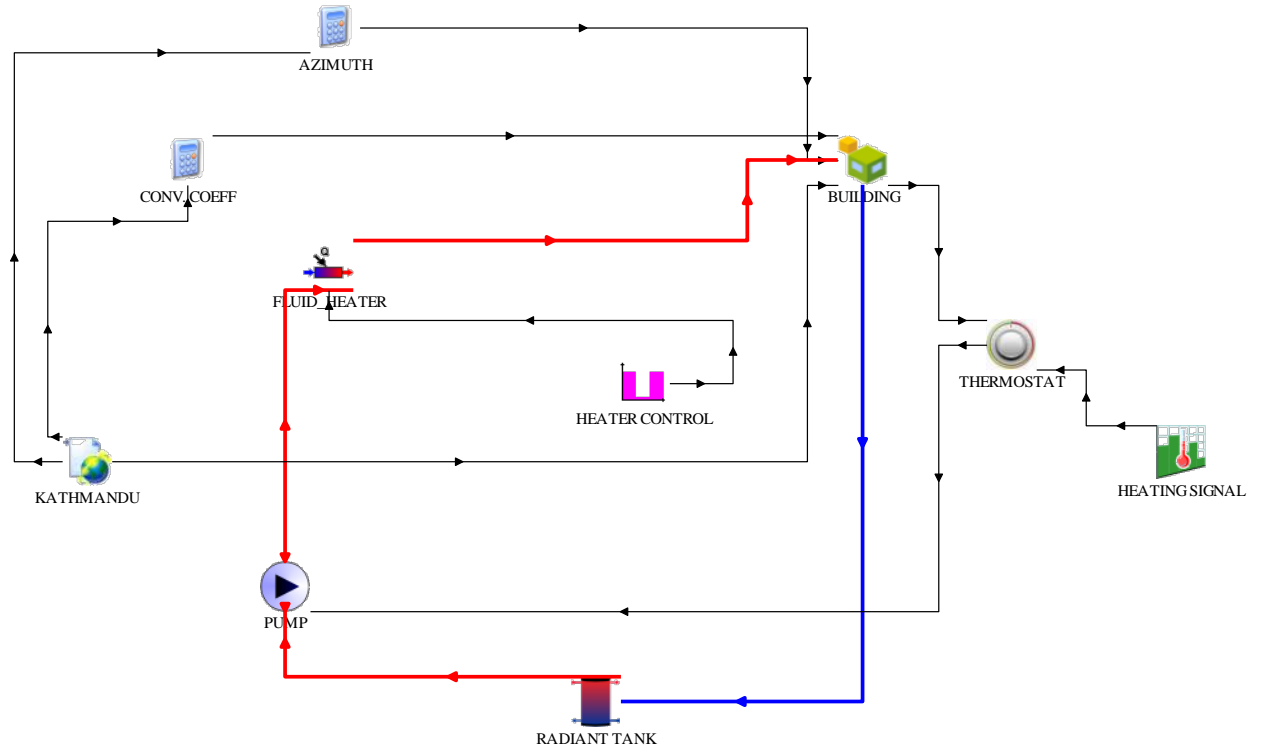


FIGURE 17: Modeling of space heating in TRNSYS

The space heating loop consists of the storage tank, a circulation pump, an electric instantaneous water heater, and radiant floors as shown in FIGURE 17. When the space temperature falls below the thermostat set point, the pump is on and it supplies water to the building. The instantaneous heater is available during the heating season only. During the no-heating seasons, the heating system is always off to avoid the risk of house overheating. All TRNSYS types used to model the space heating loop are described below.

#### 4.2.3.1 Storage Tank – Type 534

This TRNSYS type and its parameter setting were described earlier.

#### **4.2.3.2 Pump –Type 114**

GRUNDFOS Alpha 2 pump is used here and it has a rated power between 5-45 W depending upon the speed of the pump (Derived from TAS Pvt. Ltd. Nepal as of Nov. 18, 2018). The 45 W pump is used for the initial design.

Type 114 is used to model the recirculating pump with a rated flow rate of 800 kg/hr for the initial design. This initial setting was decided from a number of parametric simulations run by observing the impact of flow rate on the number of hours with space temperature not meeting the thermostat setpoint. Through the parametric simulation runs, it was found that setting a reasonable water flow rate for the space heating loop is not straightforward. A large flow rate requires a large capacity of the instantaneous heater, which may be not available on the market. On the other hand, a small water flowrate may not be sufficient to address the space heating load.

#### **4.2.3.3 Thermostat – Type 166**

TRNSYS Type 166 thermostat controls the space temperature. Because of the use of radiant floor heating, the thermostat control is based on the operative temperature. Depending on the sensed space operative temperature and the thermostat setpoint, the thermostat sends a control signal to turn on/off the space heating loop pump. In this work, the space thermostat set point temperature is set at 21°C from 7 am to 10 pm and at 18°C from 10 pm to 7 am. A deadband of 4°C is applied. This means that the pump will be turned on when the space operative temperature falls below 19°C from 7 am to 10 pm and 16°C from 10 pm to 7 am. Similarly, the pump will be turned off when the space operative temperature exceeds 23°C from 7 am to 10 pm and 20°C from 10 pm to 7 am.

#### **4.2.3.4 Instantaneous Water Heater- Fluid Heater Type 138**

The instantaneous (tankless) water heater plays the role of heating up the water temperature to 50°C for space heating when the inlet water temperature from the storage tank is less than 50°C. Since the auxiliary heat must be added instantaneously, it has a high-power rating. The maximum available market size for tankless water heater is 36 kW. For the initial design, the sizes of tankless water heaters vary with locations.

The instantaneous water heater operating status is subject to the control of Type 14k, shown in FIGURE 17 as “Heater control”. Type 14 stores the instantaneous water heater availability schedule. If the schedule is indicated as unavailable (i.e., during the non-heating season), the instantaneous is never turned on.

#### **4.2.3.5 Multi-zone Building-Type 56**

TRNSYS Type 56 is used to model the house. This component models the thermal behavior of a building divided into different thermal zones. In order to use this component, a separate pre-processing program was executed. The TRNBuild program reads in and processes a file containing the building description and generates two files viz. (. Bui) and (. b18). These two files are then used by Type 56 component during TRNSYS simulation.

There are two methods to model HVAC (heating, ventilation and air conditioning) systems in TRNSYS. The two methods correspond respectively to the "energy rate" and "temperature level" control. With the "energy rate" control, a simplified HVAC model is embedded within Type 56. Detailed HVAC models can be established only by the "temperature level" approach. In this case, separate HVAC components need to be created and modeled together. Type 56 simulation outputs can be used as the inputs to HVAC equipment models, which in turn produce heating and cooling inputs to Type 56. The

“temperature level” approach is employed in this work because the solar combisystem is used to supply hot water to address the space heating need.

To create a house model with TRNSYS Type 56, a three-dimensional (3D) geometry of the house needs to be modeled in Google Sketch up along with the windows. TRNSYS 3D plugin provides the necessary interface between TRNSYS and sketch up to build the basic geometry of the building. Building envelope information on window types, wall and roof types, wall and roof materials are defined in the library. Then, after defining the thermal zones, the desired inputs and outputs are selected for plotting later during the simulation.

### **Zone Definition**

The modeled house is based on a real reference building located in Kathmandu, Nepal. The building faces directly to south and it has two and- half-stories and 18 small windows. The house is modeled as a single zone building. The modelled house has the same floor area, house volume, and window area as the real reference building. However, the following simplification is made during the model development: all windows on each orientation are combined together and represented by a big window but keeping the same window area. This simplification does not affect the thermal load but reduces the modeling efforts.

Building envelope including external walls, ground floor and external roof are defined in Type 56 in the same manner. For example, for external walls, the wall type is selected through the ‘Wall Type Manager’ in Type 56. Then, based on the selected wall type, all layer types are defined through the ‘Layer Type Manager’. Finally, each layer material and its thickness are specified.

## External Wall Construction

The left of FIGURE 18 shows the external wall construction of the real reference building. The right of FIGURE 18 illustrates the wall modeled in TRNSYS. As described in Chapter 3, typical external wall construction is composed of 230 mm (9") of brick wall and 12.5-25 mm (0.5-1") cement plaster on the both sides. When modeling the exterior wall in TRNSYS, EPS insulation is inserted between the brick and cement plaster. The insulation layer thickness will be varied during optimization to explore the impact of building envelope variables on system performance. For the initial design without insulation materials, the insulation thickness is set at 1 mm, which is the minimum value accepted by TRNSYS for material thickness.

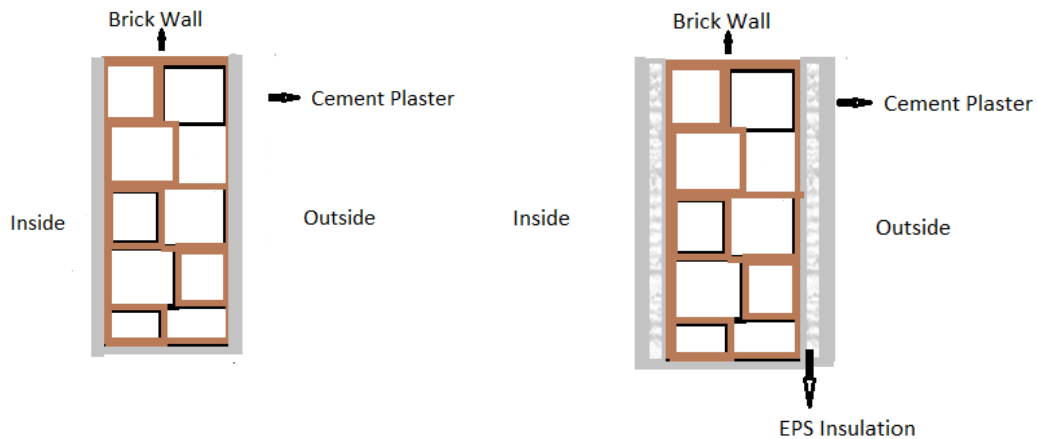


FIGURE 18: External wall construction for reference building and its TRNSYS representation (right)

## Roof Construction

Roof construction is modeled similarly as the wall construction by introducing the insulation layer in between the concrete roof and the cement plaster as shown in FIGURE 19. For the initial design without insulation materials, the insulation thickness is set at 1 mm.



FIGURE 19: Roof construction for reference building and its TRNSYS representation (Right)

## Window

Subedi (2010) stated that in Kathmandu and even across the entire country of Nepal, single-pane windows with 5-mm glazing and wood or aluminum frames are commonly used in residential buildings. Based on TRNSYS, single-pane windows with wooden frames have a U-factor of 5.72 and g-value 0.837. U-factor indicates the potency of heat loss from the window- which in the case of single pane window is highest. G-value measures the amount of solar radiation allowed from the window (Integrated Environmental Solutions, 2019). Windows account for the major heat loss of the building because of the high thermal conductivity of single pane glazing and the large window area.

Infiltration, ventilation, internal gains, occupancy schedule are not considered in this study for the purpose of simplification and their minor impact on the thermal load.

## **Radiant Floor Heating System**

Radiant floor heating is the system used for space heating. Internationally, there is an increase use of radiant floor heating in new residential constructions in the last two decades. Radiant floor heating is used in 30% to 50% of the total number of new residential constructions in Germany, Austria, and Denmark and up to 90% in Korea. The growing interest is due to the many advantages associated with radiant floor heating. Radiant floor heating is thermally more comfortable than forced air systems and baseboard heaters. Radiant floors provide uniform warm surfaces as well as uniform air temperature from floor to ceiling, have quiet operation, and do not cause drafts. Also, this type of heating allows for the room air temperatures to be slightly lower compared to other heating systems, which prevents indoor air from getting excessively dry (Patil 2010).

Radiant floors using water as the heat transfer fluid. The design temperature range for supply water is between 38°C to 65°C for heating (ASHRAE 2000). As prescribed in ASHRAE Standard 55 (2004), the floor surface temperature inside occupied zones with people wearing normal indoor shoes is 29°C maximum and 19°C minimum. This recommendation is based on the criteria of 10% of people dissatisfied (Patil 2010).

The entire radiant floor system consists mainly of (i) the actual energy delivering network of tubing in the floor, (ii) the supply loop including the storage tank and the accessories including the pump, the controller, manifolds, and (iii) the return loop. Both the supply and the return loops are modeled outside of Type 56 in TRNSYS studio. Floor tubing is simulated in TRNSYS within Type 56 as an ‘active layer’ of the floor and is described next.

## Modelling Radiant System in TRNSYS: Active Layer

There are various methods to incorporate the hydronic radiant system in a building depending upon whether the building is a retrofit or a new construction. A system with concrete slab and embedded pipes is used in this work because 1) the concrete floor matches the construction convention in Nepal; and 2) the concrete's high thermal mass and high thermal conductivity (0.8 W/m-K) are the desired properties for radiant floor applications. A concrete layer with embedded water tubes is shown in FIGURE 20.

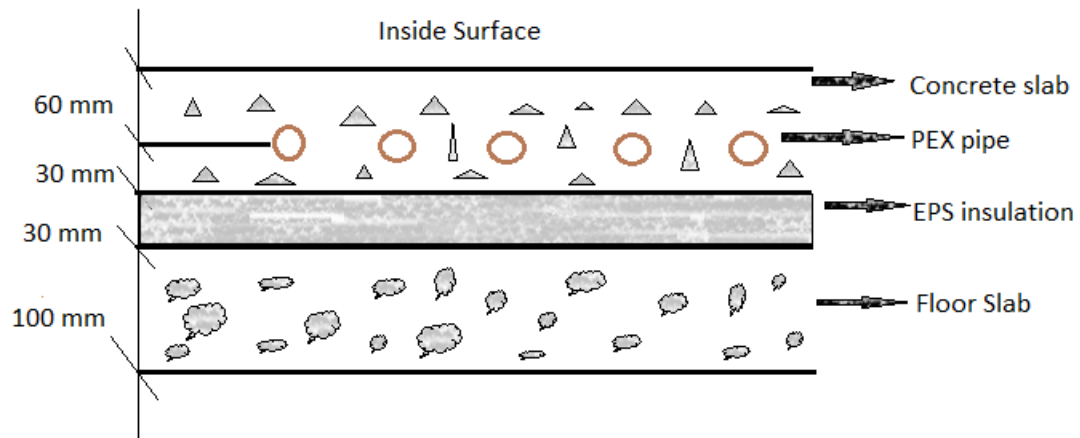


FIGURE 20: Construction of radiant floor heating system in TRNSYS

Cross Linked Polyethylene (PEX) is an ideal tubing material for radiant floors because it is noncorrosive and is not affected by the chemical composition of concrete. It is a strong and flexible product that can withstand temperatures in the range of  $-17^{\circ}\text{C}$  to  $93^{\circ}\text{C}$ . Due to the cost effectiveness, flexibility and ease of installation, a 12.5 mm (0.5 inch) diameter PEX tubing is commonly used for residential buildings. The turning radius of the tube needs to be at least six times of the tube diameter. This in turn determines the center to center distance of two tubes. To summarize, for the 12.5 mm ( $\frac{1}{2}$ " ) tubing used in

this case with 75 mm (3”) of turning radius, the center to center distance is 200 mm (6”) (Patil 2010).

## **Insulation**

The most commonly found insulation in Nepal is Expanded Polystyrene (EPS) locally known as thermocol. EPS is a lightweight, closed cell, rigid, plastic foam insulation material produced from solid beads of polystyrene (as mentioned in starrfoam). The low density ( $30 \text{ kg/m}^3$ ) and low thermal conductivity ( $0.0325 \text{ W/m-K}$ ) are two attractive properties that make EPS effective to be used as the insulation material (as mentioned in b-foam). The thickness of floor insulation is a variable to be optimized.

### **4.2.4 Thermal Comfort Measurement -Type 584**

Maintaining thermal comfort is a major objective of HVAC systems. ASHRAE Standard 55-2017 defines thermal comfort as the condition of the mind that expresses satisfaction with the thermal environment and is a subjective evaluation. Thermal comfort is affected by the following four environmental factors:

- The dry bulb temperature of the surrounding air
- The humidity of the surrounding air
- The relative velocity of the surrounding air
- The temperature of any surfaces that can directly view any part of the body and thus exchange radiation

In this research, the level of thermal comfort is measured in terms of the number of hours with an operative temperature less than the predefined thermostat setpoint throughout a whole year. Operative temperature considers the combined impact from the room air temperature and the surrounding surface temperature.

TRNSYS Type 584 is used to count the number of thermostat setpoint unmet hours as shown in FIGURE 21. Type 584 can watch up to 100 different parameters, but only one parameter “operative temperature” is watched here. Type 584 accumulates all the time when the sensed space operative temperature is below the setpoint minus the temperature dead band. When the simulation is complete, Type 25 e prints the output in the form of number of heating setpoint unmet hours in a year. Modeling of whole combisystem is represented in FIGURE 22.

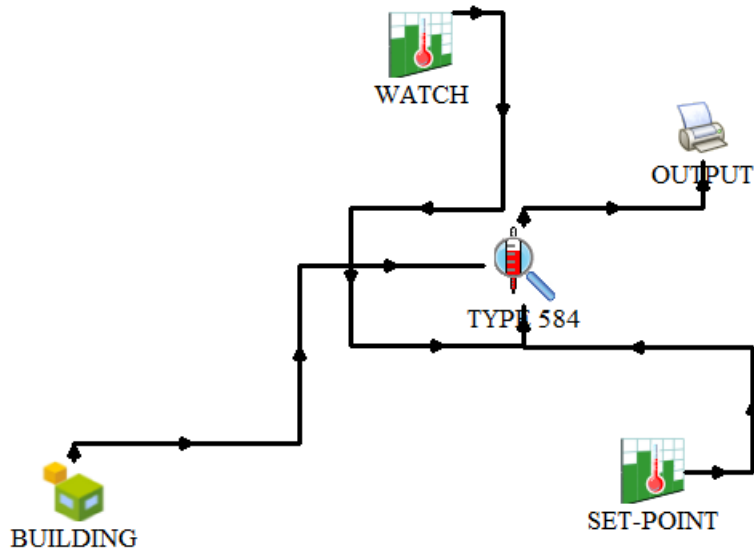


FIGURE 21: Calculation of thermal comfort by Type 584

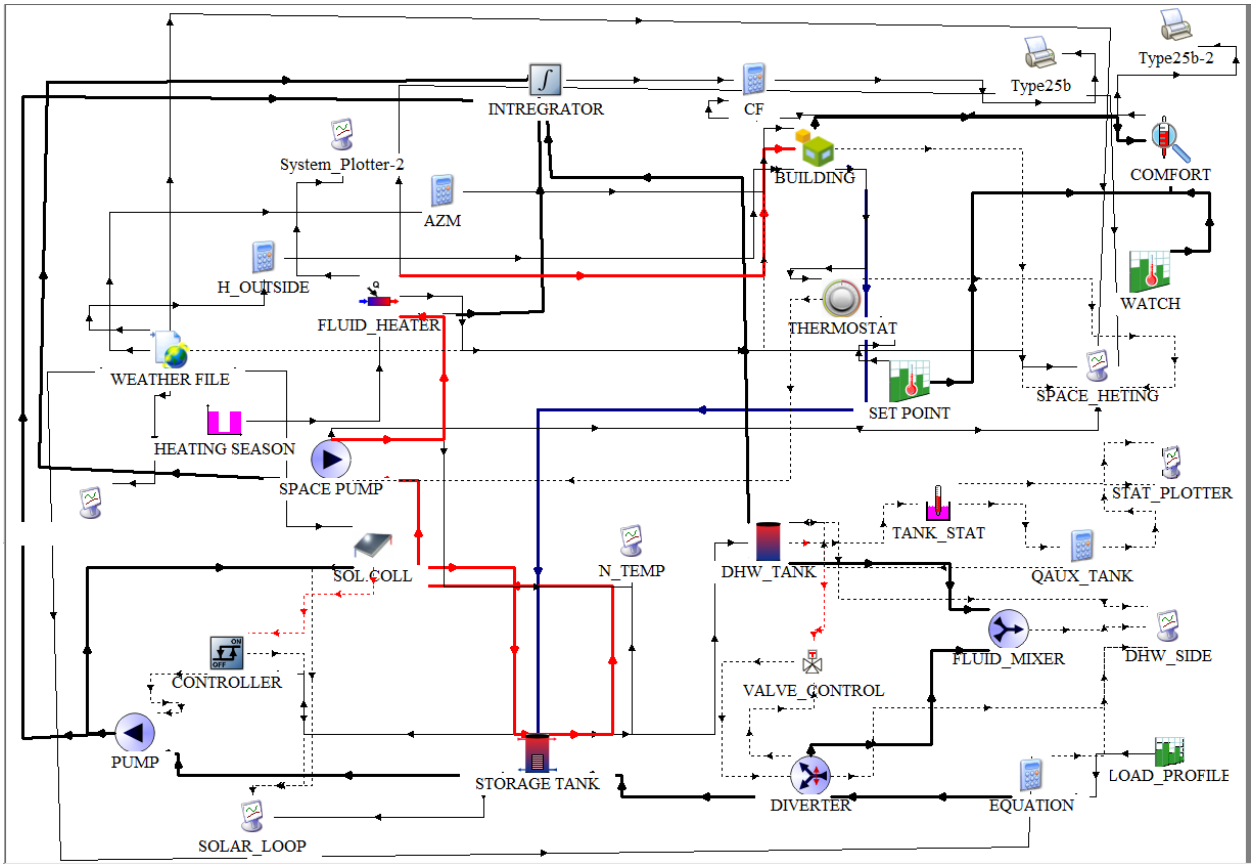


FIGURE 22: TRNSYS model of the solar combisystem

## CHAPTER 5: LIFE CYCLE COST OPTIMIZATION

A solar combisystem consists of several interacting components with many design parameters. It is not a trivial task to determine the most favorable design alternative from a large number of possible combinations of design variable values. Many designers used parametric analysis to improve the combisystem design. The parametric analysis involves an iterative procedure to perturb one variable a time, run the system simulation, and observe the impact of changing the variable value on the simulated system performance. When no further improvement can be made, another variable is chosen and perturbed gradually. Even though the parametric analysis is a straightforward approach to apply, the problem is that it cannot find the optimal solution or even the near-optimal solution. In addition, the manual procedure of perturbing variables and running simulations is very time-consuming and often impractical for cases with more than two or three independent variables (Wetter 2016). Therefore, in order to address the limitations of parametric analysis, the optimization technique is used in this study. Optimization is the process of automatically searching for the most favorable solution from a large design space. The performance of the designed system could be analyzed with respect to energy, economics and emission, depending on the formulated objective function. This research focuses on the optimization of life cycle cost. The variables, constraints, the life cycle cost objective function and the optimization approaches are described in this chapter.

### 5.1 Variables

TABLE 4 lists the total of 12 variables considered in this study. Each variable is presented with its name, boundary conditions, initial value, unit, and variable type (i.e., continuous or discrete).

TABLE 4: Optimization variables used with their boundary conditions

S.N.	Optimization Variables	Boundary Conditions	Initial Value	Step Size	Unit	Type
1.	Area of solar collector	2-40	20	0.5	m <sup>2</sup>	Continuous
2.	Collector slope	0-90	28	1	degree	Continuous
3.	Collector fluid rate	200-800	100	50	kg/hr	Continuous
4.	DHW tank volume	0.1-1	0.3	0.1	m <sup>3</sup>	Continuous
5.	Storage tank volume	0.1-10	1	0.1	m <sup>3</sup>	Continuous
6.	DHW auxiliary power	3,600-18,000	3,600	3600	kJ/hr	Continuous
7.	Instantaneous water heater power	3,6000-129,600	36,000	3600	kJ/hr	Continuous
8	Flow rate of space heating loop pump	800-4,600	800	50	kg/hr	Continuous
9	Roof insulation	1, 25, 50	1	-	mm	Discrete
10	Ground floor insulation	30, 60, 90	30	-	mm	Discrete
11	Wall insulation inside	1, 25, 50	1	-	mm	Discrete
12	Wall insulation outside	1, 25, 50	1	-	mm	Discrete

The area of solar collectors is normally limited by the space available on the south facing roof of the house. Considering that the whole system is installed on the roof, the collector area is varied from 2 to 40 m<sup>2</sup>. Since a solar combisystem needs to have at least one collector, the area of 2 m<sup>2</sup> for one collector is set as the lower boundary condition. The initial design has a 20 m<sup>2</sup> of collector area, as explained in Chapter 4.

The collector slope is varied from 0 to 90 degrees, where the upper boundary condition of 90 degree implies that the solar collectors are placed vertically and while the lower boundary condition of 0 degree implies that collectors are placed horizontally. The

general rule of thumb states that the collector slope should be set at the latitude of the location to maximize annual solar energy utilization (Leckner 2008). Therefore, for initial design, solar collectors are inclined at latitudinal angle of  $27^\circ$  for Hilli region and  $29^\circ$  for the Terai region. However, it is also recommended to have solar combisystems installed 10-15 degree more than the latitudinal angle to collect more heat during winter season when sun is low in the sky (Hin 2013).

Pump sizing also affects the performance of solar combisystems. Parametric analysis was conducted to see the effect of the collector loop flowrate. When the collector flow rate was 100 kg/hr, the collector outlet temperature was as high as  $250^\circ\text{C}$ , which is unacceptable. Therefore, the flow rate was doubled based on the parametric analysis. The boundaries for the variable of collector fluid flowrate is set at 200 kg/hr and 800 kg/hr, and the former one is the used for the initial design.

The storage tank volume has a big impact on combisystem's performance. The tank volume needs to consider the balance between the amount of energy that can be stored and the storage water temperature that can be reached. A very large tank can end up with a low storage water temperature, which implies the instantaneous heater for space heating and the auxiliary heater for DHW heating may be always activated whenever there is a water flow. On the other hand, although a very small tank can have a high storage water temperature, but some solar energy may not be able to be collected due to the maximum setting of storage water temperature. Hin (2013) assumed his system installed in the basement. Therefore, the basement height is used as the constraint to size the storage tank based on the correlation between tank height and tank volume. My research assumes that the combisystem is installed on the roof, so there is no constraint on the tank height except

for the additional structural load consideration. The storage tank is varied from 0.1 m<sup>3</sup> to 10 m<sup>3</sup>, with 1 m<sup>3</sup> used for the initial design.

Relative to the storage tank, the DHW tank does not have to store energy for longer hours. The DHW tank volume is varied from 0.1 m<sup>3</sup> to 1 m<sup>3</sup>, with 0.3 m<sup>3</sup> used for the initial design, which is the typical DHW tank size for a family of five. Auxiliary heating is required for the DHW tank during the time when solar energy is not sufficient. Thus, the auxiliary electric heater capacity is varied from 1 kW to 5kW, with 1 kW used for the initial design.

For the sizing of the instantaneous water heater used for space heating, it was observed that the capacity of 36 kW is a good choice for the initial size design. This value is used as the upper boundary for the instantaneous water heater size for two reasons. The initial design of combisystem does not consider building insulation but when the building insulation is applied during the optimization, the instantaneous heater size required will be less. In addition, the maximum available size on market is 36 kW. During optimization this parameter is considered as continuous variable from 5-36 kW with step size of 1 kW. The water flowrate in the space heating loop has crucial effect on thermal comfort because it determines the amount of heating energy supplied to the radiant floor system and eventually transferred to the space. For a give heating load, a lower flow rate means that a higher supply water temperature is needed. The supply water temperature is fixed at 50°C in this work. The water flowrate in the space heating loop is varied between 800 kg/hr to 4600 kg/hr. The lower boundary is determined by TRNSYS, and the upper boundary is based on the maximum flowrate that the selected pump can deliver.

Subedi (2010) compared the thermal analysis of buildings with modern construction vs. vernacular construction in Kathmandu in terms of the time lag. The vernacular construction comprises of brick walls with mud mortar, clay tile roof covering and wooden roof structures, window shutters and frames. The brick walls have a thickness of a half meter to a meter depending upon the building height and size. The time lag is about 12.5 hours for the half-meter-thickness walls and is about 4.8 hours for the roof. The modern construction comprises of reinforced concrete structural frame, brick walls, concrete roof, single-pan gal zings, wooden doors and windows, and no insulation in walls and roofs. The time lag is about 6 hours for the 0.254-meter-thickness brick walls and is 3.7 hours for the 0.615-meter-thickness concrete roof. The time lag of modern constructions has decreased from vernacular constructions, which could create a potential thermal comfort problem if the building is not actively heated. Although the use of insulation in building envelope is not a common practice, adding insulation to building envelop is important to reduce the heating load, and thereby reduce the size of solar combisystems and the initial system cost. Therefore, expanded polystyrene (EPS) is used in external walls, roofs and ground floor. The building insulation is varied during optimization as described below.

### **For External Walls and Roof**

The insulation thickness in external walls and roof will be varied discretely from lower boundary of 1 mm to 50 mm respectively. While there is no constraint on the choice of upper boundary condition, the lower boundary represent “no insulation scenario” of initial design discussed earlier. A minimum thickness of 1 mm has to be defined.

### **For Ground Floor**

Recall that radiant floor inside TRNSYS is modeled by an “Active Layer”. The inherent part of this set up is TRNSYS requires an insulation of at least 30 mm beneath the radiant floor. Therefore, 30 mm EPS sheet is considered as the lower boundary of the ground floor insulation and the insulation thickness is varied from 30 mm to 90 mm during optimization. Considering the standard thickness of EPS sheet to be 30 mm, the floor thickness is varied in three steps of 30 mm, 60 mm and 90 mm thickness.

## **5.2 Objective Function**

Life cycle cost (LCC) is formulated as the objective function in this work. LCC of the solar combisystem includes the initial cost, the replacement and maintenance cost and the operating cost. The life span needs to be decided first for the LCC calculation. Previous researches have assumed building’s life span as the analysis period of solar combisystem (Leckner (2008); Patil (2010); and Hin (2013)). Since the building structure lasts much longer than the equipment life, replacement must be considered in the life cycle cost. My work treats the LCC analysis period as the service life of solar collectors, which last at least 25 years without serious performance degradation. Therefore, replacement cost of the solar combisystem is not considered. Maintenance and reparation costs are not considered either due to the lack of reliable data. Operating cost includes the energy cost only. The cost

associated with the radiant floor heating system is excluded from the scope because no optimization variable is directly related to the radiant system design and operation. LCC can be expressed mathematically by the formula given by Fuller and Petersen in 1996 (Hin 2013).

$$LCC = PW_{inv} + PW_{op} \dots \dots \dots .6$$

where  $PW_{inv}$  and  $PW_{op}$  are the present value of investment cost and operating cost, respectively.

### 5.2.1 Investment Cost

The investment cost represents the capital cost incurred at the beginning of the combisystem installation. It does not need to be discounted because it is already in the present value. The calculation of investment cost can be expressed as:

$$PW_{inv} = PW_{inv.coll} + PW_{inv.pump} + PW_{inv.dhw\ tank} + PW_{inv.sto.tank} + PW_{inst.heater} + PW_{inv.insu} \dots \dots \dots 7$$

where,  $PW_{inv.component\ name}$  is the initial costs associated with respective components.

TABLE 5: The cost of major solar combisystem components

Components	Cost (Dollars)	Source
Solar collector	225 per m <sup>2</sup>	TAS Pvt. Ltd
Storage tank	1950 per m <sup>3</sup>	TAS Pvt. Ltd
Domestic hot water tank	1950 per m <sup>3</sup>	TAS Pvt. Ltd
Pumps	550 per pump	TAS Pvt. Ltd
Instantaneous water heater	Represented by equation	Rheem

In TABLE 5, the initial investment costs of most components of the combisystem are provided by local installer and service provider of solar thermal systems from Nepal (TAS Pvt. Ltd). The costs were provided in Nepalese currency, but they were converted to U.S. Dollars for the calculation.

Because instantaneous water heaters are not available on the Nepalese market, the costs of various sizes from the Rheem company in the U.S. are referred to. Rheem manufactures instantaneous water heaters with the capacity ranging from 18 kW to 36 kW. During the optimization, the instantaneous water heater capacity is varied in a wider range than Rheem’s off-the-shelf product availability. To facilitate the optimization, a linear regression was made to correlate the cost and the instantaneous water heater power rating based on the quotes provided by Rheem. The regressed equation is shown in FIGURE 23.

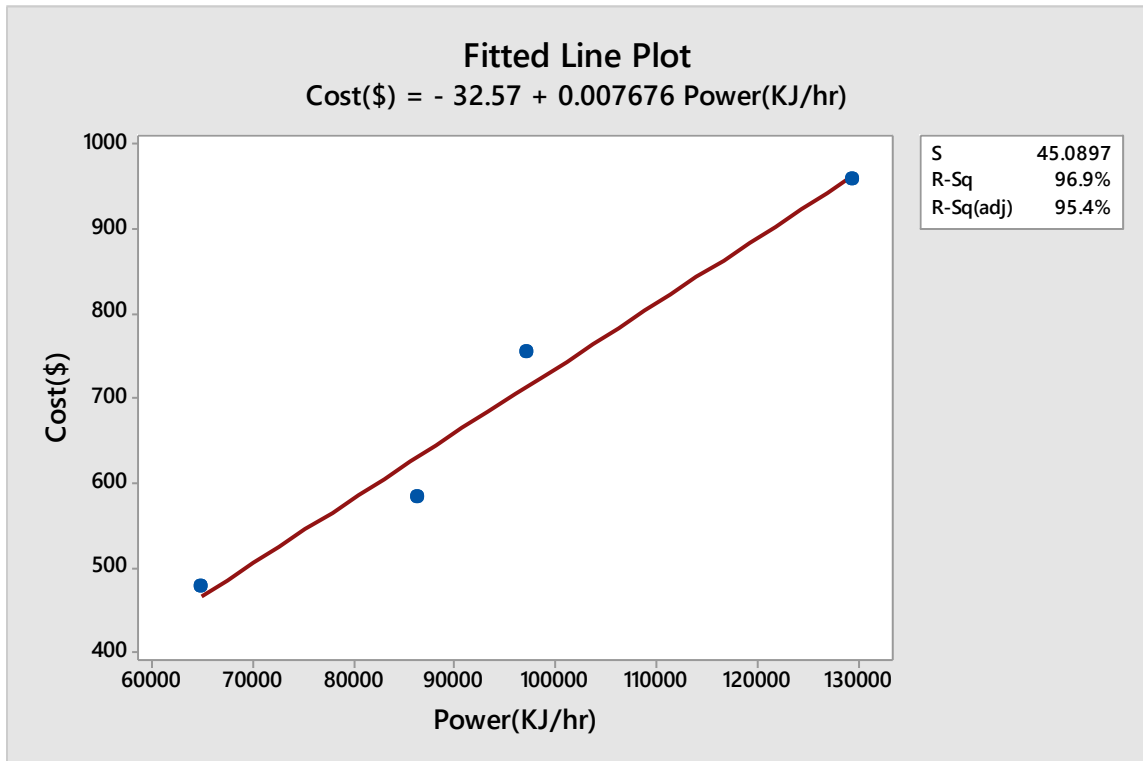


FIGURE 23: Cost vs. Power of instantaneous heater

### 5.2.2 Operating Cost

The operating cost covers the cost of energy consumed by the auxiliary heater for domestic water heating, the instantaneous water heater for space heating, and the two pumps. The operating cost  $PW_{op}$  is calculated with the equation (Hin 2013):

$$PW_{op} = C * \frac{1 - (1 + a)^{-n}}{a} \dots \dots \dots 8$$

where,  $n$  is the number of years for life cycle analysis (25 years),  $C$  is the annual energy cost, and  $a$  is the effective interest rate

The effective interest rate is calculated as:

$$a = \frac{i_d - e}{1 + e} \dots \dots \dots 9$$

where,  $e$  is the escalation rate of electricity price, and  $i_d$  is the discount rate including inflation. The annual energy cost is calculated by multiplying the annual electricity consumption of the combisystem with the electricity price. The average electricity price for residential buildings is \$0.096 per kWh in Nepal (accessed from website of Nepal Energy Forum). The effective interest rate considers the time value of money during the analysis period. It has been observed that for the past half-decade, the escalation rate of electricity price is 3.44% per year (accessed from website of Nepal Energy Forum). The discount rate after considering for inflation is set at 9.71% (NRB 2019).

### 5.2.3 Penalty Function

Based on the variables defined in TABLE 5, the optimization algorithm would likely select the configuration with the smallest size of collectors, the smallest storage tank size and the smallest instantaneous water heater capacity because of their high capital costs. However, such design is far from sufficient to meet the thermal load and will cause many hours not meeting the thermostat

setpoint. Therefore, we must apply the number of thermostat setpoint unmet hours as a constraint for the optimization problem (Hin 2013). The unmet hours hereinafter is called as the Hours Under Set Point (HUSP). Recall that the operative temperature is used for the space thermostat control. The HUSP is the sum of the total number of hours that the space operative temperature falls below the setpoint throughout the whole year. Due to the sudden change of setpoint temperatures from the setback period to the normal operation period, a certain amount of HUSP is inherent in the system operation. The Appendix G of ASHRAE 90.1 states that the unmet hours for the proposed design should not exceed 300 hours for a whole year. Although AHSRAE 90.1 is for commercial buildings, the number specified there can be reasonably used a reference for this work. During the optimization, the constraint is implemented as a penalty function, which is then added to the original objective function. The penalty function works in the following manner. If the combisystem ends up with less than 300 HUSP, the penalty function takes a value of zero. Otherwise, if the combisystem ends up with more than 300 HUSP, the penalty function takes a very large value, which is set at \$200,000 for this work. Such a high penalty cost ensures that no system design with more than 300 HUSP is considered optimal. Overall, the final LCC objective function, including all the costs and the penalty function, is formulated as below.

$$LCC = \text{Total Initial cost} + P W_{\text{energycost}} + LT(300, HUSP) * 200,000 \dots \dots \dots 10$$

$$= [\text{Total initial cost}] + \left[ C \times \frac{1 - (1+a)^{-n}}{a} \right] + LT(300, HUSP) \times 200,000 \dots \dots \dots 11$$

$$\begin{aligned} & [P W_{\text{inv. coll}} + 2 \times P W_{\text{inv. dhw, tank}} + 2 \times P W_{\text{inv. sol. pump}} \\ & + P W_{\text{inv, instantaneous heater}} + (\text{SOL\_PUMP} + \text{SPACE\_PUMP} \\ & + \text{DHW\_AUX} + \text{SPACE\_AUX}) \times \text{COST\_UNIT} \times 12.70 \\ & + LT(300, HUSP) \times 200,000 \dots \dots \dots 12 \end{aligned}$$

### 5.3 Selection of Optimization Tool

GenOpt is an open source generic optimization program developed by Lawrence Berkley National Laboratory. GenOpt has been specially designed to address the optimization problems that rely on building simulations to evaluate the objective function. A mechanism is provided to couple GenOpt with the simulation programs such as Energy-Plus, SPARK, DOE-2, and TRNSYS by simply modifying configuration files. GenOpt has an open interface on both the simulation program side and the minimization algorithm side (Wetter, 2016). GenOpt requires the following files to start the optimization:

- **Simulation template files:** They contain all the information of the model and how each component is linked with others. The numerical values are replaced with variable names in order to facilitate optimization.
- **Command file:** It stores all the variables that are being optimized and the algorithm that is being used for optimization with termination criteria.
- **Configuration file:** It contains the information related to simulation program and how to start the simulation engine.
- **Initialization file:** This file contains the location of template files, configuration file and command file which are necessary to start the optimization. It also tells GenOpt the name of objective function and the location to find it.

After completing the file setup, GenOpt automatically generates input files based on the input template of the simulation program. GenOpt then launches the simulation program, reads the function value being minimized from the simulation result file, checks possible simulation errors and determines a new set of input parameters for the next run as

shown in FIGURE 24. The whole process is repeated iteratively until a minimum of the function is found or a certain stopping criterion is satisfied (Wetter 2016).

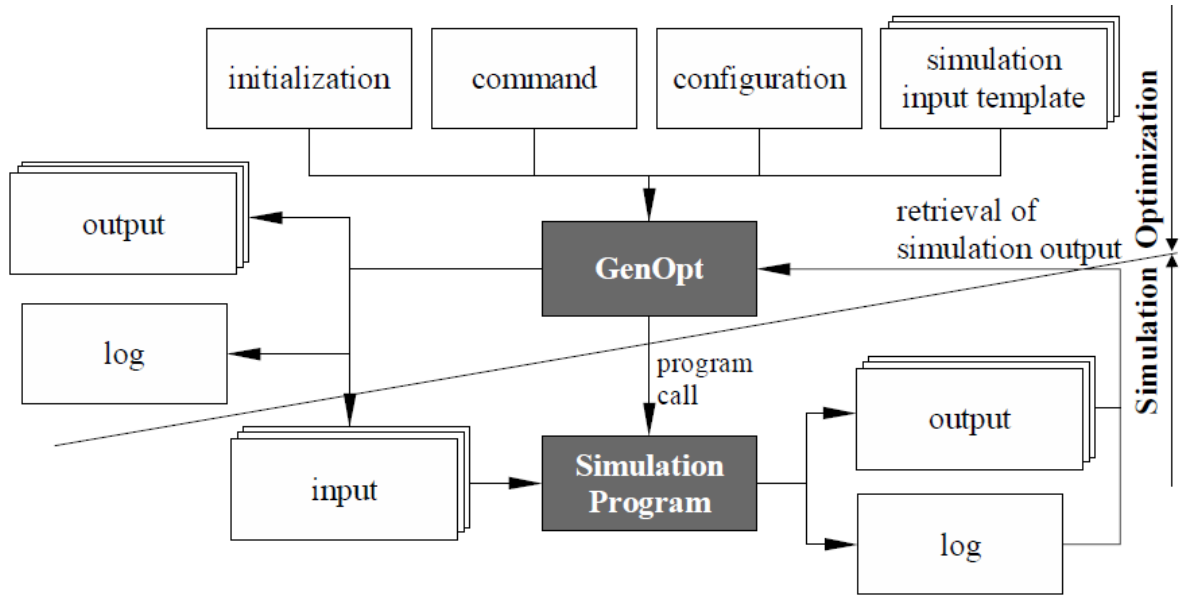


FIGURE 24: Interface between GenOpt and simulation program (Wetter 2016)

### 5.4 Optimization Algorithm

GenOpt has implemented a number of algorithms and it also provides the interface to add the user-developed algorithms. The choice of optimization algorithms is based on the type of variables (i.e., continuous or discrete) to be optimized and the performance space shape. For a problem having both discrete and continuous variables, it is advised to use either the Particle Swarm Optimization (PSO) algorithm alone or the hybrid PSO and Hooke-Jeeves (HJ) algorithm. Because the formulated optimization problem has both continuous and discrete variables and the performance space shape is unknown, the hybrid use of PSO and HJ is an appropriate choice, as demonstrated by several previous studies (Hin 2013).

### 5.4.1 Particle Swarm Optimization

Introduced by Kennedy and Eberhart in 1995, PSO is regarded as an artificial intelligence-based algorithm by emulating the behavior of a school of fish or a flock of birds in finding their shelter or food. Analogical to flocks of birds or schools of fish that the group can combine their own knowledge and the group's knowledge to accurately locate a food source within a wide search space, PSO is a stochastic, probability-based algorithm that uses a finite set of individuals, called particles, to perform a global search of optimal positions for non-linear optimization problems. Each particle has a value of the cost function that is being optimized. After each generation, the particles attempt to improve their cost function values from the last step. Each particle remembers its own best value, called the cognitive behavior, and it also knows the best value obtained by all other particles in the swarm, called the social behavior. These cognitive and social values influence the direction and velocity that each particle moves for the next generation seeking for a lower cost function value. The algorithm has two basic governing equations, Equations 13 and 14, for the position and velocity vectors of individual particles, respectively. It needs to be noted that each optimization variable represents a dimension in the search space (Hin 2013).

$$x_i^{k+1} = x_i^k + v_i^{k+1} \dots \dots \dots 13$$

$$v_i^{k+1} = v_i^k + c_1 r_1 (p_i^k - x_i^k) + c_2 r_2 (G - x_i^k) \dots \dots \dots 14$$

where,

i = Particle index

k = Generation index

x = Particle position

v = Particle velocity

$p_i$  = Best individual particle position

$G$  = Best swarm position

$c_1, c_2$  = Cognitive and social parameters

$r_1, r_2$  = Random numbers between 0 and 1

Although there are numerous variations and versions in implementing the particle swarm optimization, the following steps are generally used:

- 1) Randomly initialize particle positions and velocities;
- 2) Set  $k = 1$ ;
- 3) Evaluate function value of each particle given its coordinates;
- 4) If  $f_i^k \leq f_{i, best}$  then  $f_{i, best} = f_i^k, p_i^k = x_i^k$
- 5) If stopping condition is satisfied then go to 8);
- 6) Set  $k = k + 1$ , and

$$x_i^{k+1} = x_i^k + v_i^{k+1} \dots \dots \dots 15$$

$$v_i^{k+1} = v_i^k + c_1 * r_1 * (p_i^k - x_i^k) + c_2 * r_2 * (G - x_i^k) \dots \dots \dots 16$$

- 7) Repeat 3) to 6)
- 8) Terminate

The algorithm stops when the “number of generations” has reached a user-specified value. GenOpt has three PSO variations, of which the PSO on Mesh is selected for this research. The continuous variables are modified so that they belong to a fixed mesh, whose parameters are provided in TABLE 6. By constraining the variables to a mesh, the number of simulation calls made during the optimization is reduced when the particles start to

cluster. That is, if several particles are on adjacent mesh nodes and their velocities are not high enough to move them to the next nodes, the particles remain on those nodes and the simulations are not repeated. The algorithm simply reuses the value of the cost function previously obtained at those positions. Therefore, the PSO on mesh has the advantage of reducing the number of simulation calls. The disadvantage of this variation is that all continuous variables essentially become discrete. Because the variables are confined to the mesh that does not change in size or configuration, the variable's step size cannot change either (Hin 2013).

TABLE 6: Optimization parameter for PSO algorithm (Hin 2013)

Parameter	Value
Main	PSOCC (Particle Swarm Optimization with Constriction Coefficient)
Neighborhood Topology	Von Neumann
Neighborhood size	5
Number of Particles	15
Maximum Number of Generation	50
Seed	1
Cognitive acceleration	2.8
Social acceleration	1.3
Maximum velocity gain continuous	0.5
Maximum velocity gain discrete	4

In TABLE 6, the neighborhood topology defines the particles from which the social best value is taken to establish particle velocities and positions. This value does not need to be chosen from the entire swarm but rather can be chosen from a smaller group

surrounding the particle in question. The size of this group is determined from the value of neighborhood size parameter. The shape is determined by the neighborhood topology type. The two most common neighborhood topology types are known as gbest and lbest (Hin 2013).

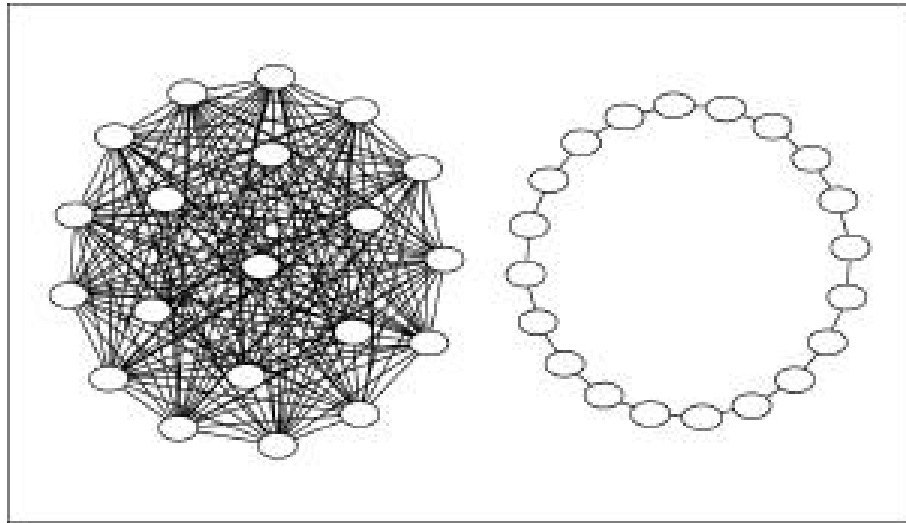


FIGURE 25: Gbest and lbest neighborhood topology

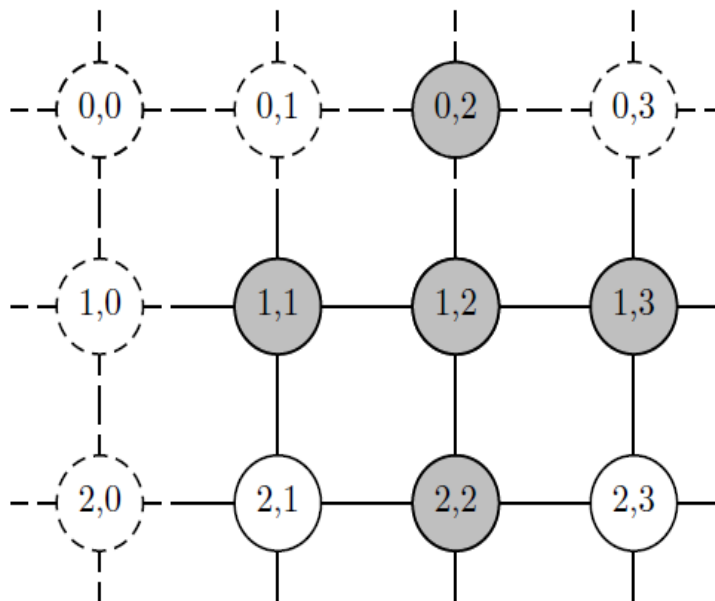


FIGURE 26: Von Neumann neighborhood topology

FIGURE 25 shows the difference between the gbest and lbest topologies. In gbest, the trajectory of each particle is influenced by the best point found by any member of the entire population. The lbest topology only lets the trajectory of a particle be influenced by a smaller proportion of the population, typically only two other particles located on either side of the particle in question. These topology types, however, have distinct disadvantages. Gbest tends to converge quickly on a solution, however it often tends to get stuck in a local minimum. Lbest is capable of “flowing around” local minima, however, lbest tends to take longer to converge (Kennedy 2001). A third type of neighborhood, known as the Von Neumann neighborhood, is also commonly used. A Von Neumann neighborhood with a neighborhood size of 1 takes into consideration the best point found by the particles located above, below and on either side of the particle in question on a two-dimensional lattice. FIGURE 26 shows an example of the Von Neumann topology with a neighborhood size of 1. In the case of this thesis, the von Neumann topology is used since Wetter (2009) states that “best performance has been achieved with the von Neumann topology”. The number of particles and number of generations determine how many iterations are performed before the PSO terminates. Carlisle and Dozier (2001) recommend using a population size of 30 for a standard PSO algorithm. However, because a hybrid algorithm is used in my work, a smaller population size of 15 is used in this work to save computation time. Carlisle and Dozier (2001) do not recommend a standard number of generations to use. Wetter (2004) completed optimization of a system having four variables using a maximum number of generations of 20. Hin (2013) completed his optimization of solar combisystem having 8 variables using max generation of 50. Trial runs with maximum generation of 50 for my model also yields reasonable accuracy. The seed

parameter is simply used to initialize the random number generator. The random numbers are used for the values of  $r_1$  and  $r_2$  in equation 16. The value of the seed parameter is normally set as 1. The cognitive and social acceleration parameters represent the values of  $c_1$  and  $c_2$  in Equation 16. Carlisle and Dozier (2001) recommended the values of 2.8 and 1.3 for cognitive and social acceleration factors, respectively. These values work well for a general-purpose PSO, or at least work well as a starting point before tweaking certain parameters to improve the performance of the algorithm. The continuous and discrete maximum velocity gains are normally set to 0.5 and 4, respectively for standard PSO problems (Wetter 2009). The constriction gain helps to control the spread of the particles. A larger constriction gain means the particles tend to clump together less often and helps keep a bigger spread of particles in later generations. This however comes at the expense of more simulations. Wetter (2004) showed that by increasing the number of particles and increasing the constriction gain from 0.5 to 1, a larger cost reduction was obtained at the expense of twice the amount of simulations. In order to keep the number of simulations required for the optimization relatively low, a constriction gain of 0.5 is used. The mesh size parameters are used by both the PSO algorithm and the HJ algorithm (Hin 2013).

#### **5.4.2 Hooke Jeeves Algorithm**

The Hooke-Jeeves (HJ) algorithm has a simple procedure as shown in FIGURE 27.

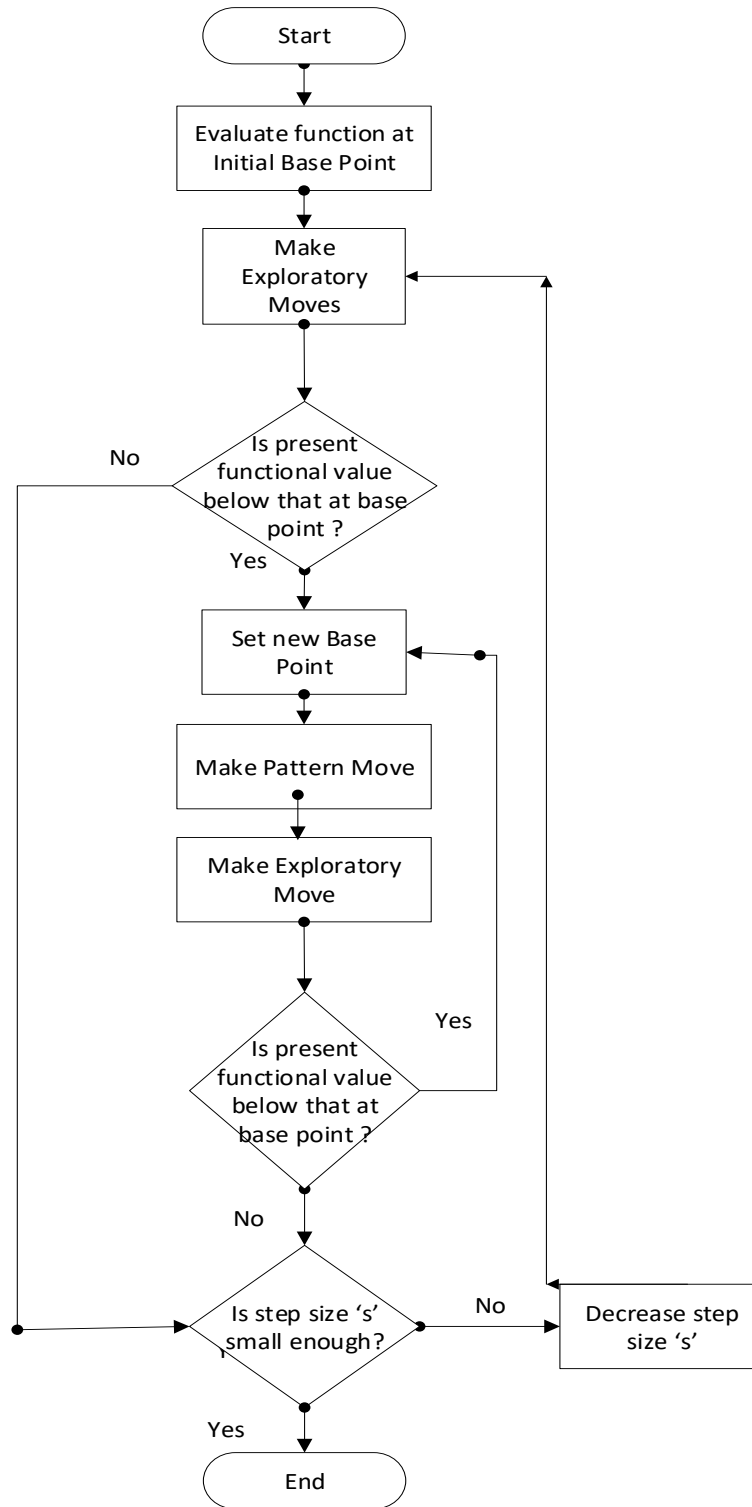


FIGURE 27: Pattern move of Hooke-Jeeves algorithm

The HJ algorithm starts with evaluating the objective function at an initial point that can be user-defined. In the case of the hybrid algorithm, the initial point for Hooke Jeeves algorithm is the terminating point of the Particle Swarm Optimization. The second step of the algorithm involves an exploratory move around the initial individual. The process of an exploratory move is depicted in FIGURE 27.

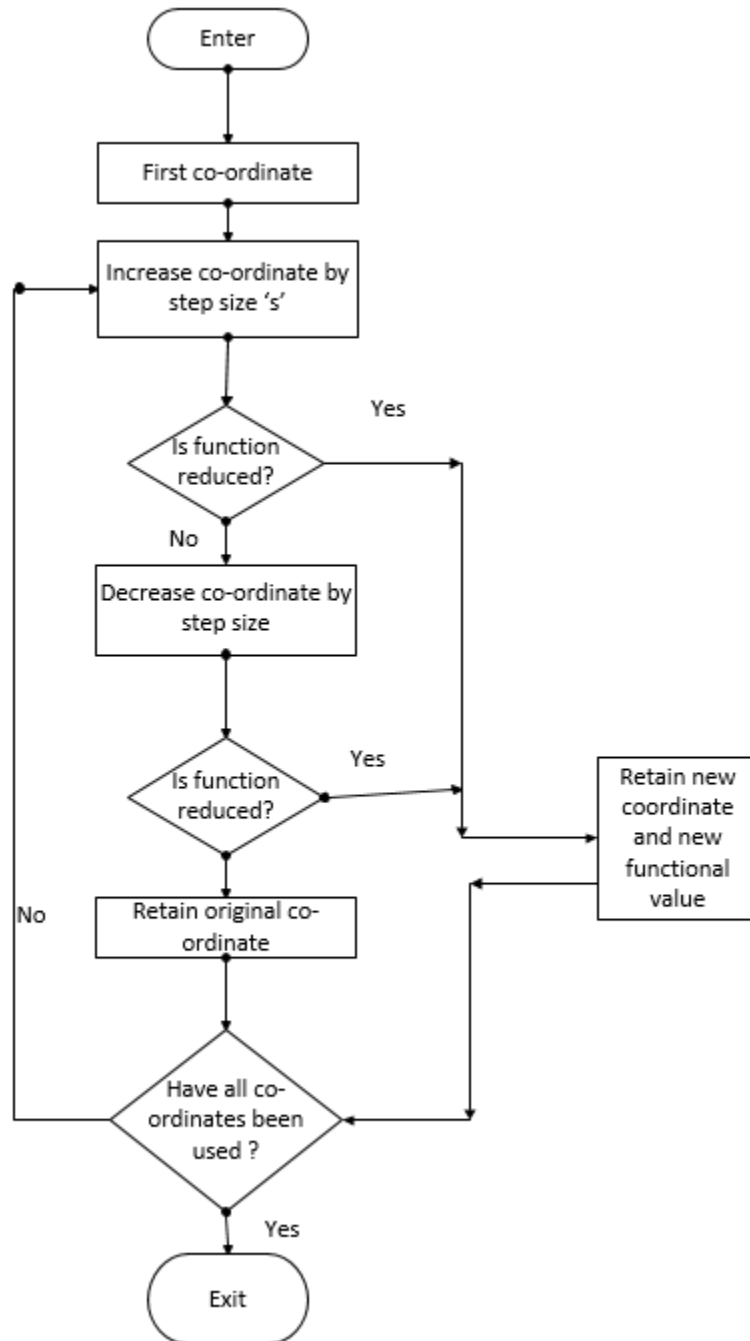


FIGURE 28: Exploratory move of the Hooke-Jeeves algorithm

In a pattern move, the algorithm sequentially increases and decreases the value of each optimization variable by its corresponding step size. In FIGURE 28, this step is described as increasing or decreasing the coordinate. The objective function is evaluated

after the variable is changed. If the objective function value decreases, the changed variable value is retained. Otherwise, the variable is reset to its original value. This step is also referred to as the ‘global search’. Once the exploratory move is completed for all variables, the algorithm continues from the first decision box. By now, the algorithm establishes a new base point based on the lowest objective function value obtained so far. According to the new base point and the previous base point, a “pattern move” can be made. The exploratory moves are then repeated around this new base point. If this step produces a point that has a value of the objective function that is lower than the lowest found so far, the algorithm sets this point as the new base point and repeats the exploratory moves around this new base point. This is often referred to as the ‘local search’. In FIGURE 28 the local search is shown as the second set of exploratory moves. If the local search fails to produce a value of the objective function that is lower than the lowest obtained so far, the algorithm reduces the step size and performs a new global search. This process is repeated until the step size has reached its minimum or there is no further decrease of the objective function value in both the local and global searches.

The step size is reduced according to the following equations.

$$y_j = y_{j-1} + 1 \dots \dots \dots .17$$

$$s_j = \frac{1}{r^{y_j}} \dots \dots \dots .18$$

where,

j = Step reduction index;

y = Mesh size exponent;

t = Mesh exponent increment;

r = Mesh size divider;

The mesh size exponent mesh exponent increment, mesh size divider and the initial mesh exponent are all optimization parameters that are specified at the before running the HJ algorithm. The algorithm repeats the entire process above until a maximum number of step size reductions has been reached. The maximum number of step size reductions is also an optimization parameter that is supplied during the optimization set-up. The values for these parameters used in this thesis are found in TABLE 7.

TABLE 7: Optimization parameters for the Hooke-Jeeves algorithm

<b>Parameters</b>	<b>Value</b>
Constriction gain	0.5
Mesh size divider	2
Initial Mesh size exponent	0
Mesh size exponent increment	1
Number of step reductions	2

Wetter (2009) recommended using common values of 2, 0, and 1 for mesh size divider, initial mesh size exponent, and mesh size exponent increment respectively. The value of step size determines how many iterations of the process shown in FIGURE 28 are completed before the algorithm terminates. Hin (2013) found out that increasing the number of step reduction does not necessarily minimize the cost function for his model but certainly increased the number of simulation and time. Therefore, considering the complexity of model, Hooke-Jeeves algorithm will undergo two stages of “step reduction”.

## CHAPTER 6: OPTIMIZATION RESULTS

The initial design is optimized with the hybrid application of the Particle Swarm Optimization (PSO) algorithm and the Hooke-Jeeves optimization (HJ) algorithm. The hybrid use of these two optimization algorithms intends to combine their unique strengths. The PSO is applied first because it is good at performing global search in a large space. Then, using the optimum found from the PSO as the starting point, the HJ is applied because it is good at performing local search. The GenOpt software provides the mechanism of setting up the hybrid application of PSO and HJ in a single run. For this mechanism, the number of simulations needs to be specified as one of the parameters to control the optimization run. The simulation number, however, includes the number of simulations call by both PSO and HJ. It is difficult to control how much efforts are taken by each of the optimization algorithms. To address this problem, the application of PSO and HJ are applied sequentially in two separate steps. The first step is to run the PSO which uses the number of generations as the stopping criterion. After the PSO is complete, the obtained optimum is manually specified as the starting point for the HJ, which uses the number of simulations as the stopping criterion.

### 6.1 Results for the Terai Region

FIGURE 29 shows the evolution of the life cycle cost along with the 50 generations when particle swarm optimization was implemented. For each generation, the objective function values for all 15 individuals are plotted. There are three individuals with very high life cycle cost, and they are generated at the first several generations. This can be explained by the stochastic characteristics of PSO. When performing the global search, PSO may generate design alternatives (e.g, a design with the minimum thickness of envelop

insulation, the minimum solar collector area, and minimum capacity of the instantaneous water heater) that have the number of thermostat unmet hours more than the maximum requirement. In this case, the penalty function is triggered and leads to a very high objective function value. As FIGURE 29 shows, this phenomenon occurs only at the first several generations because the algorithm can quickly identify the promising region for the optimum.

To show the evolution process more clearly, those outliers caused by the penalty function are removed, which leads to FIGURE 30. This figure shows the following:

- The life cycle cost is reduced from \$27,918 for the initial design (the individual marked with green color) to \$16,195 for the best design at the end of optimization (the individual marked in red color).
- The best design solution obtained by the end of the 20<sup>th</sup> generation (the individual marked with blue color) has a life-cycle cost of \$16,226 which is only \$33 greater than the best design solution obtained at the end of the 50<sup>th</sup> generation.
- Initially, all individuals in the particle are diversified with a large range of objective function values between \$31,398 and \$20,296 (excluding outliers). By the end of the 20<sup>th</sup> generation, all individuals in the particle have a small range of objective function values between \$17,100 and \$16,226, which indicates the convergence of the optimization algorithm. The convergence is kept from the 20<sup>th</sup> generation to the final 50<sup>th</sup> generation. After the 20<sup>th</sup> generation, several individuals clearly deviate from the converged region, which is normal for PSO because of its global exploration of the solution space.

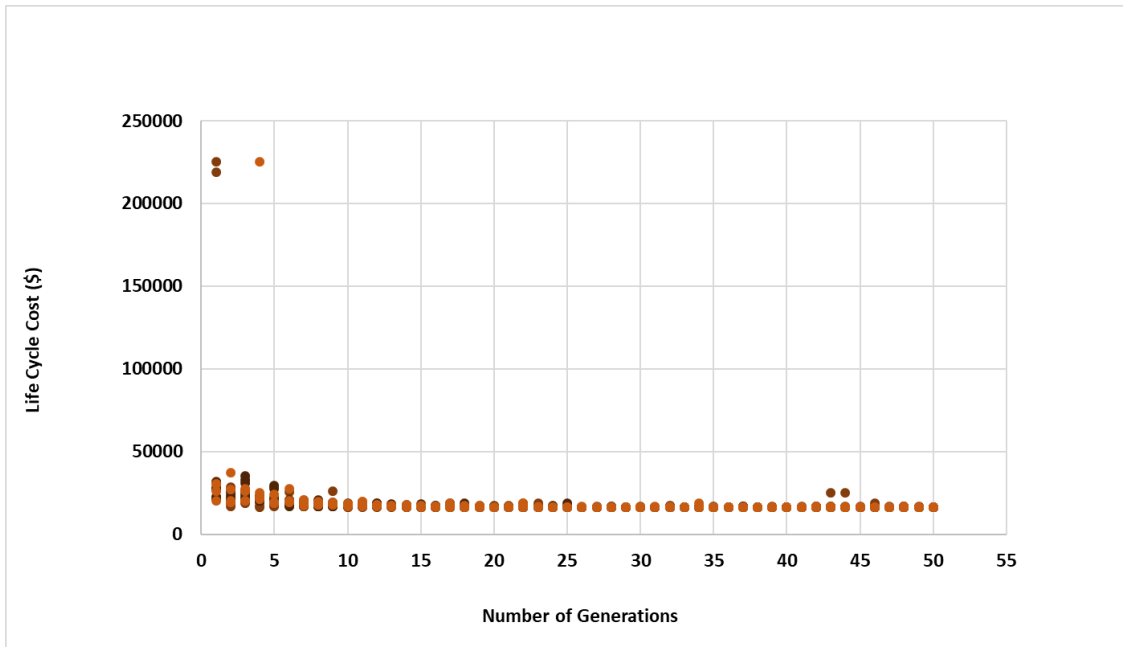


FIGURE 29: Evolution of the objective function values with the generation for the particle swarm optimization in Terai region

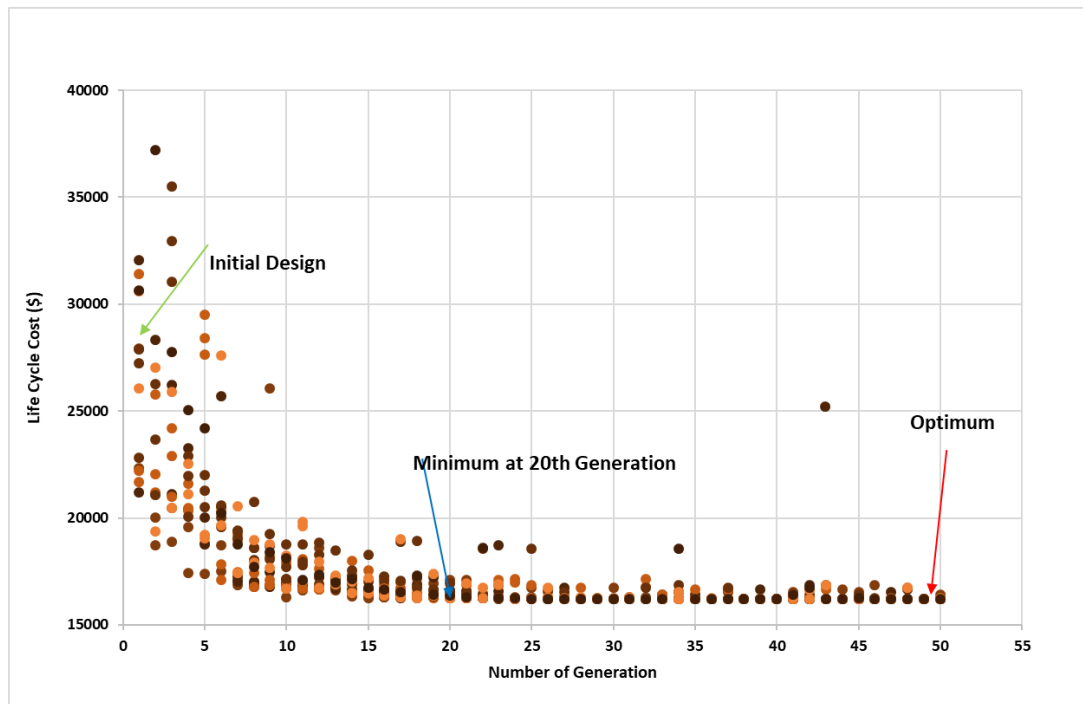


FIGURE 30: Evolution of the objective function values with the generation for the particle swarm optimization in Terai, after excluding the outliers due to the triggering of the penalty function

Using the best individual found from the PSO as the starting point, the HJ is applied. Because the HJ algorithm is not able to deal with discrete variables, the variables on building envelope insulation, which have been considered discrete during PSO, are replaced with specific numerical values in the HJ input file.

The HJ is run for a total of 12 iterations. FIGURE 31 shows that the life cycle cost is reduced by \$5,884 from \$16,196 to \$10,312 at the end of optimization. Because the HJ is a local search optimization algorithm that maintains only one solution, the objective function always reduces from one iteration to the next iteration. By the end of hybrid algorithm, life cycle cost for the Terai region is reduced by 63%.

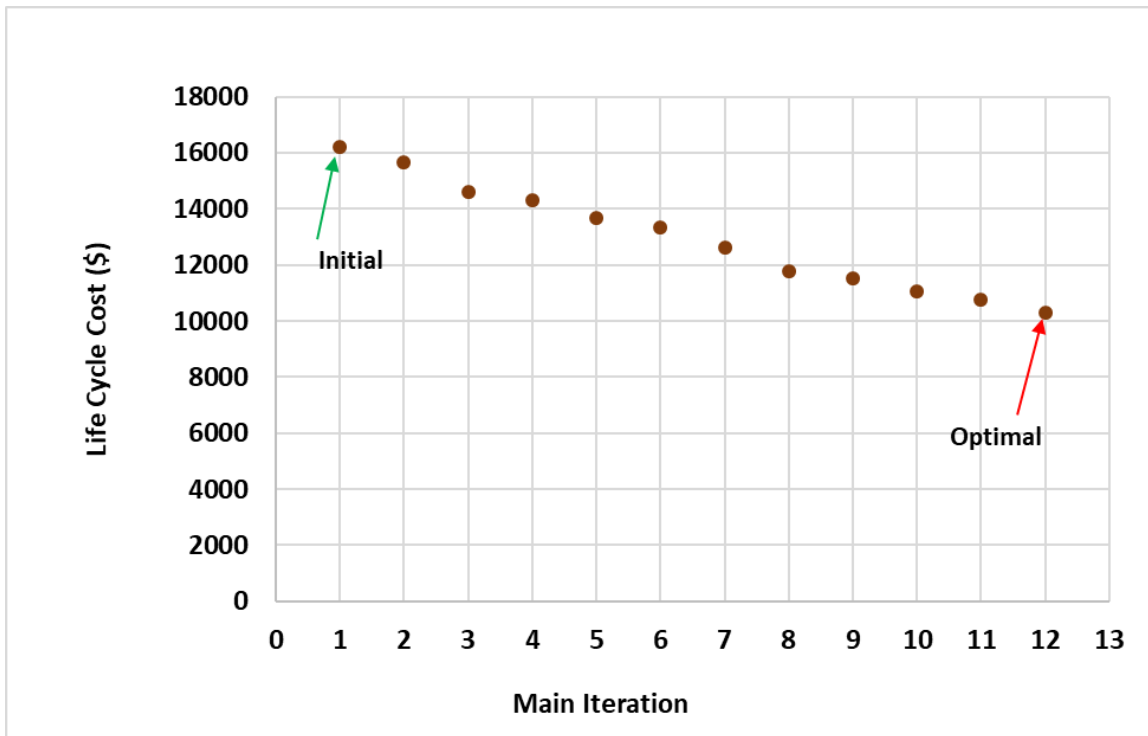


FIGURE 31: Evolution of the objective function with the iteration for the Hooke-Jeeves optimization

TABLE 8 lists the optimal values for all optimization variables. For the convenience of comparison, the initial design values at the beginning of the optimization,

which are based on the design convention, engineering judgement, and a number of parametric runs of the TRNSYS simulation model, are also presented in TABLE 8.

TABLE 8: Initial values and final values of the optimization variables for Terai region

S.N.	Optimization Variables	Unit	Initial Value	Optimal Value PSO	Optimal Value HJ
1	Area of solar collector	m <sup>2</sup>	20	11.40	5.9
2	Collector slope	degree	29	19.65	32.65
3	Collector fluid rate	kg/hr	200	607	757
4	DHW tank volume	m <sup>3</sup>	0.3	0.486	0.186
5	Storage tank volume	m <sup>3</sup>	1	1.181	0.181
6	DHW auxiliary power	kJ/hr	3,600	12,385	5,185
7	Instantaneous water heater power	kJ/hr	129,600	73,755	12,555
8	Flow rate of space heating loop	kg/hr	800	3,855	3,205
9	Roof insulation	mm	1	50	50
10	Ground floor insulation	mm	30	60	60
11	Wall insulation inside	mm	1	1	1
12	Wall insulation outside	mm	1	50	50

The solar collector area is reduced from 20 m<sup>2</sup> to 5.9 m<sup>2</sup> mainly because 1) solar collectors have a much high initial cost while the price of electricity for heating is low; and 2) the location has a mild climate, which does not need a large collector area for space heating. The solar collector slope is found to be 33° for the final optimal design. The location has a latitude of 29° and an elevation of 91 m above the sea level. Any slope in

the range from the location latitude (i.e., 29°) to 15° above the latitude (i.e., 44°) can be regarded as a reasonable design (Hin 2013).

The solar collector fluid flow rate is increased from 200 kg/hr for the initial design to 757 kg/hr for the optimal design. The most possible reason is that the increase of the flowrate slows down the increase of the storage water temperature, which thereby is favorable for the solar collector efficiency. As a rule of thumb, IEA suggested using 50-100 L for every square meter of flat-plate solar collector area (Weiss, 2003). The optimal storage size selected during optimization (186 L) is low for the optimal collector area of (5.9 m<sup>2</sup>). This causes the outlet temperature from the solar collector to rise rapidly. In order to keep the outlet temperature of the solar collector low, the propylene glycol mixture is accelerated. This also ensures maximum heat collected during the day time from the solar collector.

The sizes of both the storage tank and the DHW tank are decreased from the initial design. This is mainly for two reasons: 1) both tanks have high capital cost while the electricity price is very low; and 2) the solar collector area is small and it is not necessary to have a large storage tank.

The space heating loop flowrate is increased from 800 kg/hr for the initial design to 3200 kg/hr for the optimal design. This increase is to compensate the significant decrease of instantaneous water heater power as discussed earlier. As we know, for the same amount of energy delivered to the radiant floor, increasing the supply water flowrate means the decrease of the supply water temperature. Instead of supplying water to the radiant system at maximum initial design temperature of 50° with average flow rate of 800 kg/hr, optimal

design sends water at low temperature 25° but high flow rate of 3200 kg/hr. In fact, heat supplied during the latter case is almost double with the optimal design condition.

Building envelope insulation has a big impact on the space heating load and thereby the sizing of the equipment used in the combisystem. Meanwhile, the insulation initial cost is much lower than the equipment cost. Therefore, it is reasonable to expect that relative to the initial design, a higher level of insulation should be used in the envelope, as demonstrated from the optimal insulation values in TABLE 8. The roof insulation is increased from the minimum of 1 mm (a proxy of no insulation because TRNSYS does not accept a zero value for the layer's thickness) for the initial design to the maximum of 50 mm for the optimal design. The ground insulation is increased from 30 mm for the initial design to 60 mm for the optimal design. The external part of the wall insulation is increased from the minimum of 1mm for the initial design to the maximum of 50 mm for the optimal design. However, the internal part of the wall insulation is kept at the minimum. Such a wall design is reasonable because applying the thermal insulation outside of the structure is favorable for using the thermal mass to reduce the impact of diurnal outdoor temperature change on the space temperature.

## **6.2 Results for the Hilli Region**

FIGURE 33 shows the optimization results of PSO for Kathmandu, the representative city in the Hilli region. It can be noticed that there are more individuals with very high life cycle cost for this location than for the Terai region. In pursuit of the global minimum, PSO may generate design alternatives (e.g, a design with the minimum thickness of envelope insulation, the minimum solar collector area, and minimum capacity of the instantaneous water heater) that have the number of thermostat unmet hours more than the

maximum requirement. In this case, the penalty function is triggered and leads to a very high objective function value.

To show the evolution process more clearly, those several outliers caused by the penalty function are removed from FIGURE 32, which leads to FIGURE 33. Following observations are made from FIGURE 33.

- The life cycle cost is reduced from \$57,540 for the initial design (the individual marked red in the figure) to \$22,061 for the best design at the end of optimization (the individual marked green in the figure).
- The best design solution obtained by the end of the 20<sup>th</sup> generation (the individual marked blue in the figure) has a life-cycle cost of \$22,136.81, which is only \$76.24 greater than the best design solution obtained at the end of the 50<sup>th</sup> generation. The best design occurs at the 47<sup>th</sup> generation.
- Initially, all individuals in the swarm are diversified with a large range of objective function values between \$57,540 and \$24,907. By the end of the 20<sup>th</sup> generation, all individuals in the swarm have a small range of objective function values between \$23,374 and \$22,137, which indicates the convergence of the optimization algorithm. The convergence is kept from the 20<sup>th</sup> generation to the final 50<sup>th</sup> generation with occasional deviation from the optimal area of solution. After the 20<sup>th</sup> generation, several individuals clearly deviate from the converged region, which is normal for PSO because of its global exploration of the solution space.

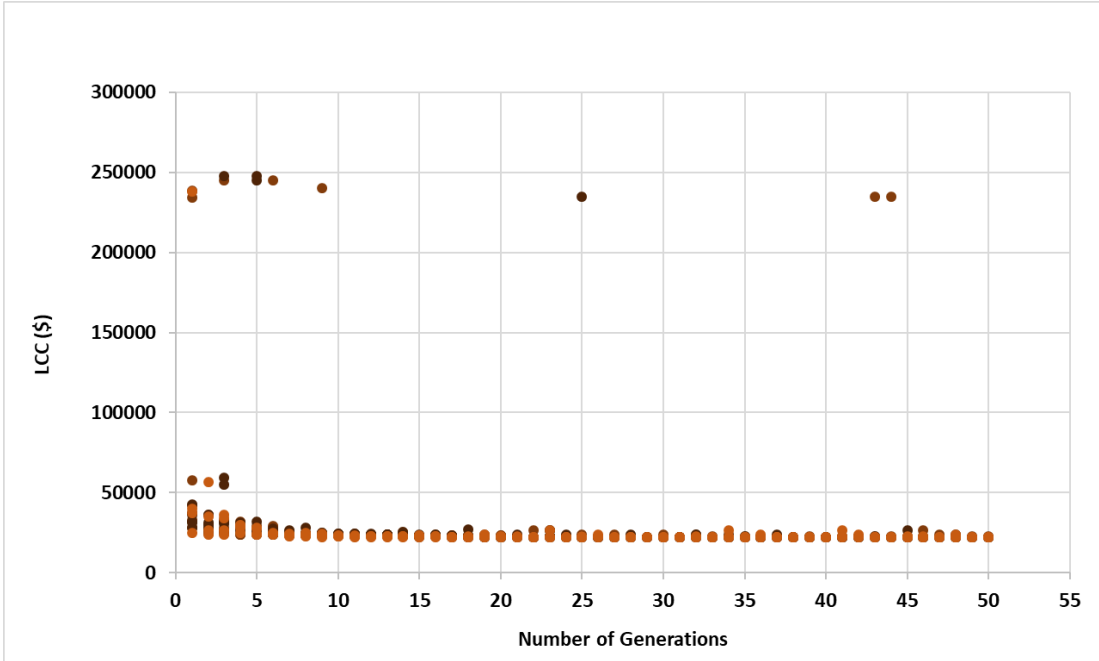


FIGURE 32: Evolution of the objective function values with the generation for the particle swarm optimization in Hilli region.

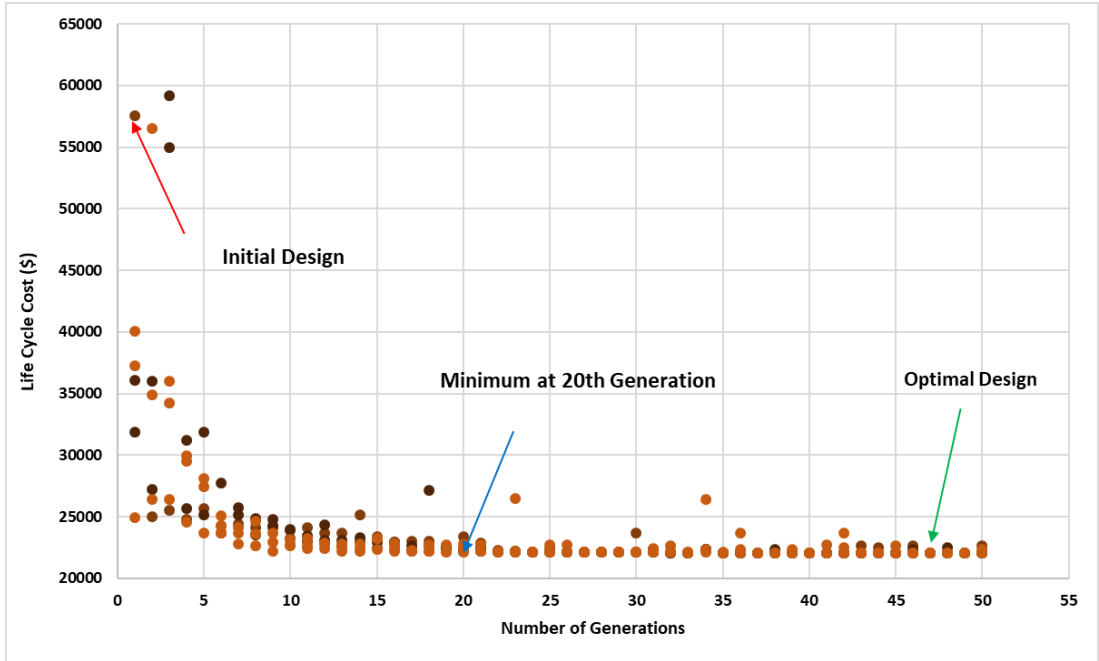


FIGURE 33: Evolution of the objective function values with the generation for the particle swarm optimization in Hilli region without outliers

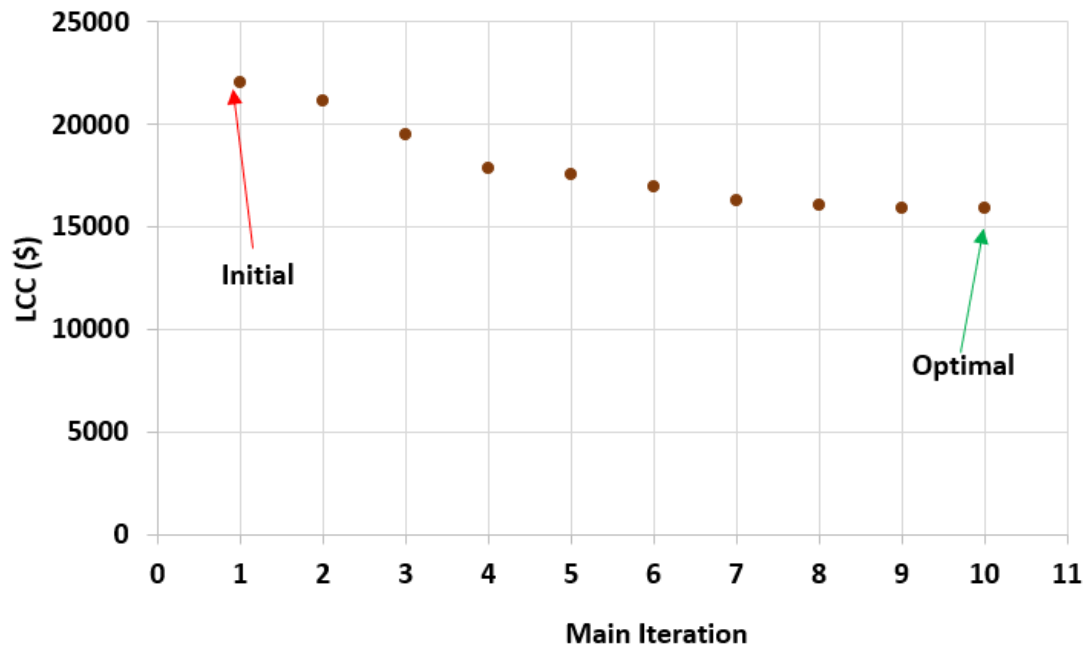


FIGURE 34: Evolution of the objective function values in Hooke-Jeeves for Hilli region

Using the best individual found from the PSO as the starting point, the HJ is applied. Because the HJ algorithm is not able to deal with discrete variables, the variables on building envelope insulation, which have been considered discrete during PSO, are replaced with specific numerical values in the HJ input file.

The HJ is run for a total of 10 iterations. FIGURE 34 shows that the life cycle cost is reduced by \$6,136 from \$22,057 to \$15,921 at the end of optimization. Because the HJ is a local search optimization algorithm that maintains only one solution, the objective function always reduces from one iteration to the next iteration.

When the hybrid algorithm is applied to the initial design, the life cycle cost is reduced by 72% for the Hilli region.

TABLE 9 lists the optimal values of the 12 variables obtained at the end of the HJ. For the convenience of comparison, the initial design values at the beginning of the

optimization, which are based on the design convention, engineering judgement, and a number of parametric runs of the TRNSYS simulation model, are also presented in the table.

TABLE 9: Initial values and final values of the optimization variables for Hilli region

S.N.	Optimization Variables	Unit	Initial Value	Optimal Value PSO	Optimal Value HJ
1	Area of solar collector	m <sup>2</sup>	20	31.33	24.33
2	Collector slope	degree	28	50	60
3	Collector fluid rate	kg/hr.	500	470	770
4	DHW tank volume	m <sup>3</sup>	0.3	0.333	0.133
5	Storage tank volume	m <sup>3</sup>	1	1.678	0.378
6	DHW auxiliary power	kJ/hr.	3,600	8,905	8,906
7	Instantaneous water heater power	kJ/hr.	129,600	30,524	12,524
8	Flow rate of space heating loop	kg/hr.	2500	3,350	2,700
9	Roof insulation	mm	1	50	50
10	Ground floor insulation	mm	30	60	60
11	Wall insulation inside	mm	1	1	1
12	Wall insulation outside	mm	1	50	50

Recall the solar collector results for the southern belt in Nepal. It showed that the solar collector area is reduced from the initial design of 20 m<sup>2</sup> to 6 m<sup>2</sup>. For this belt, the collector area of the optimal design is increased from initial design. The major reason lies in the larger space heating load than the southern belt. It has already been presented in Chapter 3 that major cause of temperature difference within the country is due to rapid

change in altitude (at every 1000 m rise in altitude, the temperature decreases by 6°C). When there is a high space heating load, the contribution of solar collectors weighs more and overpowers the operating cost of the auxiliary heater.

The optimal design of solar collector slope is found to be double the initial value. In order to better understand the impact of solar collector slope on LCC, the optimal design is perturbed with the change of only the collector slope while keeping all other variables unchanged. The perturbed collector slope includes 10° less than the latitude, the latitude, 15° more than the latitude, 10° more than the optimal solution in TABLE 9, and 20° more than the optimal solution FIGURE 35 shows how the LCC changes with the perturbed collector slope. This figure shows that there is no significant difference in LCC when the collector slope varies from 18° to 80°. However, a research led by NREL recommends having solar collector tilted at 72° for Sterling, VA which has latitudinal angle of 39°N as shown in FIGURE 36. From the two researches it can also be concluded that the impact of collector slope is hard to notice when the objective function is life cycle cost which is an indirect consequence of energy. In the light of above researches conducted by NREL and output from this study, the solar collector slope of 60° for Kathmandu is validated.

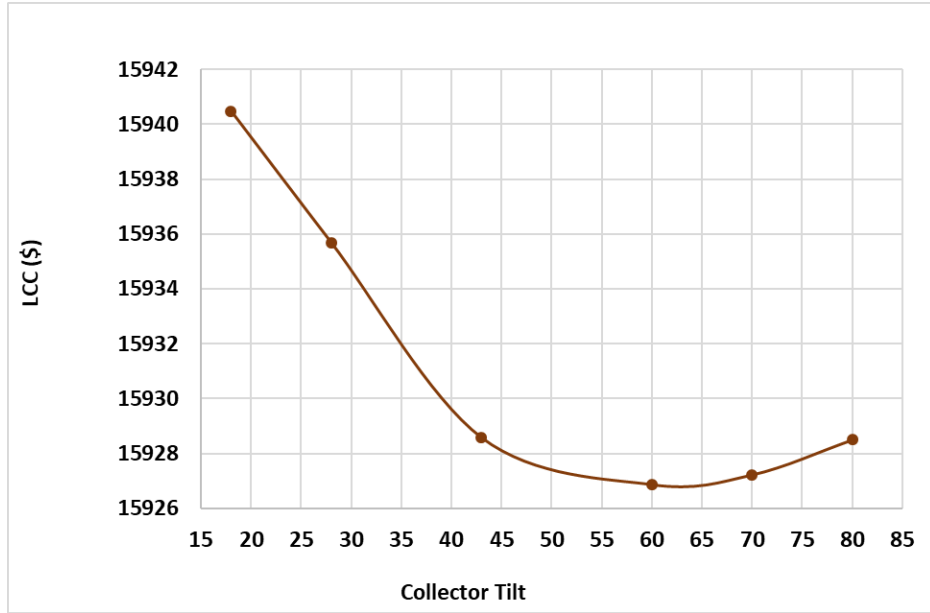


FIGURE 35: Impact of collector slope on Life Cycle Cost

**Graph 3** Solar space heating load profiles are nonlinear and require careful analysis to optimize annual heat generation and minimize overproduction during the summer months. For this modeled system incorporating 320 square feet of collectors, a tilt angle of 72° is good.

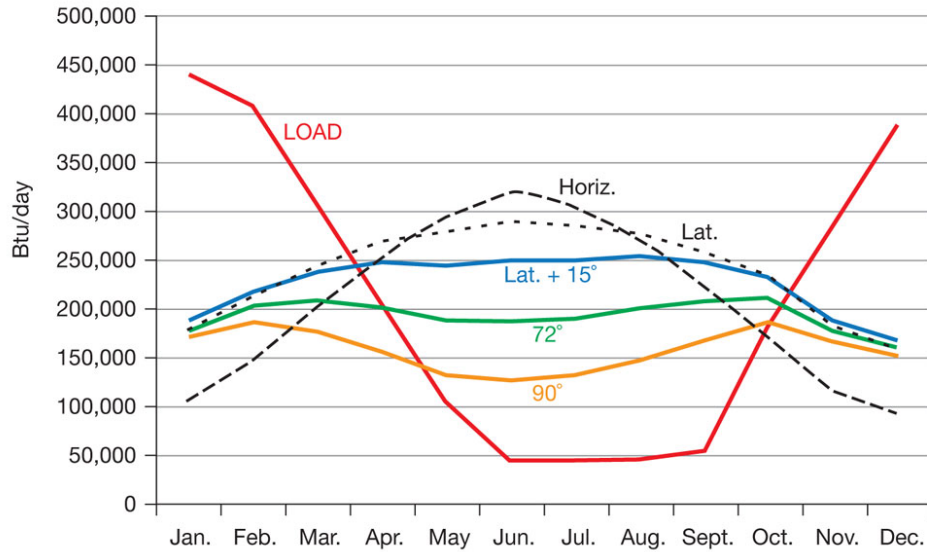


FIGURE 36: Impact of collector slope on annual energy generation for Sterling, VA

The sizes of both the storage tank and the DHW tank are decreased from the initial design. This is mainly due to the high capital cost while the electricity price is very low.

The solar collector fluid flow rate is increased from 500 kg/hr. for the initial design to 770 kg/hr for the optimal design. Solar thermal installers in Canada recommended having collector fluid flow rate in between 10 and 115 kg/hr per m<sup>2</sup> collector area (Hin 2013). The collector flow rate of the optimal design is 32 kg/hr per collector area, which lies in the installer-recommended range.

The space heating loop flowrate is increased from 2500 kg/hr for the initial design to 2700 kg/hr for the optimal design. As we know, for the same amount of energy delivered to the radiant floor, increasing the supply water flowrate means the decrease of the supply water temperature. Instead of supplying water to the radiant system at high temperature, which is not ideal for radiant floor heating system, supplying water at a large flow rate and low temperature is more effective.

Similar to the Terai region, building envelope insulation has a big impact on the space heating load and the sizing of the equipment used in the combisystem and thereby on the life cycle cost. Meanwhile, the insulation initial cost is much lower than the equipment cost. Therefore, it is reasonable to expect that relative to the initial design, a higher level of insulation should be used in the envelope, as demonstrated from the optimal insulation values in TABLE 8. The roof insulation is increased from the minimum of 1 mm (a proxy of no insulation because TRNSYS does not accept a zero value for the layer's thickness) for the initial design to the maximum of 50 mm for the optimal design. The ground insulation is increased from 30 mm for the initial design to 60 mm for the optimal design. The external part of the wall insulation is increased from the minimum of 1mm for

the initial design to the maximum of 50 mm for the optimal design. However, the internal part of the wall insulation is kept at the minimum. Such a wall design is reasonable because applying the thermal insulation outside of the structure is favorable for using the thermal mass to reduce the impact of diurnal outdoor temperature change on the space temperature. The size of instantaneous water heater is reduced from staggering 36 kW to 3.5kW due to the effect of building insulation.

## CHAPTER 7: CONCLUSIONS

### 7.1 Summary of Results

The work presented in the thesis includes the design, modeling, and optimization of a solar combisystem for typical single-family houses in Nepal. The proposed solar combisystem consists of solar thermal collectors, one preheating water tank, one domestic hot water tank with auxiliary electric resistance heating, an electric instantaneous water heater and circulation pumps. TRNSYS software is used to model the solar combisystem.

For optimization, life cycle cost is the objective function. The life cycle cost was calculated to include the initial cost of the combisystem components, and the present value of the cost of electricity consumed over the operating life of the combisystem. The present value calculations considered the inflation rate, the discount rate, and the escalation rate of electricity price in Nepal. The number of hours not satisfying the thermostat set points is treated as the constraint of the optimization problem. Major optimization variables include the thermal collector area, the volumes of both tanks, the flow rate of water circulating between the thermal collectors and the preheating tank, and several building envelope variables such as the wall insulation and roof insulation. The particle swarm optimization and the Hooke-Jeeves algorithms are combined to solve the optimization problem.

The solar combisystem was modeled and optimized in two different climatic regions in Nepal: the Terai region and the Hilli region. For both regions, the optimization starts from an initial design based on guidelines, conventional construction practices, and engineering judgement. Though the initial design is technically feasible and provides acceptable thermal comfort, the optimization ends up with an optimal design with significant reduction of the life cycle cost from the initial design. Life cycle cost for system

in the Terai region was reduced by 63% and by 72% for system in Hilli region. This demonstrates the importance of optimization even during the initial design phase. For the Terai region, the size of solar combisystem has been reduced dramatically from the initial design. This is because the space heating load in the Terai region is not large enough to overcome the upfront cost of the solar combisystem. It is favorable to have a system with a small solar collector area of 6 m<sup>2</sup> and the DHW and storage tanks with a volume of 180 L for this region.

For the Hilli region, the optimal design has a collector area of about 24 m<sup>2</sup>, due to the large space heating load in the region as compared to Terai region. The storage tank volume is also increased to about 380 L.

For both regions, the optimization shows that building envelope insulation is important to minimize the life cycle cost. This indicates that the need of requiring a minimum thermal insulation in residential buildings to deploy solar combisystems.

## **7.2 Future Work**

The research could be extended in future along the following avenues:

- This research showed that the solar combisystem is expensive and it is best to rely upon electricity to achieve DHW and space heating for the Terai region in Nepal. It would be interesting to investigate the amount of subsidies required to make solar combisystem economically feasible.
- Nepal has three distinct climate zones, two of which were analyzed in this work. Due to the lack of data of typical building constructions in Himalayan region, the combisystem could not be analyzed for that location. However, the most common complaints of trekkers in the Himalayan region is unavailability of hot water and

warm rooms. Therefore, it is worthwhile to pursue further research on the feasibility of solar combisystems in the Himalayan region.

- This thesis optimizes the life cycle cost of the solar combisystem. In order to reveal the trade-off between the economic performance and other criteria (e.g., life cycle energy), a multi-objective optimization could be pursued.

## REFERENCES

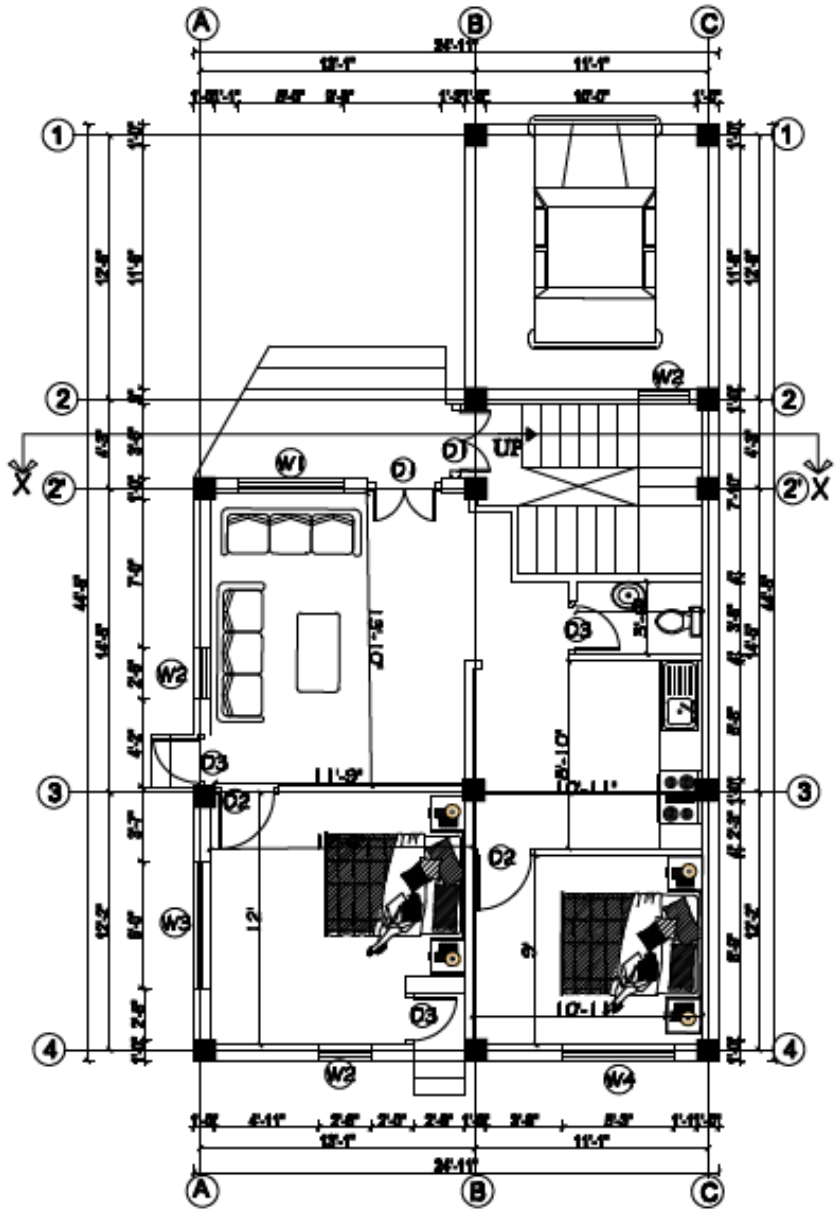
- Andersen, E. and S. Furbo. 2009. Theoretical variations of the thermal performance of different solar collectors and solar combi systems as function of the varying yearly weather conditions in denmark. *Solar Energy* 83, no 4: 552-65.
- Ardente, F., G. Beccali, M. Cellura and V. Lo Brano. 2005. Life cycle assessment of a solar thermal collector. *Renewable Energy* 30, no 7: 1031-54.
- Asaee, S., V. Ismet Ugursal and I. Beausoleil-Morrison. 2016. Techno-economic study of solar combisystem retrofit in the canadian housing stock. *Solar Energy* 125: 426-43.
- Asaee, S.R., V.I. Ugursal, I. Beausoleil-Morrison and N. Ben-Abdallah. 2014. Preliminary study for solar combisystem potential in canadian houses. *Applied Energy* 130: 510-18.
- Ashrae. 2007. *2007 ashrae handbook- fundamentals*. Atlanta, GA, USA: American Society of Heating, Refrigerating and Air-conditioning Engineers.
- Bales, C. and T. Persson. 2003. External dhw units for solar combisystems. *Solar Energy* 74, no 3: 193-204.
- Banister, C.J. and M.R. Collins. 2015. Development and performance of a dual tank solar-assisted heat pump system. *Applied Energy* 149: 125-32.
- Battisti, R. and A. Corrado. 2005. Environmental assessment of solar thermal collectors with integrated water storage. *Journal of Cleaner Production* 13, no 13-14: 1295-300.
- Bhandari, R. and S. Pandit. 2018. Electricity as a cooking means in nepal—a modelling tool approach. *Sustainability* 10, no 8: 2841.
- Bornatico, R., M. Pfeiffer, A. Witzig and L. Guzzella. 2012. Optimal sizing of a solar thermal building installation using particle swarm optimization. *Energy* 41, no 1: 31-37.
- Calise, F., M.D. D'accadia and L. Vanoli. 2011. Thermoeconomic optimization of solar heating and cooling systems. *Energy Conversion and Management* 52, no 2: 1562-73.
- Chow, T.T., G. Pei, K.F. Fong, Z. Lin, A.L.S. Chan and J. Ji. 2009. Energy and exergy analysis of photovoltaic-thermal collector with and without glass cover. *Applied Energy* 86, no 3: 310-16.
- Crawford, R.H. and G.J. Treloar. 2004. Net energy analysis of solar and conventional domestic hot water systems in melbourne, australia. *Solar Energy* 76, no 1-3: 159-63.

- Esmap. 2017. Solar resource and photovoltaic potential of nepal. In *Global ESMAP Initiative Renewable Energy Resource Mapping and Geospatial Planning – Nepal*, 77.
- Fairy, P. and D. Parker. 2004. A review of hot water draw profiles used in performance analysis of residential domestic hot water systems.
- Fraisse, G., Y. Bai, N. Le Pierrès and T. Letz. 2009. Comparative study of various optimization criteria for sdhws and a suggestion for a new global evaluation. *Solar Energy* 83, no 2: 232-45.
- Giri, D.J., Govinda ; Pokhrel, Benit ; Shrestha, Biswas 2013. Room heating by solar air collector for residential purpose. Bachelor in Engineering, Tribhuvan University.
- Hernandez, P. and P. Kenny. 2012. Net energy analysis of domestic solar water heating installations in operation. *Renewable and Sustainable Energy Reviews* 16, no 1: 170-77.
- Hin, J.N.C. 2013. Life cycle optimization of a residential solar combisystem for minimum cost, energy use and exergy destroyed. Masters Degree, Concordia University.
- Hugo, A. 2008. Computer simulation and life cycle analysis of a seasonal thermal storage system in a residential building. Degree of Master of Applied Science, Concordia University.
- Kalogirou. 2004. Optimization of solar systems using artificial neural-networks and genetic algorithms. *Applied Energy* 77, no 4: 383-405.
- Kalogirou. 2009. Thermal performance, economic and environmental life cycle analysis of thermosiphon solar water heaters. *Solar Energy* 83, no 1: 39-48.
- Klein, S., W.A. Beckman, J.A. Duffie and J.W. Mitchell. 2018. Trnsys.
- Leckner, M. 2008. Life cycle energy and cost analysis of a net zero energy house (nze) using a solar combisystem. Degree of Master of Applied Sciences (Building Engineering) Concordia University.
- Leconte, A., G. Achard and P. Papillon. 2012. Solar combisystem characterization with a global approach test and a neural network based model identification. *Energy Procedia* 30: 1322-30.
- Letz, T., C. Bales and B. Perers. 2009. A new concept for combisystems characterization: The fsc method. *Solar Energy* 83, no 9: 1540-49.
- Lima, J.B.A., R.T.A. Prado and V. Montoro Taborianski. 2006. Optimization of tank and flat-plate collector of solar water heating system for single-family households to

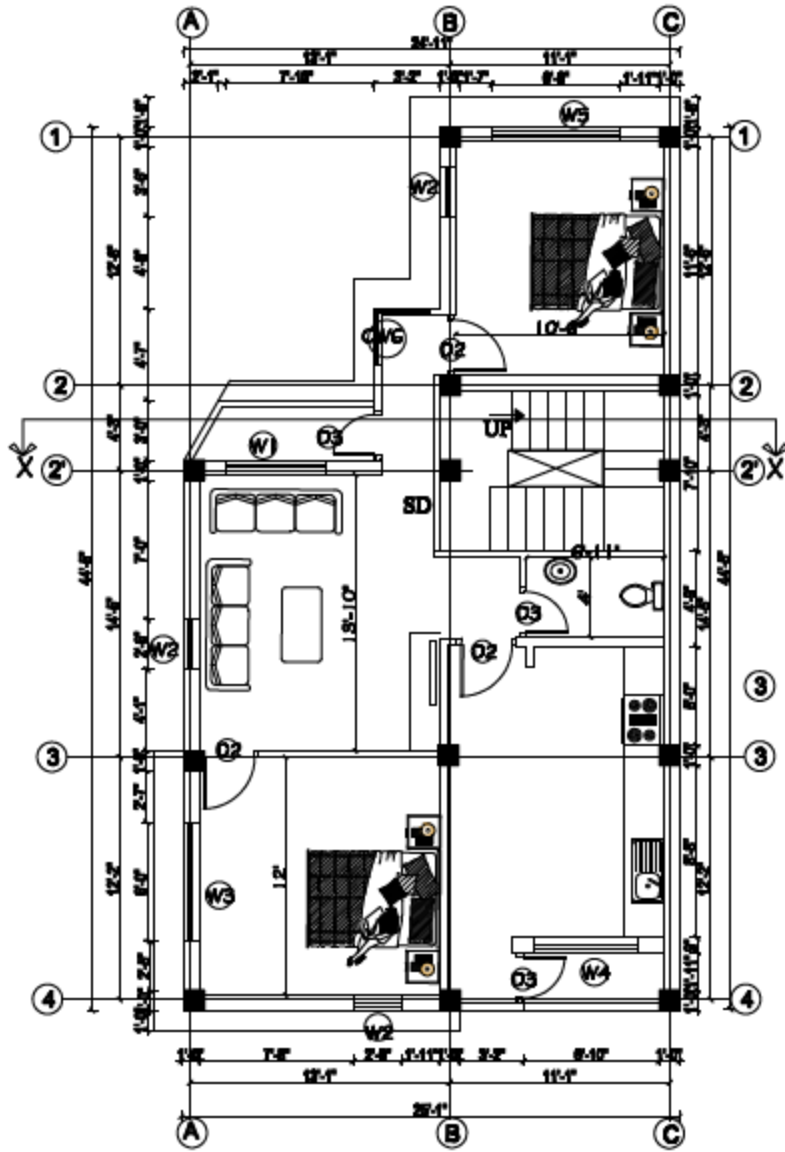
- assure economic efficiency through the trnsys program. *Renewable Energy* 31, no 10: 1581-95.
- Loomans, M.V., Huib. 2002. Application of the genetic algorithm for optimization of large solar hot water systems. *Solar Energy* 72, no 5: 427-39.
- Lund, P.D. 2005. Sizing and applicability considerations of solar combisystems. *Solar Energy* 78, no 1: 59-71.
- Lundh, M., K. Zass, C. Wilhelms, K. Vajen and U. Jordan. 2010. Influence of store dimensions and auxiliary volume configuration on the performance of medium-sized solar combisystems. *Solar Energy* 84, no 7: 1095-102.
- Nrb. 2019. Nepal rastra bank current macroeconomic and financial situation of nepal.
- Papillon, P., A. Leconte, M. Albaric, B. Mette and J. Ullmann. 2010. Solar combisystems promotion and standardisation : Final report. Intelligent energy europe. .
- Patil, R. 2010. Impact of climate change on an r-2000 and a net zero energy home. Master of Applied Sciences, Concordia University.
- Peuser, F., K.H. Remmers and M. Schnauss. 2011. *Solar thermal systems - successful planning and construction*. Berlin, Germany: Beuth Verlag GmbH.
- Pradhan, B., P. Sharma and P. K. Pradhan. 2019. Impact of cold wave on vulnerable people of tarai region, nepal.
- Rajbhandari, U.S. and A.M. Nakarmi. 2015. Energy consumption and scenario analysis of residential sector using optimization model – a case of kathmandu valley. In *IOE Graduate Conference*. Kathmandu.
- Rey, A. 2017. Multi-objective optimization of solar thermal combisystems. Doctor of Philosophy, Concordia University.
- Sengupta, U. and V. Upadhyaya. 2016. Lost in transition? Emerging forms of residential architecture in kathmandu. *Cities* 52: 94-102.
- Shakya, S. and T. Bajracharya. 2003. Technology analysis of domestic solar water heater systems in nepal : Needs a revamp. Paper presentat at the 8th National Convention and FEISCA Regional Meet, in Kathmandu.
- Streicher, E., W. Heidemann and H. Muller-Steinhagen. 2004. Energy payback time – a key number for the assessment of thermal solar systems. In *EuroSun*, 10. Freiburg, Germany.
- Subedi, P. 2010. A sustainable housing approach to kathmandu, nepal. M.S. in Building Construction, University of Florida.

- Sustar, J. 2011. Performance modeling and economic analysis of residential solar combisystems. Masters Degree, University of Colorado.
- Timilsina, A.B., S.K. Mishra, R.N. Bhattaraiai and T.R. Bajracharyaa. 2018. Variable refrigerant flow (vrf) system for space heating: A case study of resort. *Journal of the Institute of Engineering* 14, no 1: 1-13.
- Ulrike, J. and V. Klaus. 2000. Influence of the dhw load profile on the fractional energy savings : A case study of a solar combi-system with trnsys simulations. *Solar Energy* 69: 197-208.
- Weiss, W. 2003. *Solar heating systems for houses- a design handbook for solar combisystems*. London: James & James (Science Publishers) Ltd.
- Weiss, W., F. Mauthner and M. Spork-Dur. 2013. Solar heat worldwide. In *Markets and Contribution to the Energy Supply 2013*, 68. 2013: AEE - Institute for Sustainable Technologies, A-8200 Gleisdorf, Austria, IEA Solar Heating & Cooling Programme.
- Weiss, W. and M. Spork-Dur. 2018. Solar heat worldwide. In *Global Market Development and Trends in 2017 Detailed Market Figures 2016*, 94. 8200 Gleisdorf, Austria: AEE - Institute for Sustainable Technologies.
- Wetter, M. 2016. Generic optimization program user manual version 3.1.1. Lawrence Berkeley National Laboratory.

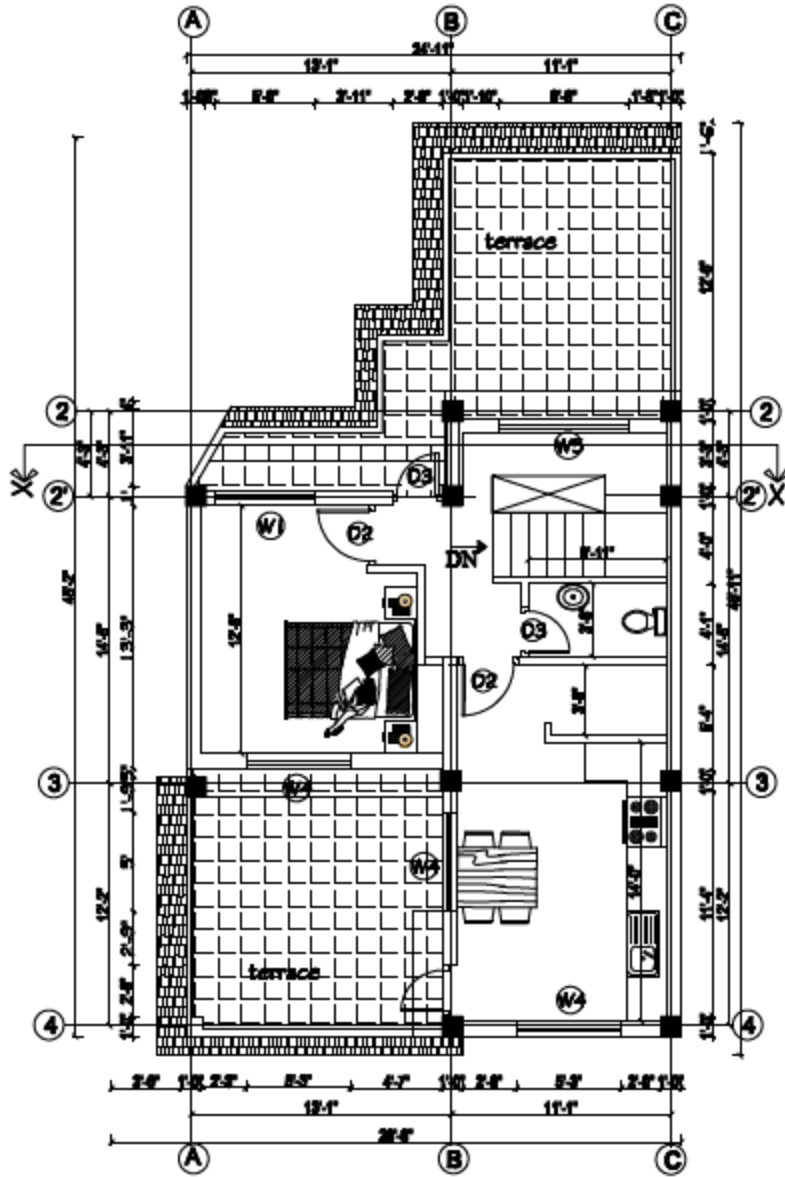
# APPENDIX A



Ground Floor of the reference house



First floor plan of the building



Second floor plan of the reference building

## APPENDIX B

### Properties of Storage Tank

<b>Particulars</b>	<b>Value</b>	<b>Unit</b>	<b>Source</b>
Number of tank nodes	5	-	
Number of ports	1	-	
Number of immersed heat exchangers	2	-	
Number of miscellaneous heat flows	0	-	
Tank volume	STO_VOL	string	
Tank height	1.5	m	Leckner,2008
Tank fluid	0	-	
Fluid specific heat	4.19	kJ/kg.K	TESSS,2019
Fluid density	1000	kg/m <sup>3</sup>	TESSS,2019
Fluid thermal conductivity	2.14	kJ/hr.m.K	TESSS,2019
Fluid viscosity	3.21	kg/m.hr	TESSS,2019
Fluid thermal expansion coefficient	0.00026	1/K	TESSS,2019
Top loss coefficient	1.181	kJ/hr.m <sup>2</sup> . K	Leckner,2008
Edge loss coefficient for node-1	1.181	kJ/hr.m <sup>2</sup> . K	Leckner,2008
Edge loss coefficient for node-2	1.181	kJ/hr.m <sup>2</sup> . K	Leckner,2008
Edge loss coefficient for node-3	1.181	kJ/hr.m <sup>2</sup> . K	Leckner,2008
Edge loss coefficient for node-4	1.181	kJ/hr.m <sup>2</sup> . K	Leckner,2008
Edge loss coefficient for node-5	1.181	kJ/hr.m <sup>2</sup> . K	Leckner,2008
Bottom loss coefficient	1.181	kJ/hr.m <sup>2</sup> . K	Leckner,2008
Additional thermal conductivity	0	kJ/hr.m.K	
Inlet flow mode	1	-	
Entry node	5	-	
Exit node	1	-	
Flue loss coefficient for node-1	0	kJ/hr.m <sup>2</sup> . K	
Flue loss coefficient for node-2	0	kJ/hr.m <sup>2</sup> . K	
Flue loss coefficient for node-3	0	kJ/hr.m <sup>2</sup> . K	

Flue loss coefficient for node-4	0	kJ/hr.m <sup>2</sup> . K	
Flue loss coefficient for node-5	0	kJ/hr.m <sup>2</sup> . K	
Type of HX (HX1)	3	-	
Number of HX nodes (HX1)	5	-	
HX fluid (HX1)	0	-	
HX fluid specific heat (HX1)	4.19	kJ/kg.K	TESS,2019
HX fluid density (HX1)	1000	kg/m <sup>3</sup>	TESS,2019
HX fluid thermal conductivity (HX1)	2.14	kJ/hr.m.K	TESS,2019
HX fluid viscosity (HX1)	3.21	kg/m.hr	TESS,2019
Multiplier for natural convection (HX1)	0.6	-	TESS,2019
Exponent for natural convection (HX1)	0.25	-	TESS,2019
Geometry factor for natural convection (HX1)	1.0	-	TESS,2019
Geometry exponent for natural convection (HX1)	1.0	-	TESS,2019
Inner tube diameter (HX1)	0.01587	m	Leckner,2008
Outer tube diameter (HX1)	0.018	m	Leckner,2008
HX wall thermal conductivity (HX1)	385	W/m.K	
Length of coiled tubes (HX1)	36.6	m	Leckner,2008
Number of tubes (HX1)	1	-	Leckner,2008
HX header volume (HX1)	0	m <sup>3</sup>	
HX cross sectional area (HX1)	0.05	m <sup>2</sup>	
Coil diameter (HX1)	0.53	m	Leckner,2008
Coil pitch (HX1)	0.03	m	Leckner,2008
Tank node for HX node (HX1)-1	1	-	
Fraction of HX length (HX1)-1	0.2	-	
Tank node for HX node (HX1)-2	1	-	

Fraction of HX length (HX1)-2	0.2	-	
Tank node for HX node (HX1)-3	2	-	
Fraction of HX length (HX1)-3	0.2	-	
Tank node for HX node (HX1)-4	2	-	
Fraction of HX length (HX1)-4	0.2	-	
Tank node for HX node (HX1)-5	3	-	
Fraction of HX length (HX1)-5	0.2	-	
Type of HX (HX2)	3	-	
Number of HX nodes (HX2)	5	-	
HX fluid (HX2)	0	-	
HX fluid specific heat (HX2)	3.747	kJ/kg.K	
HX fluid density (HX2)	973	kg/m <sup>3</sup>	
HX fluid thermal conductivity (HX2)	0.206	W/m.K	
HX fluid viscosity (HX2)	0.025	poise	
Multiplier for natural convection (HX2)	0.6	-	
Exponent for natural convection (HX2)	0.25	-	
Geometry factor for natural convection (HX2)	1.0	-	
Geometry exponent for natural convection (HX2)	1.0	-	
Inner tube diameter (HX2)	0.01587	m	Leckner,2008
Outer tube diameter (HX2)	0.018	m	Leckner,2008
HX wall thermal conductivity (HX2)	385	W/m.K	Leckner,2008
Length of coiled tubes (HX2)	36.6	m	Leckner,2008
Number of tubes (HX2)	1	-	Leckner,2008
HX header volume (HX2)	0.001	m <sup>3</sup>	

HX cross sectional area (HX2)	0.05	m <sup>2</sup>	
Coil diameter (HX2)	0.053	m	Leckner,2008
Coil pitch (HX2)	0.03	m	Leckner,2008
Tank node for HX node (HX2)-1	3	-	
Fraction of HX length (HX2)-1	0.2	-	
Tank node for HX node (HX2)-2	4	-	
Fraction of HX length (HX2)-2	0.2	-	
Tank node for HX node (HX2)-3	4	-	
Fraction of HX length (HX2)-3	0.2	-	
Tank node for HX node (HX2)-4	5	-	
Fraction of HX length (HX2)-4	0.2	-	
Tank node for HX node (HX2)-5	5	-	
Fraction of HX length (HX2)-5	0.2	-	

